Study of a sociable molecule

Mapping the binding interfaces of the cell division regulator MipZ in *Caulobacter crescentus*

Dissertation

zur Erlangung des Doktorgrades

der Naturwissenschaften

(Dr. rer. nat.)

dem

Fachbereich Biologie

der Philipps-Universität Marburg

von

Binbin He

aus Yakeshi, P. R. China

Marburg (Lahn), April 2014

Vom Fachbereich Biologie der Philipps-Universität Marburg (Hochschulkennziffer: 1180)
als Dissertation angenommen am: ___.___.2014

Erstgutachter: Jun.-Prof. Dr. Martin Thanbichler
Zweitgutachter: Prof. Dr. Lotte Søgaard-Andersen
Tag der mündlichen Prüfung am: ___.___.2014

Die Untersuchungen zur vorliegenden Arbeit wurden von Oktober 2010 bis April 2014 am Max-Planck-Institut für terrestrische Mikrobiologie unter der Leitung von Jun.-Prof. Dr. Martin Thanbichler durchgeführt.

ABSTRACT

In most bacteria, cell division requires assembly of FtsZ, the tubulin homologue, into a ring-like structure, the so-called Z-ring. The Z-ring acts as a scaffold for the cell division machinery and marks the future division site. To precisely localize the Z-ring, bacteria have evolved different regulatory mechanisms. In the model organism *Caulobacter crescentus*, Z-ring positioning depends on a P-loop ATPase, MipZ.

MipZ forms bipolar gradients within the cell and acts as an inhibitor of FtsZ polymerization, thereby restricting assembly of the Z-ring to the midcell region. Gradient formation is driven by the alternation of MipZ between a monomeric and dimeric state with distinct interaction patterns and diffusion rates. This alternation results in a dynamic localization cycle, in which MipZ continuously oscillates between non-specific chromosomal DNA and the polarly localized ParB protein.

In this study, we investigated the function of MipZ by mapping its interaction interfaces with FtsZ, ParB and DNA. We systematically exchanged surface-exposed residues using alanine-scanning mutagenesis. Analyzing the subcellular distribution of the mutant proteins as well as their ability to support division site placement, we identified four clusters of residues that are important for MipZ activity. Two of them are likely responsible for contacting FtsZ and chromosomal DNA, respectively, whereas the other two appear to be involved in the interaction with ParB. Notably, the DNA-binding and FtsZ-binding interfaces of MipZ comprise residues from both monomeric subunits and are located on opposite sides of the dimer. This result is consistent with the previous finding that the regulatory effect of MipZ is specific for its dimeric form and that only the dimeric form contacts DNA and FtsZ. We also found that the DNA-binding region mainly consists of positively charged arginine and lysine residues. *In vivo* and *in vitro* studies showed that mutation of these residues impairs the DNA-binding activity of MipZ to different extents; moreover, mutation of R194 and R198 abolished the MipZ-DNA interaction. These results provide the first detailed analysis of the interaction determinants of MipZ and deepen our knowledge of the molecular mechanism underlying the function of this intriguing cell division regulator.

ZUSAMMENFASSUNG

In den meisten Bakterien wird die Zellteilung durch die Assemblierung des Tubulin-Homologs FtsZ in eine ringähnliche Struktur, den sogenannten „Z-Ring“ eingeleitet. Der Z-Ring markiert die zukünftige Teilungsebene und rekrutiert direkt oder indirekt alle weiteren Zellteilungsproteine. Bakterien haben unterschiedliche regulatorische Mechanismen entwickelt, um die korrekte Positionierung des Z-Rings sicherzustellen. Im Modellorganismus *Caulobacter crescentus* ist die Positionierung des Z-Rings von der P-loop ATPase MipZ abhängig.

MipZ bildet einen bipolaren Gradienten in der Zelle und agiert als Inhibitor von FtsZ, welches dadurch ausschließlich in der Zellmitte polymerisieren kann. Die Bildung des Gradienten beruht auf einem Wechsel von MipZ zwischen einem monomeren und dimeren Zustand, welche unterschiedliche Interaktionspartner und Diffusionsraten aufweisen. Aus diesem Verhalten ergibt sich ein dynamischer Lokalisationzyklus, in dem die MipZ-Moleküle zwischen unspezifischer chromosomaler DNA und polar lokalisiertem ParB oszillieren.

In dieser Studie wurde die Funktion von MipZ untersucht, indem die Bindestellen von FtsZ, ParB und chromosomaler DNA auf MipZ kartiert wurden. Dazu wurden systematische oberflächenexponierte Reste mit Hilfe von ortsgerichteter *alanine-scanning* Mutagenese ausgetauscht. Die mutierten Proteine wurden anschließend auf ihre zelluläre Verteilung sowie auf ihre Fähigkeit, die Zellteilungsebene korrekt zu platzieren, untersucht. Es konnten vier Aminosäuren-Cluster identifiziert werden, welche eine entscheidende Rolle für die Aktivität von MipZ hatten. Zwei von ihnen sind für die Bindung von FtsZ und chromosomaler DNA verantwortlich, die anderen zwei vermitteln die Interaktion mit ParB. Bemerkenswert ist, dass sich die DNA- und die FtsZ-Bindetasche aus Resten von beiden monomeren Untereinheiten zusammensetzen und einander gegenüber liegen. Diese Beobachtung steht in Einklang mit bisherigen Ergebnissen, welche darauf hindeuten, dass die Zellteilung auschließlich durch die dimere Form reguliert wird und nur diese zur Interaktion mit DNA und FtsZ fähig ist. Es zeigte sich zudem, dass die DNA-Binderegion zum Großteil aus positiv geladenen Arginin- und Lysin-Resten besteht. *In vivo* und *in vitro* Experimente zeigten, dass Mutationen in diesen Resten die DNA-Bindekapazität von MipZ in unterschiedlichem Maß verringern. Mutationen in R194 und R198 führten darüberhinaus zur vollständigen Inhibition der MipZ-DNA-Interaktion. Diese Ergebnisse liefern erstmals detaillierte Einblicke in die Interaktionsdeterminanten von MipZ und erweitern unser Verständnis des molekularen Mechanismus, der der Aktivität dieses faszinierenden Zellteilungsregulators zu Grunde liegt.

CONTENT

1 INTRODUCTION

Nowadays, it is well-accepted that bacterial cells are not simply bags of enzymes. Bacterial cell division is a good example to show the complexity of bacteria. Although the general idea is that bacteria undergo binary fission for division, there are an increasing number of studies that focus on asymmetric and even irregular cell division mechanism. *Caulobacter crescentus*, the organism used in this study, is intensively studied for its asymmetric division and tightly regulated cell cycle (1). *C. crescentus*, an α-proteobacterium, is ubiquitous in fresh water (2). It undergoes an asymmetric cell division, which gives birth to two distinct daughter cells, a smaller motile, flagellated swarmer cell and a bigger sessile stalked cell (Figure 1.1) (3). The stalked cell is able to start the cell cycle immediately, whereas the swarmer cell needs to differentiate into a stalked cell before it can enter a new cell cycle. In every cell cycle, *C. crescentus* only replicates its chromosome once (4).

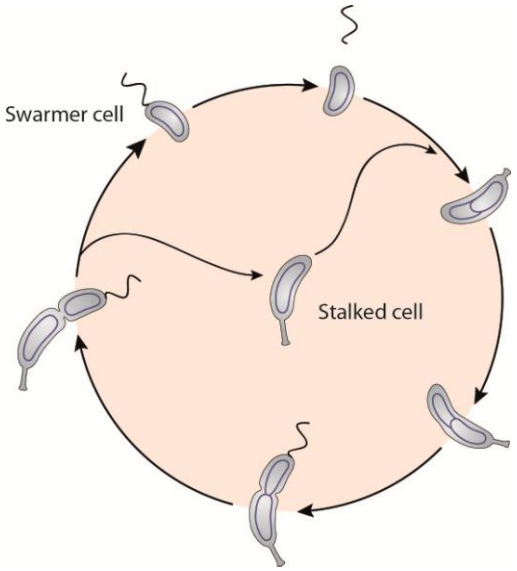

Figure 1.1 Cell cycle of *C. crescentus*. The two daughter cells, the swarmer cell and the stalked cell, enter the cell cycle differently. The swarmer cell needs to transform to a stalked cell to start the cell cycle, while the stalked cell can start replication immediately. Figure adapted from M. Thanbichler (unpublished).

1.1 Chromosome segregation in bacteria

Bacteria evolved a variety of delicate mechanisms to ensure precise and faithful chromosome segregation. Unlike eukaryotic cells, which separate chromosome replication and segregation in time, bacteria usually replicate and segregate their chromosome concomitantly (5-7). How bacteria manage to regulate and coordinate the complicated processes is still poorly understood. However, owing to advances in microscopy technology, some mechanisms and many proteins

involved in bacterial chromosome segregation have been discovered in recent years. Surprisingly, even though chromosome segregation is a crucial step for bacterial survival, only a small set of highly conserved proteins have been discovered; moreover, these proteins are not essential in most bacteria (6). In the following section, bacterial chromosome segregation is reviewed with a focus on three chromosome segregation-related components: the ParAB-*parS* system, the SMC (structural maintenance of chromosomes) complex, and FtsK.

1.1.1 Important components involved in bacterial chromosome segregation

Generally, bacterial chromosome segregation can be divided into three steps: the segregation of the replication origins, the segregation of the bulk of the chromosome, and the segregation of the terminus region (5). Both the SMC complex and ParAB-*parS* system are mainly involved in separating the newly replicated origins, while FtsK segregates the terminus region (5, 6, 8-10).

The ParAB-*parS* system was found to mediate the segregation of both low-copy number plasmids and chromosomes (11), although the plasmid-encoded ParAB-*parS* system is relatively well-studied (12), here I mainly focus on the chromosome-encoded system. The ParAB-*parS* system consists of three parts: the two proteins ParA and ParB, as well as a DNA sequence, *parS* (6). ParA, an ATPase, is generally believed to form dimers or polymers in a nucleotide-dependent manner (13, 14). ParA binds non-specifically to chromosomal DNA and drives the separation of the duplicated sister origin regions (5). ParB specifically binds to *parS* sequences; simultaneously it also interacts with ParA and stimulates the ATPase activity of ParA, thereby disassembling ParA (6, 14, 15). *parS*, the centromere-like DNA element, is usually close to the origin and present in multiple copies (6). It is generally accepted that ParA moves the ParB-*parS* complex together with the newly replicated origin to the opposite cell pole (6). However, the mechanism underlying the process is still under debate. One model suggests that ParA forms filaments, which pull the two newly replicated origins apart (14, 16). By contrast, the diffusion-ratchet model, although proposed for ParAB-*parS* mediated plasmid segregation, explains the segregation by the directed movement of the ParB-*parS* complex along local gradient of ATP-bound ParA, in this model, ParA does not form filaments but dimmers that cover the nucleoid (17, 18). The formation of the ParA gradient is dependent on the non-specific binding of ParA to chromosomal DNA, its ParB-stimulated ATPase activity, and the different binding affinities of the ADP-bound and ATP-bound ParA for chromosomal DNA (17-19). Besides mediating chromosome segregation, the ParAB-*parS* system also contributes to other aspects of cellular organization in different bacterial species. In *C. crescentus* and *Corynebacterium glutamicum*, ParAB-*parS* system plays a role in division site placement (20-23). The system is also involved in the regulation of sporulation in *Bacillus subtilis* and *Streptomyces coelicolor* (24, 25). Over 65% of sequenced bacterial genomes encode *parAB* loci (6, 26) while *E. coli* belongs to the other 35% that do not have a ParAB-*parS* system. However, in most of the species that have a ParAB-*parS* system, the system is not essential (6). The essentiality of ParAB-*parS* has only been shown in *C. crescentus* (27) and *Myxococcus xanthus* (7, 28).

The SMC complex is found in eukaryotes, prokaryotes, as well as archaea (10). The bacterial SMC complex (or its analogue MukBEF in many γ-and δ-proteobacteria, including *Escherichia coli*) consists of three parts: the V-shaped SMC homodimer with ATPase activity and the two

accessory proteins ScpA and ScpB that bridge between the dimer and participate in the regulation of the ATPase activity of the SMC dimer (10). Mutations in the SMC complex usually increase the fraction of anucleate cells (29-31), suggesting that SMC has a chromosome segregation-related function. Microscopy studies show that SMC fluorescent protein fusions are associated with the chromosome (10). Moreover, some of the *E. coli* MukB foci are colocalized with the origin region (32). In *B. subtilis*, ParB loads SMC onto the origin region from where it is distributed over the chromosome (33). A recent study (34) revealed that in *B. subtilus* the SMC complex plays a central role in resolving and segregating the newly replicated origins, particularly, in conditions of fast growth. In *C. crescentus*, a SMC fluorescent protein forms multiple foci in the cell but rarely colocalizes with ParB (29), and the ATPase activity of *C. crescentus* SMC is crucial for its function in segregating newly replicated origins (35).

It is still unclear what mechanisms drive the separation of the bulk of the chromosome. However, it was proposed that chromosome condensation and entropic effects, as well as DNA replication and transcription drive the separation process (5, 36). Moreover, the SMC complex is also proposed to contribute to segregating the bulk of the chromosome by introducing lengthwise condensation (37, 38).

FtsK, a multifunctional protein is involved the chromosome segregation and cell division (39). FtsK is conserved in many bacterial species, and it consists of an N-terminal domain, a linker domain with variable length and a C-terminal ATPase domain (39). The N-terminal region contains several trans-membrane domains that anchor FtsK to the septum, whereas the C-terminal domain is responsible for DNA binding and translocation (40). FtsK assembles into a hexameric complex at the septum, and pumps the chromosome toward *dif* site, which is located in the terminus region of chromosome. The direction of DNA translocation is determined by multiple copies of KOPS (FtsK-Orienting Polar Sequences), an 8-bp DNA sequence motif, oriented toward the *dif* site (40, 41). Upon reaching the *dif* site, FtsK activates the XerCD mediated homologous recombination at the *dif* site, which resolves dimeric chromosomes resulting from an odd number of homologous recombination events between the two sister chromosomes (42, 43). Moreover, FtsK activates topoisomeriase IV to decatenate the two sister chromosomes of the replication (44). Finally, as a component of divisome, FtsK also interacts with other cell division proteins to mediate the proper cell division (45).

1.1.2 The ParAB-*parS* system of *C. crescentus*

The ParAB proteins are essential for the viability of *C. crescentus*, the depletion of ParB or overexpression of ParA results in smooth filamentation. However, co-overexpression of both proteins suppresses the filamentous phenotype and partially restores cell division, although it leads to many anucleate cells, suggesting the cell division and chromosome segregation-related function of ParAB (27, 46). The *parS* sequence is crucial for the initiation of chromosome segregation in *C. crescentus* (36). Due to the essentiality of the ParAB-*parS* system, *C. crescentus* has evolved delicate mechanisms, involving the scaffold protein PopZ and the polar landmark protein TipN, to regulate this system (Figure 1.2) (47, 48). Before the initiation of chromosome replication ParB-*parS* complex localizes at the flagellated pole (old pole) of the swarmer cell and the stalked pole (old pole) of the stalked cell, mediated by its tethering to the polarly localized PopZ matrix (49). During the initiation of chromosome replication and

segregation, the newly formed ParB-*parS* complex is quickly translocated to the opposite pole in a ParA-dependent manner, and captured by the newly accumulated PopZ at the new pole (47, 50). PopZ, a multimeric polar scaffolding protein, recruits and interacts with many proteins involved in chromosome segregation, such as ParA and ParB and cell cycle signaling, such as CckA and DivJ (47). A *popZ* null mutant displays a stalkless, filamentous phenotype, and ParB foci are no longer attached to the cell pole, indicating an important role in cell morphology, cell division and chromosome segregation (22). ParA is the main player to translocate the ParB-*parS* complex to the new pole. Moreover, it has been shown that the transition of PopZ from unipolar to bipolar localization is dependent on the accumulation of ParA at the new pole (47). The direction and dynamics of ParA-mediated DNA segregation relied on another protein, TipN (48, 51). TipN, a membrane-bound protein, is considered to act as the landmark of the new pole (51). In *tipN* null mutants, ParA structures regenerate behind the ParB-*parS* complex, so that the partition complex stalls and even moves back-and-forth (48). TipN is shown to directly interact with ParA at the new cell pole and regulate ParA-dependent movement of ParB-*parS* complex toward the new pole by recruiting the monomeric form of ParA to the new pole, thus preventing its dimerization and relocalization on the nucleoid (48). Except for regulating the dynamics of the ParAB-*parS* system, TipN also determines the cell polarity (51, 52). The *tipN* null mutant exhibits several cell polarity defects, including mislocated flagella and a reverse asymmetry of the daughter cells (51).

In *C. crescentus*, the ParAB-*parS* system also plays a crucial role in Z-ring positioning (Figure 1.2) (21). Z-ring positioning in *C. crescentus* is regulated by MipZ, a negative regulator of FtsZ polymerization, whose distribution is dependent on its interaction with ParB (20, 21). Thus proper cell division in *C. crescentus* relies on a functional ParAB-*parS* system. A more detailed explanation of the MipZ-mediated Z-ring positioning system is given in section 1.3.3.

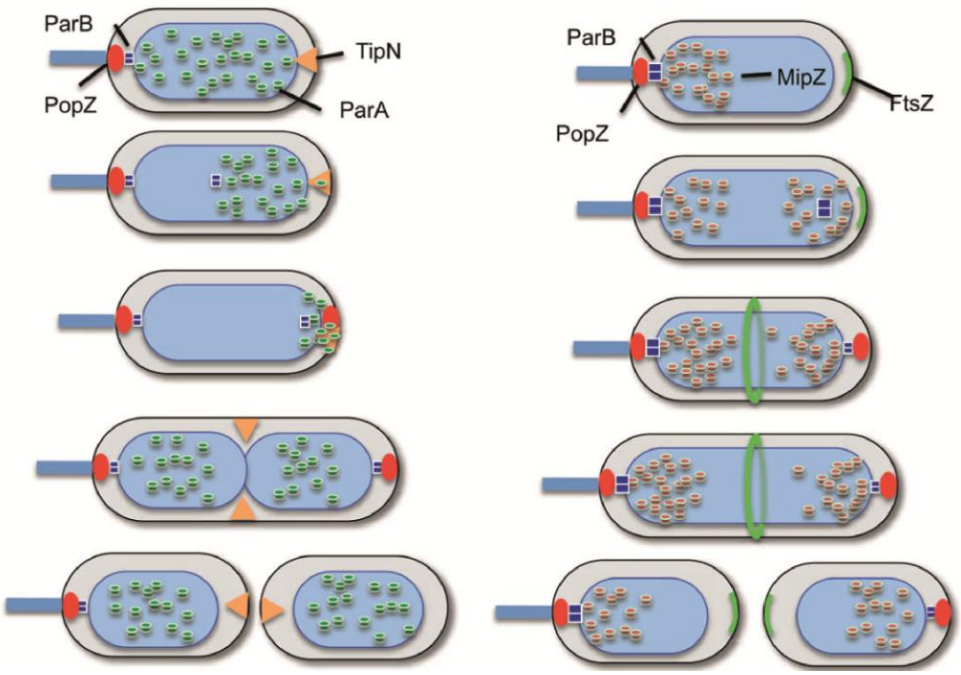

Figure 1.2 ParAB-*parS*-mediated cellular organizations in *C. crescentus*. The roles of the ParAB-*parS* system in origin segregation and Z-ring positioning are illustrated on the left and right side, respectively. More details are given in section 1.1.2. Figure adapted from (53).

1.2 FtsZ and the Z-ring

FtsZ, a tubulin homologue, is the central component of the cell division machinery in the majority of bacteria, many archaea, some mitochondria, and all chloroplasts (54). Although the amino acid sequence similarity between tubulin and FtsZ is very low, the two proteins share similar structure (55, 56). FtsZ consists of four domains: a short, unstructured N-terminal region; a globular core domain responsible for nucleotide binding; an unstructured linker of variable length; and a highly conserved C-terminal peptides involved in the interaction with some important FtsZ regulators (57).

In most bacteria, the initial step of cell division requires FtsZ polymerization into the so-called Z-ring at the future division site. The Z-ring is a dynamic structure and the half time for Z-ring subunits turnover is 8-10 s (58). The *in vivo* structure of the Z-ring is still under debate, and different architectures have been proposed, dependent on the species investigated and the visualization technology used. In *E. coli*, the Z-ring was visualized as a loose bundle of randomly overlapping protofilaments by photo-activated localization microscopy (PALM) (59). In *B. subtilis*, the Z-ring was observed to be a bead-like structure with 3D-structured illumination microscopy (3D-SIM) (60), and in *C. crescentus*, it was imaged as sparse, short, non-overlapping protofilaments by cryo-electron tomography (61) or as a patchy and open band with 3D high-throughput photoactivated localization microscopy (HTPALM) (62). It has been proposed that the Z-ring provides the force for membrane constriction; however, the mechanism of force generation is unclear (63, 64). There are two popular models proposed: the sliding and the bending model. In the sliding model, FtsZ polymerizes into short overlapping protofilaments. These protofilaments slide along each other increasing the number of lateral contacts, thereby decreasing the circumference of the Z-ring (65). The bending model, by contrast, suggests that FtsZ protofilaments change from a straight to a curved form by hydrolyzing GTP to GDP (66), and this conformational change generates the force for constriction. Remarkably, a recent study challenged the force generation function of the Z-ring during cell membrane constriction in *E. coli*. Based on fluorescence microscopy data, Söderström *et al* (67) claimed that in fact the Z-ring disassembled before the inner membrane was sealed during constriction. Therefore, they proposed that during the final stage of constriction instead of the Z-ring, fusion of the lipid bilayer and the inward growth of peptidoglycan might be the force-generating processes (67).

The Z-ring needs to be tethered to the membrane for proper function. An important Z-ring membrane-anchor protein is FtsA, a widely conserved membrane-associated protein, interacting with the extreme C-terminus of FtsZ. FtsA influences the dynamics and the organization of the Z-ring (68, 69). In *E. coli* and *B. subtilis*, FtsA is recruited to the Z-ring at the early division stage, whereas in *C. crescentus* FtsA is a late division protein (68). This finding suggests that *C. crescentus* has an alternative mechanism to tether the Z-ring to the membrane in the early division stage, which may involve the divisome components FtsE and FtsX (57). Interestingly, a recent *in vitro* study showed that FtsA has two opposing effects on FtsZ, tethering the FtsZ polymers to the membrane and disassembling the polymers, which regulate the treadmilling dynamics of FtsZ polymers (70, 71). In *E. coli* and other γ-proteobacteria, tethering of the Z-ring to the membrane is also mediated by ZipA, a protein that stabilizes the Z-ring structure by stimulating FtsZ proteofilament bundling. In *B. subtilis*, which lacks ZipA, the proteins EzrA and SepF are considered to be the functional analogues of ZipA (57, 72, 73). In *C. crescentus*

another protein, FzlA, although not acting as a Z-ring membrane anchor, is considered to stimulate FtsZ protofilament bundling (74). ZapA, another important Z-ring regulator, which is intensively-studied in *E. coli* and also encoded by *C. crescentus*, binds directly to FtsZ and promotes the bundling of FtsZ protofilaments (75, 76). The Z-ring serves as a scaffold that recruits more than 20 other cell division proteins to form the divisome at the division site (57). The precise role of every divisome component is not fully understood; however, in general, they are involved in the following roles: stabilizing the Z-ring, synthesizing and remodeling peptidoglycan, coordinating division with chromosome segregation, and stabilizing the whole divisome (76).

Due to the crucial function that the Z-ring plays in cell division, it is an attractive target for antibiotic development. There are already a number of synthetic compounds found to be the inhibitors of the Z-ring (65). These inhibitors target at different pathways to disturb Z-ring formation (77). For instance, some small molecules target at the positive Z-ring regulator ZipA (78); acyldepsipeptide antibiotics enhance the degradation of FtsZ by activating the protease ClpP (79); and GTP analogues inhibit the assembly and dynamics of the Z-ring (80). However, none of the Z-ring inhibitors has been used in clinical applications yet (81).

FtsZ is conserved in the majority of bacteria, and it is essential in most of these bacteria; however, several groups of bacteria divide without FtsZ. *Planctomycetes* do not encode *ftsZ* in their genomes (82), and in *S. coelicolor* FtsZ has been shown to be dispensable during vegetative growth (83). Moreover L-form proliferation of *B. subtilis* is also independent of FtsZ (84). However, the mechanisms underlying FtsZ-independent bacterial cell division remain elusive (83).

1.3 Z-ring positioning in bacteria

How does the Z-ring find the future division site? This question has been puzzling researchers for many years. It is still not completely solved, but the underlying mechanisms are starting to become clearer. Most data on this subject have been obtained in five model organisms (Figure 1.3), namely *E. coli, B. stubilis, C. crescentus, S. coelicolor* and *M. xanthus*. In general, the Z-ring needs specialized regulators to direct its positioning to the division site. Although FtsZ is a widely conserved protein, the mechanisms that regulate Z-ring positioning vary significantly in different bacteria (85). Before 2010, only negative cell division regulators were reported including the MinCD system and nucleoid occlusion in *E. coli* and *B. subtilis*, as well as MipZ in *C. crescentus* (85). However, in recent years, two positive regulators, SsgB and PomZ were discovered in *S. coelicolor* and *M. xanthus*, respectively (86, 87). Interestingly, some of these regulators, including, MinD, MipZ and PomZ, belong to the Mrp/MinD family of P-loop ATPases (85, 87), which may indicate a common origin of the different Z-ring positioning systems (85, 87).

1.3.1 Positive regulators of Z-ring positioning

Streptomycetes are Gram-positive soil bacteria with complex life cycles, which resemble filamentous fungi in their apical growth (88). In contrast to cell division in rod bacteria, the vegetative growth of *Streptomycetes* is based on polar growth of the vegetative hyphae (88). During sporulation, *Streptomycetes* produce long chains of spores in aerial hyphae. In this step, they require a similar cell division machinery as rod shaped bacteria (86). *Streptomycetes* do not encode any well-known FtsZ regulators, such as the Min, Noc and SlmA proteins (86). However, in *S. coelicolor*, a positive regulator, SsgB, was found to control Z-ring positioning during sporulation. SsgB has been shown to directly interact with FtsZ and tether the Z-ring to the membrane. Moreover, it promotes FtsZ polymerization and stabilizes the Z-ring. The division site localization of SsgB is directed by another protein, called SsgA (86).

Another positive regulator of Z-ring positioning, PomZ, is found in the δ-proteoabacterium *M. xanthus* (87). PomZ directs the Z-ring to the midcell (87). A *ΔpomZ* mutant exhibits both filamentous and minicell phenotype, suggesting the Z-ring positioning related function of PomZ (87). Moreover, PomZ locates to the midcell independently of FtsZ and before Z-ring formation, and it induces the polymerization of *M. xanthus* FtsZ *in vitro* (87).

1.3.2 Negative regulators of Z-ring positioning

Z-ring positioning systems were first discovered and studied in *E. coli*. In this organism, two systems, the Min system and nucleoid occlusion, cooperate to ensure the proper Z-ring placement (89-91). The Min system consists of three proteins, encoded from one operon. MinC, the FtsZ inhibitor, which directly interacts and disrupts the Z-ring formation; MinD, a Mrp/MinD P-loop ATPase, which anchors MinC to the membrane and interacts with MinE; and MinE the topological regulator of the Min system, disassembles the MinCD complex from the membrane, and thus directing the pole-to-pole oscillation of MinCD (91). The oscillation leaves the time averaged concentration of MinC lowest at the midcell and highest at the poles, allowing the Z-ring formation at the midcell and preventing division at the cell poles (91). Loss of the Min system leads to filamentation and anucleate minicells, but overexpression of FtsZ can partially rescue this phenotype (92). MinC has two similar-sized domains, and both of the two domains interact with FtsZ (93). The C-terminal domain is the dimerization domain, is also responsible for MinD binding. Furthermore, it interacts with the C-terminal region of FtsZ and interrupts the lateral interactions between FtsZ, FtsA and ZipA (94, 95); by contrast, the N-terminal domain interrupts the interaction between FtsZ molecules, thereby shortening the FtsZ protofilaments (93, 96). MinD, the link between MinC and MinE, is the central protein regulating the dynamics of the Min system by its distinct affinities to its binding partners in different forms (53). MinD forms dimer after binding ATP, and only ATP-bound dimeric MinD binds to the membrane and recruits MinC to the cell pole (97). Notably, on MinD dimer, the binding regions for MinC and MinE overlap and locate at the MinD dimer interface, which indicates that the MinD dimer is the active form for MinC and MinE interaction, and that MinE competes with MinC for binding to the MinD dimer (98). MinD is dissembled and released from the membrane by MinE stimulated ATP hydrolysis (98). The topological regulator MinE is a small membrane-bound protein consisting only 88 amino acids. It binds to the membrane-

bound MinD dimer, undergoes a conformational change, disassembles MinD, and then, releases the MinCD complex from the membrane (96).

The central component of *E. coli* nucleoid occlusion system is SlmA, a sequence-specific DNA-binding protein belonging to the TetR family (99). SlmA acts as an antagonist of FtsZ polymerization, and prevents division over the unsegregated chromosome (99). It does so by binding to specific palindromic DNA sequences: SlmA-binding sequences (SBS), which are spread all over the chromosome except for the terminus region (99). Tonthat *et al.*, suggested that SBS binding induces SlmA to assemble into higher-order oligomers that interact with FtsZ protofilaments and disrupt their proper arrangement into the Z-ring (100). Neither the Min system nor SlmA is essential in *E. coli*, but the combination of *min*$^-$ and *slmA*$^-$ mutations was shown to be synthetic lethal (92, 99).

Both the Min system and nucleoid occlusion are present in the Gram-positive bacterium *B. subtilis* (101). The Min system of *B. subtilis* comprises four proteins, MinC, MinD, MinJ and DivIVA. The functions of MinC and MinD are similar in *E. coli* and *B. subtilis*. Moreover, a study showed that *E. coli* MinD can partially substitute for *B. subtilis* MinD (102). *B. subtilis* does not encode the topological regulator *minE*. Instead, it regulates the positioning of MinCD by DivIVA (103). DivIVA, a conserved protein in Gram-positive bacteria, is considered to be a scaffold protein, which is involved in many cellular processes including cell division, cell wall biosynthesis, secretion, genetic competence, or chromosome segregation; strikingly, the localization of DivIVA is determined by the shape of the membrane (104). It binds to the membrane, senses membrane curvature, and accumulates at the membrane regions with high negative curvature, which are the cell poles and the constriction site (104). DivIVA does not directly interact with MinD, but the interaction between MinD and DivIVA is bridged by another protein, MinJ (103). In contrast to the dynamic pole-to-pole oscillation observed in *E. coli*, the Min system in *B. subtilis* is more static (105). A model, based on the results from structured illumination microscopy suggests that DivIVA forms two rings that flank the divisome; MinCD is recruited to the two DivIVA rings at the beginning of membrane constriction. The division machinery between the two rings is not affected, but the FtsZ assembly outside the two rings is interrupted by MinC (106). The main function of the Min system in *B. subtilis*, unlike in *E. coli*, may be to disassemble the divisome, to prevent the reinitiation of Z-ring formation adjacent to recently completed division sites, ensuring that cell division occurs only once per cell cycle (107, 108).

The DNA-binding protein mediating nucleoid occlusion in *B. subtilis* is called Noc (109). Similar to SlmA, Noc also binds to specific sequences, which are widely distributed on the chromosome but excluded from the terminus region, thereby interrupting Z-ring formation over the chromosome (110). However, Noc, a ParB-like protein, shares no sequence similarity with SlmA (100). Furthermore, no direct interaction has been reported between Noc and FtsZ *in vitro* (110).

It is generally accepted that the Min system and nucleoid occlusion are the two systems that regulate Z-ring positioning in *B. subtilis* and *E. coli*. However, several recent studies indicate that other mechanisms besides the Min system and nucleoid occlusion could be involved in Z-ring positioning in these two bacteria (97). Rodrigues e*t al* showed that in outgrown spore of *B. subtilis*, the Z-ring is still positioned correctly at midcell, without both the Min and Noc

proteins, although Z-ring formation was delayed and less efficient (97). In *E. coli*, it has been proposed that passive mechanisms such as the incompletely replicated or unsegregated chromosome also contributes to Z-ring positioning in addition to the Min and SlmA proteins (111).

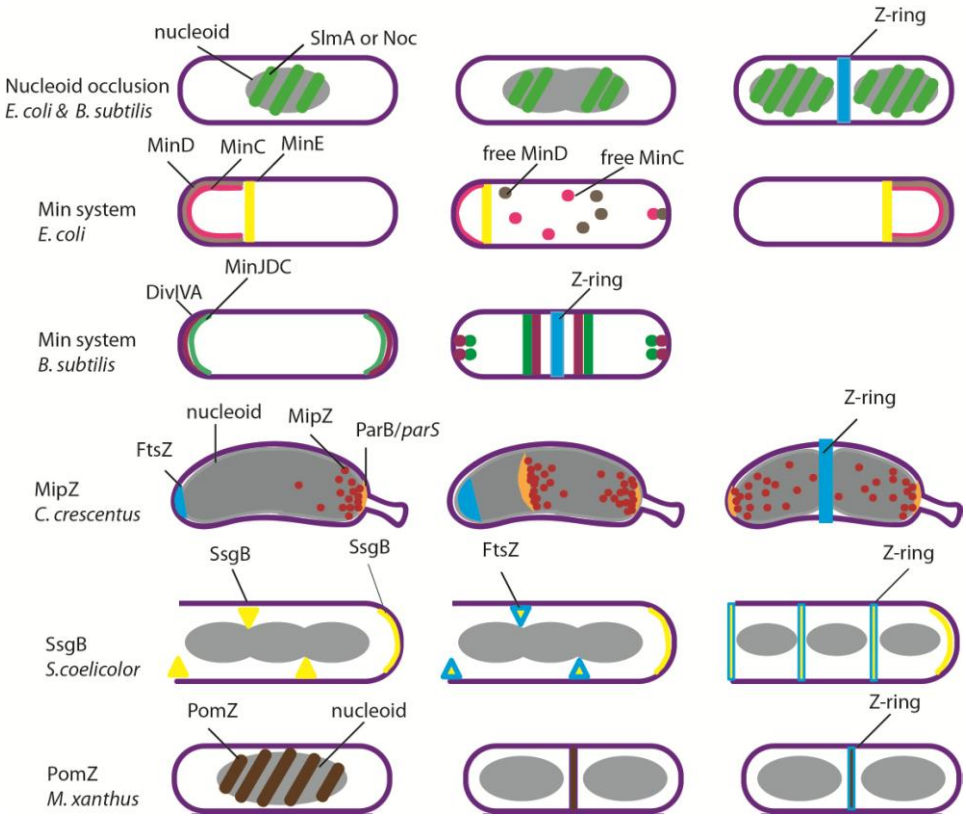

Figure 1.3 Z-ring positioning systems in bacteria. Z-ring positioning systems from *E. coli*, *B. subtilis*, *C. crescentus*, *S. coelicolor* (during sporulation) and *M. xanthus* are shown, More details are given in section 1.3. Figure modified from (85).

Apart from the relatively well-studied Z-ring positioning systems in rod-shaped bacteria, the mechanisms adapted in coccoid bacteria have also been characterized (112, 113). The Min system and nucleoid occlusion are also found in some coccoid bacteria, such as *Staphylococcus aureus* which encodes Noc, *Neisseria gonorrhoeae*, which possesses the Min system (112, 114, 115). However a big challenge of coccoid bacteria is to select a midcell plane as the future division site in the absence of a longitudinal axis. For example *S. aureus* has three alternative division planes and *N. gonorrhoeae* has two (112). Although the mechanisms behind Z-ring positioning in coccoid bacteria are still not clear, it has been proposed that the cell wall architecture and components are involved in division site positioning (112).

1.3.3 MipZ regulates Z-ring positioning in *C. crescentus*

In *C. crescentus*, both the Min system and nucleoid occlusion are absent, but another Mrp/MinD P-loop ATPase, MipZ, regulates Z-ring positioning (21). MipZ is conserved in many α-proteobacteria. Interestingly, several α-proteobacteria encode both the Min system and MipZ in their genomes, but it is unknown how these bacteria coordinate these two systems. MipZ is

essential in *C. crescentus*, and its depletion causes the formation of both minicells and filamentous cells, whereas MipZ overexpression induces smooth filamentous growth (21). The mechanism of Z-ring positioning by MipZ is shown in Figure 1.4. MipZ interacts with FtsZ both *in vivo* and *in vitro* (21). *In vitro* studies showed that MipZ stimulates the GTPase activity of FtsZ and turns the straight FtsZ protofilaments into an arc-like form (21).

Remarkably, MipZ displays a gradient-like distribution in predivisional cell, with a concentration maximum in the two polar regions and a concentration minimum at the midcell (20). Due to this gradient-like distribution, Z-ring formation is only allowed at the midcell, where the concentration of MipZ is the lowest (21). *C. crescentus* has evolved a unique way to control the MipZ distribution, which is closely linked with chromosome segregation. Before chromosome segregation, MipZ binds to the ParB-*parS* complex at the stalked pole (old pole), while FtsZ is located at the opposite pole (new pole). After replication of the origin region and the *parS* sequences, the replicated *parS*-ParB-MipZ complex is translocated to the opposite pole in a ParA-dependent manner, and FtsZ is forced to reassemble to the midcell by the inhibitory function of MipZ (21).

ParB recruits MipZ to the polar regions of the cell, but how does MipZ form a concentration gradient? The gradient-like distribution of MipZ depends on a nucleotide-induced monomer-dimer switch and on its interaction with ParB and non-specific chromosomal DNA (20). MipZ forms dimers, with each monomer binding one molecule of ATP. Because of an intrinsic ATPase activity, MipZ eventually hydrolyzes ATP, and the dimer disassembles (20). The monomeric and dimeric forms of MipZ have different affinities to FtsZ and chromosomal DNA. Both *in vivo* and *in vitro* studies indicate that only the MipZ dimer interacts with FtsZ and DNA, but ParB interacts with both MipZ forms. In addition, ParB has been suggested to stimulate MipZ dimerization (20). Based on the facts above, MipZ gradient formation can be explained by the following model (Figure 1.4) (20): ParB recruits monomeric MipZ to the cell poles and stimulates MipZ dimerization. The ATPase activity of MipZ is rather low, with a turnover number of 0.4 /min, retaining most MipZ proteins in the dimeric form. After release from ParB, chromosomal DNA interacts with the MipZ dimer and slows down its diffusion; MipZ dimmers accumulate close to the cell poles, and their concentration decreases towards midcell. This bipolar gradient ensures that the Z-ring is precisely placed at the midcell region of *C. crescentus* (20).

1.4 Scope

The correct placement of the Z-ring is crucial for bacteria to produce viable progeny. Since the discovery of the Min and nucleoid occlusion systems in the late 1980s (89), Z-ring positioning systems have been studied intensively for almost three decades. Many mechanisms were clarified, and several new systems were discovered, including MipZ, SsgB and PomZ. However, more questions are raised by these new discoveries. This study aims to provide more information about the regulatory function of MipZ in *C. crescentus.*

A remarkable feature of MipZ is its gradient-like distribution in the *C. crescentus* cell. Previous studies (20, 21) revealed that this distribution is achieved through the dynamic interaction of

MipZ with ATP, ParB, DNA and FtsZ. Except for the conserved nucleotide-binding region of P-loop ATPases, it is unclear which regions of MipZ are involved in ParB, DNA and FtsZ binding. Moreover, the mechanisms underlying these interactions have remained incompletely understood. Although it is clear that MipZ interacts with DNA, there is no known DNA-binding motif found in the crystal structure of MipZ. How does MipZ interact with DNA? How does ParB interact with MipZ and stimulate its dimerization? How does MipZ interact with FtsZ and stimulate the GTPase activity of FtsZ?

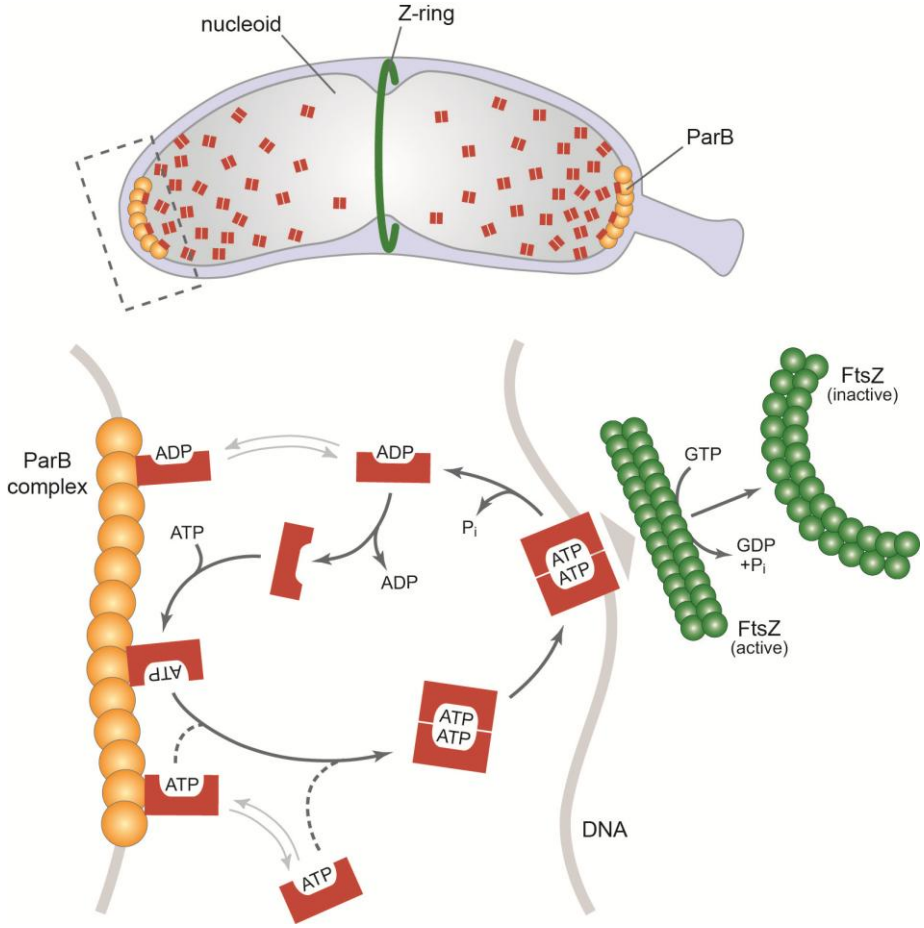

Figure 1.4 MipZ regulated Z-ring positioning in *C. crescentus*. The upper panel shows the gradient distribution of MipZ in *C. crescentus*. The lower panel shows the detailed interactions between MipZ and its interaction partners, nucleotide, ParB, chromosomal DNA and FtsZ. More details are given in section 1.3.3. Figure adapted from (20).

To address these questions, we set out to map the interaction regions on the MipZ surface. Taking the advantage of the crystal structure of MipZ, we performed a site-directed alanine-scanning-mutagenesis of MipZ focusing on residues that are exposed at the surface and carry charged or bulky hydrophobic side chains. To this end, we constructed a series of MipZ mutants, and analyzed the subcellular distributions of the MipZ variants and cell division phenotypes of these mutants by microscopy. According to the different phenotypes displayed by the mutants, we were able to identify candidate residues responsible for FtsZ, ParB, and DNA interaction, respectively. The roles of these residues were further characterized by cell biological and

biochemical methods. To this end, we are able to map the FtsZ-, ParB- and DNA-binding regions on the MipZ dimer surface.

2 RESULTS

2.1 Alanine-scanning mutagenesis of the MipZ surface

Previous studies (20, 21) revealed that MipZ mediates Z-ring positioning in *C. crescentus* and that the regulatory function of MipZ depends on its interaction with FtsZ, ParB and chromosomal DNA. However the exact mechanisms behind these interactions and the regions of MipZ responsible for these interactions are still unknown. In order to further investigate the regulatory mechanisms of MipZ, we started to map the MipZ interaction regions using site-directed alanine scanning mutagenesis, an approach in which candidate amino acids are substituted one after another by alanine. Due to the crucial role of MipZ in *C. crescentus* cell division (21), a defective interaction caused by the substitution of an interactive residue with an alanine should be reflected by a cell division defect of the respective mutant strain. Moreover, the interaction defect with FtsZ, ParB or chromosomal DNA should cause distinct phenotypes, because these interactions have different roles in MipZ function and localization. It should, therefore, be possible to pin-point the MipZ residues involved in FtsZ, ParB or chromosomal DNA interaction based on the phenotypes and localization patterns observed from the MipZ mutant proteins

To test the function of mutant MipZ variant, we constructed experimental strains (Figure 2.1A) that carried an in-frame deletion (amino acids 37-801) in the endogenous *mipZ* gene, a wild-type copy of *mipZ* under the control of the vanillate inducible promoter P_{vanA}, and a *mipZ* variant fused with e*yfp* (enhanced yellow fluorescent protein) inserted at the chromosomal *xylX* locus downstream of the xylose-inducible promoter P_{xylX}. In these constructs the synthesis of wild-type (WT, henceforth) MipZ or the mutant MipZ-eYFP fusion can be easily controlled by adding vanillate or xylose into the culture. Upon growth in medium only containing xylose, $MipZ_{WT}$ is depleted and replaced with the fluorescent protein fusion, making it possible to analyze both the functionality and the localization of the mutant proteins. To ensure the validity of this screening approach, we first analyzed a strain (BH64) producing $MipZ_{WT}$-eYFP in place of the native protein. Analysis of BH64 showed that the protein was fully functional, producing normal cell shape and the characteristic unipolar or bipolar gradient-like YFP pattern in swarmer and predivisional cells, respectively (Figure 2.1C).

Based on the different roles of the interactions in the function of MipZ, we expected mutations to cause distinct phenotypes in the experimental strains (Figure 2.1A). Functional MipZ is able to control the Z-ring positioning, yielding cells with normal cell lengths and constriction in the midcell region (21). Cells producing FtsZ-binding defective MipZ would divide randomly at mis-localized Z-rings. However, FtsZ is not involved in MipZ distribution, thus the FtsZ-binding defective mutants should still display the WT-like distribution. ParB recruits MipZ to the cell poles and stimulates MipZ dimerization, mutants defective in ParB binding would have less MipZ in the polar regions and more freely diffusive monomeric MipZ in the cell, indicated by fainter polar foci and a higher YFP background. Because only dimeric MipZ has inhibitory

effect on FtsZ, a mutant with less dimeric MipZ should display a similar cell division defect as FtsZ-interaction defective mutants. However, it is possible that despite a decrease in the concentration of dimeric MipZ, the inhibitory effect of MipZ is still enough to support the normal cell division, therefore, the mutants would have normal cell length. MipZ interacts with chromosomal DNA, which prevents MipZ from free diffusion and thus enabling the gradient-like distribution of MipZ. If the interaction between MipZ and chromosomal DNA were impaired, the MipZ dimers would freely diffuse in the cell, disassembling the Z-ring, and thus blocking cell division throughout the cell, thereby inducing filamentous growth.

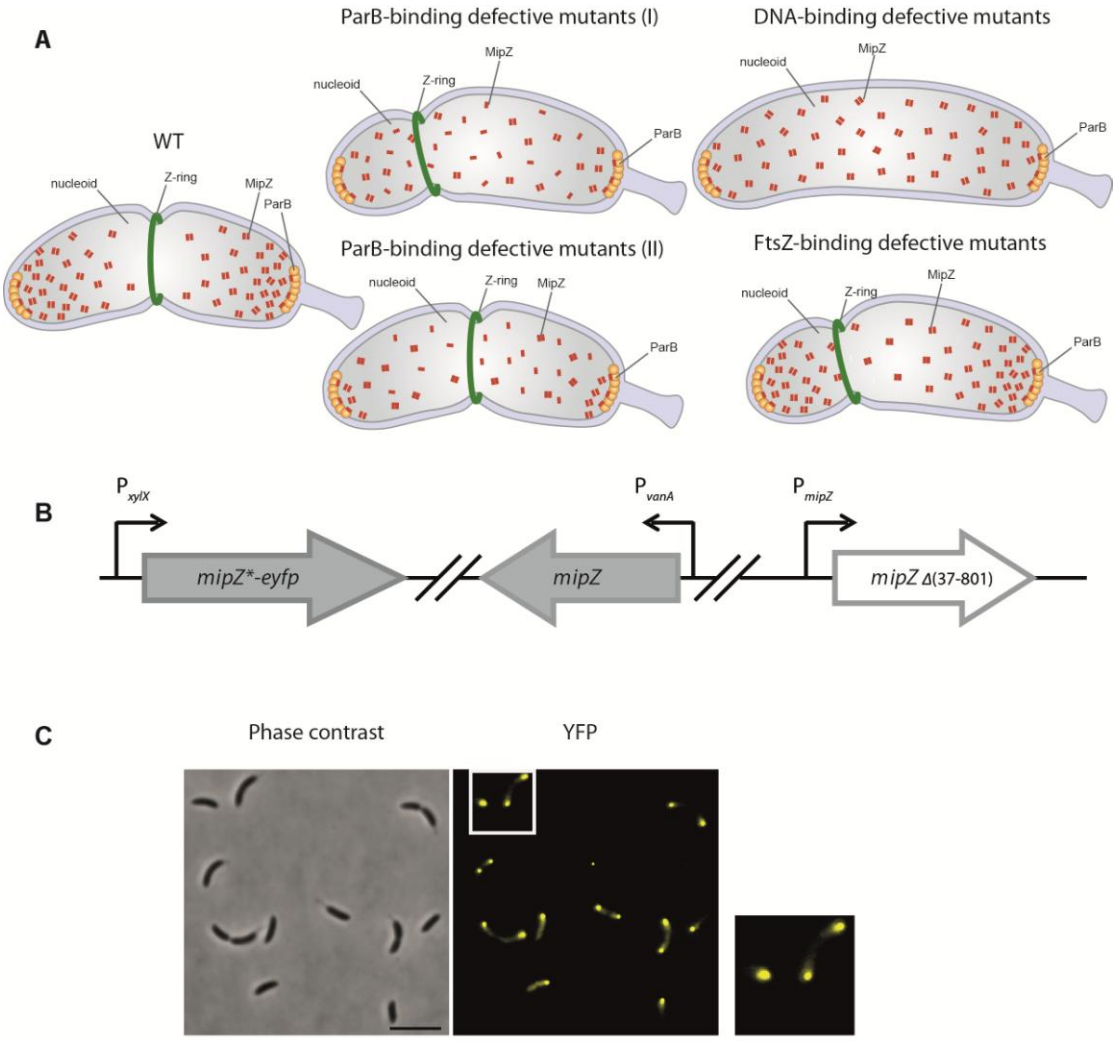

Figure 2.1 Expected phenotypes of binding defective MipZ mutants and construction of the experimental strains. (A) The expected phenotypes of the WT, FtsZ-, ParB-, and DNA-binding defective MipZ mutants of *C. crescentus*. **(B)** Construction of the experimental strain. The white box indicates the in-frame deletion of the native *mipZ* (amino acids 37-801). A copy of $mipZ_{WT}$ was placed under the control of the chromosomal P_{vanA} promoter and a mutant allele of *mipZ* fused with *eyfp* was placed under the control of the chromosomal P_{xylX} promoter. **(C)** Phenotype of a *C. crescentus* strain producing $MipZ_{WT}$-eYFP. *C. crescentus* strain BH64 (CB15N Δ*mipZ* P_{vanA}-*mipZ* P_{xylX}- *mipZ-eyfp*) was grown overnight in PYE medium containing 0.5 mM vanillate. The cells were washed twice with PYE medium and grown for 8 h in PYE containing 0.3% xylose, and then were then visualized by phase contrast and fluorescence microscopy. An enlargement of the area in the white box is given on the right side. Bar: 5 µm

Taking advantage of the crystal structure of MipZ dimer (20) (PDB 2XJ9) we picked 35 surface-exposed amino acids with either charged or bulky hydrophobic side chains (Figure 2.2). We reasoned that these residues were likely to be involved in specific interactions. We only selected residues that were not located in the MipZ dimerization interface or the nucleotide binding region, to avoid adverse effects on nucleotide binding and dimerization (20, 21).

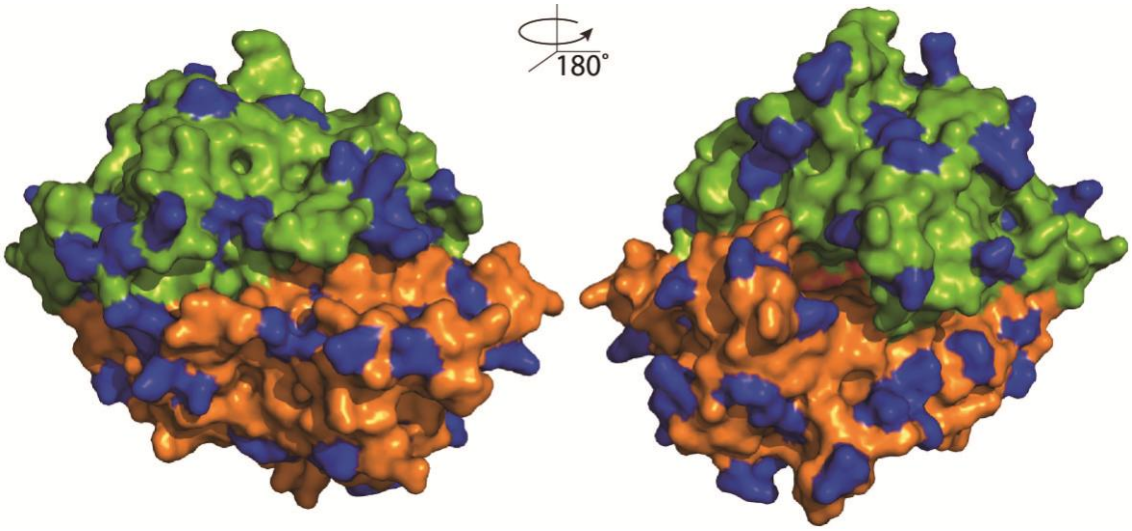

Figure 2.2 Surface-exposed residues of MipZ targeted by site-directed mutagenesis. The MipZ homodimer (PDB 2XJ9) structure is shown one monomer in green and the other in orange. The amino acids selected for alanine substitution are highlighted in blue. The structures were rendered in PyMOL.

2.1.1 Screening for MipZ interaction defective mutants

To analyze whether the selected residues were involved in contacts with MipZ interactors, 39 conditional MipZ mutants carrying mutant *mipZ*-eyfp* integrated at the *xylX* locus were constructed (Figure 2.1B). The fusion proteins studied included 35 variants obtained in the alanine scanning mutagenesis, as well as $MipZ_{WT}$ and variants of MipZ defective in ATP binding and hydrolysis ($MipZ_{K13A}$, $MipZ_{D42A}$ and $MipZ_{G14V}$) (20) as controls (Table 2.1). The sorting of different mutations into different binding-defective groups was based on their distinct phenotypes, which largely fit our expectations. All the MipZ variants and their phenotypes are listed in Table 2.1. In summary, during the screening we identified sixteen mutants without obvious phenotypes. Three mutants showed the phenotype expected for a defect in FtsZ-binding: a broad spectrum of cell lengths but a WT-like subcellular MipZ distribution. Seven mutants had the expected ParB-binding defective phenotype: diminished or even invisible eYFP foci and a higher eYFP background. Nine mutants showed the expected DNA-binding defective phenotype: filamentous cells and higher eYFP background. Three mutants displayed both a ParB and the DNA binding defective phenotype: filamentous cells, diminished eYFP foci and higher YFP background. In addition, three mutant constructs were unstable (Figure 2.3B).

Table 2.1 MipZ point mutations and their phenotypes

Point mutation	Phenotype
E53A K155A E165A	FtsZ-binding defect
W58A D147A L172A V246A	ParB-binding defect
R194A K197A R198A R219A L237A R242A	DNA-binding defect
D236A L248A R221A	ParB and DNA binding defect
E3A K35A R55A E65A D76A R84A E86A R99A E103A R125A E152A W164A E200A R213A H262A Y269A	WT
R5A E94A L161A	unstable
K13A	Monomeric MipZ Control, broadly distributed cell lengths higher YFP background signal (20)
D42A	Dimeric MipZ Control, filamentous cells, patchy YFP signal(20)
G14V	Monomeric MipZ Control, broadly distributed cell lengths,higher YFP background signal (20)

The stability of the different MipZ*-eYFP variants was tested by immunoblot analysis with an antibody raised against MipZ. As shown in Figure 2.3, most of the fusion proteins were stable,

except for those carrying the R5A, E94A, L161A, and R221A mutations. Interestingly, in contrast to the other three unstable variants, the R221A variant exhibited two bands in the immunoblot, a fainter band at the size of MipZ-eYFP, and a more pronounced product band at the size of MipZ. This result indicates that although the eYFP fusion of $MipZ_{R221A}$ is cleaved in the linker region that connects MipZ with its eYFP fusion tag, $MipZ_{R221A}$ itself is a stable protein. The instability of the $MipZ_{R5A}$, $MipZ_{E94A}$, $MipZ_{L161A}$ fusions was also reflected by their much fainter YFP signals and broadly distributed cell lengths, which correspond to the typical phenotype of MipZ depletion (21) (Figure 2.3 B). On the other hand, R221A displayed a DNA and ParB-binding defective phenotype (Figures 2.3B, 2.7, and 2.10), with filamentous growth and evenly distributed YFP signal in the cell. It is not clear whether the even distribution of the YFP signal is the consequence of a ParB-binding defect or rather caused by the diffusing eYFP protein, which was cleaved from $MipZ_{R221A}$-eYFP fusion. However, a bacterial two-hybrid assay, which is explained in more detailed in section 2.3, indicated a defective interaction between $MipZ_{R221A}$ and ParB (Figure 2.8). Therefore, we assume that $MipZ_{R221A}$ is defective in both DNA and ParB-binding. The three residues R5, E94 and L161 may be involved in stabilization of the MipZ structure. Mutations in these residues may therefore cause local rearrangements in MipZ that result in MipZ degradation.

2.2 Residues involved in FtsZ interaction

Three mutants, BH68 ($MipZ_{E53A}$), BH82 ($MipZ_{E165A}$), and BH97 ($MipZ_{K155A}$) caught our attention by displaying broadly distributed cell lengths but a WT-like MipZ distribution (Figure 2.4). We reasoned that the mutant proteins were probably defective in FtsZ interaction. It has been revealed that the MipZ dimer can stimulate the GTPase activity of FtsZ approx. two fold, concomitant with a change in the conformation of the FtsZ polymers that disrupts Z-ring formation (21). In order to verify whether the three residues modified in these mutant MipZ varaints were involved in FtsZ regulation, I determined the GTPase activity of FtsZ in the presence of $MipZ_{E53A}$, $MipZ_{K155A}$, $MipZ_{E165A}$, or with $MipZ_{WT}$, $MipZ_{D42A}$, and $MipZ_{K13A}$ as controls. $MipZ_{K13A}$ is deficient in ATP hydrolysis and ATP-triggered dimerization, which keeps the protein in the monomeric state. A previous study (20) showed that only MipZ dimers but not the monomers can interact with FtsZ. $MipZ_{K13A}$ was, therefore, used as a negative control. In contrast, $MipZ_{D42A}$ is blocked in the dimeric state because of a defect in ATP hydrolysis and thus hyper-active, serving as a positive control (20, 21). The results of GTPase assay (Figure 2.5) showed that the three mutant variants $MipZ_{E53A}$, $MipZ_{K155}$ and $MipZ_{E165A}$ did not stimulate the GTPase activity of FtsZ to the same extent as $MipZ_{WT}$ or $MipZ_{D42A}$. $MipZ_{K155A}$ and $MipZ_{E165A}$ displayed significant lower GTPase activity compared with $MipZ_{WT}$, while $MipZ_{E53A}$ only displayed a minor decrease. Consistant with these data, the cell length phenotype caused by $MipZ_{E53A}$ is also not as dramatic as that observed for the other two variants, with less minicells and filamentous cells (Figure 2.4). Therefore, it appears that $MipZ_{E53A}$ is only slightly defective in FtsZ-binding.

The results from both the *in vivo* phenotype analysis (Figure 2.4) and the *in vitro* GTPase assay (Figure 2.5) suggest that the three residues E53, K155 and E165 are involved in FtsZ interaction. The location of these three residues is highlighted on the MipZ dimer in Figure 2.6.

Remarkably, they form a cluster consisting of residues from each monomeric subunit, which is in line with the previous finding that MipZ dimerization is a prerequisite for FtsZ interaction (19).

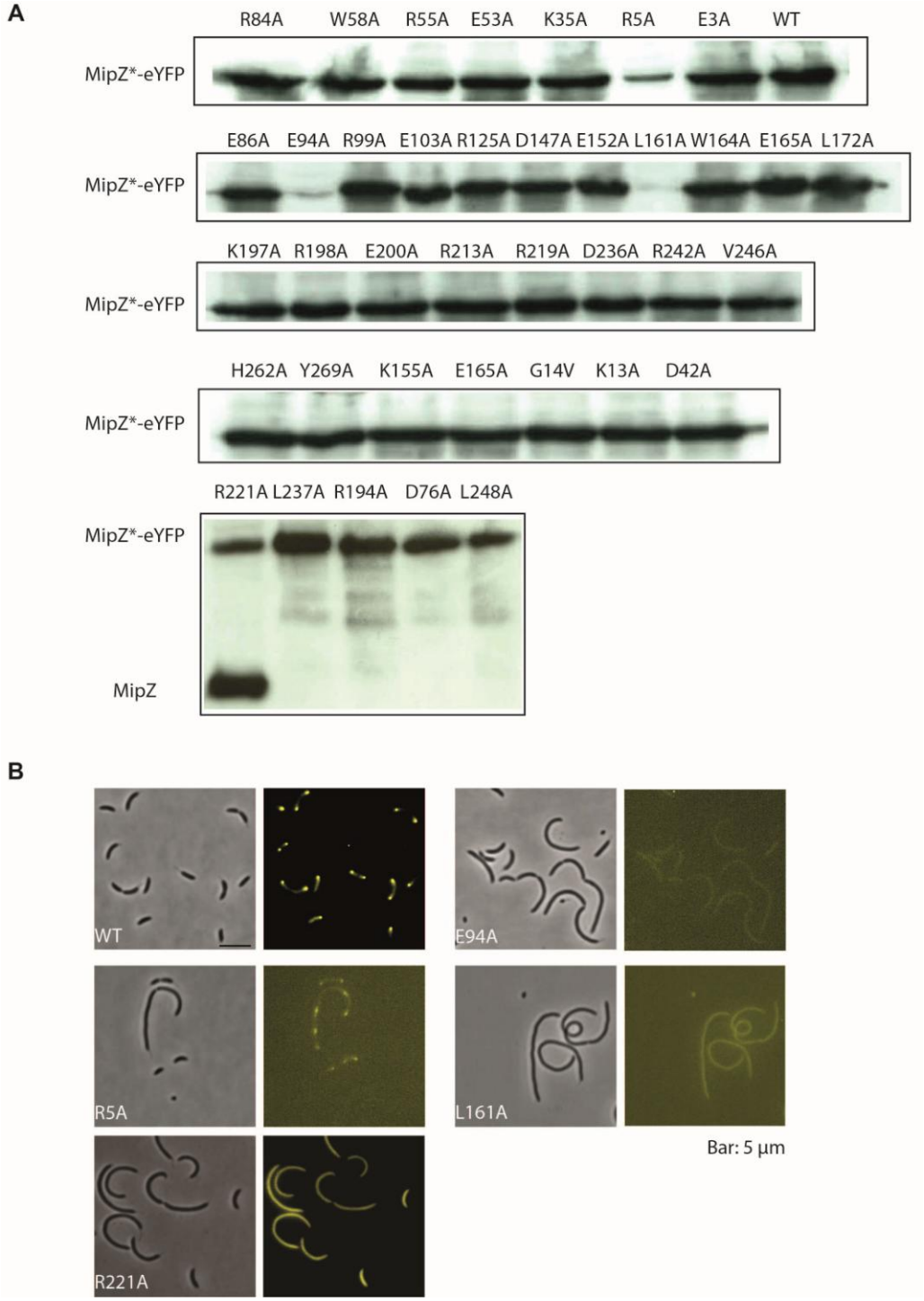

Figure 2.3 Stability of the MipZ*-eYFP fusion proteins. (A) Immunoblot analysis of strains producing mutant MipZ variants. All MipZ mutants were cultivated as described in Figure 2.1 C. Samples were withdrawn from the cultures and subjected to immunoblot analysis with anti-MipZ antibody. **(B)** Phenotype of mutants producing unstable MipZ-eYFP variants. Strains BH64 (WT), BH66 (R5A), BH74 (E94A), BH80 (L161A) and BH118 (R221A) were cultivated and visualized as described for Figure 2.1C.

2.3 Residues involved in ParB interaction

C. crescentus mutants producing potential ParB-binding defective MipZ variants were expected to show fainter polar foci and a higher YFP background, because ParB recruits MipZ to the cell poles and stimulates MipZ dimerization (20, 21). A defect in the interaction with ParB would decrease MipZ accumulation at the cell poles and, consequently, reduce the abundance of MipZ dimer in the cell. Considering that only the MipZ dimer is active in the regulation of cell division, and that the monomer does not inhibit Z-ring formation nor interact with chromosomal DNA, mutants producing ParB-binding defective MipZ may also display broadly distributed cell lengths. Seven mutants, BH70 ($MipZ_{W58A}$), BH78 ($MipZ_{D147A}$), BH83 ($MipZ_{L172A}$), BH90 ($MipZ_{D236A}$), BH93 ($MipZ_{V246A}$), BH94 ($MipZ_{L248A}$) and BH118 ($MipZ_{R221A}$) showed the described phenotypes (Figure 2.7A), indicating the respective MipZ variants were probably defective in ParB interaction. Among them, BH78 ($MipZ_{D147A}$) and BH83 ($MipZ_{L172A}$) displayed normal cell lengths, while the other five mutants exhibited broadly distributed cell lengths (Figure 2.7 A). The YFP signal of these strains was further characterized by plotting fluorescence intensity against the distance from the cell pole (Figure 2.7 B). Due to its instability, the $MipZ_{R221A}$-eYFP fusion was excluded from this analysis, leaving a total of six potential ParB-binding defective mutants analyzed. Note that, only cells with WT cell lengths were selected for this analysis in order to compare the YFP intensity distribution throughout the whole cell. Compared with BH64, which produces $MipZ_{WT}$-eYFP, all six mutants exhibited a lower fluorescence intensity at the cell poles and a higher intensity in the pole-distal region (Figure 2.7B). It should be noted that mutants BH90 ($MipZ_{D236A}$), BH94 ($MipZ_{L248A}$) and BH118 ($MipZ_{R221A}$) also exhibited a DNA-binding defective phenotype, with most cells growing filamentously (Figure 2.7A).

The interaction between these seven MipZ mutant variants and ParB was further characterized by bacterial two-hybrid analysis. To this end, the mutated *mipZ* alleles were fused with the gene encoding the T-25 fragment of the *Bordetella pertussis* adenylate cyclase, whereas the gene encoding the corresponding T-18 fragment was fused with *C. crescentus parB*. The resulting plasmids were co-transformed into the adenylate cyclase-deficient reporter strain *E. coli* BTH101. A positive interaction between MipZ variants and ParB would result in the reconstitution of a functional adenylate cyclase synthesizing 3', 5'-cyclic AMP, which would in turn facilitate the transcription of *lacZ* (116). The protein product of *lacZ* is able to utilize lactose and the metabolism of lactose decreases the pH value in the surrounding of the cells and thus turning neutral red containing MacConkey indicator agar red. Therefore, red colonies indicate a positive interaction between ParB and MipZ variants. The MipZ variants D147A, L172A, D236A, V246A, W58A, R221A, and L248A clearly exhibited a ParB-binding defect, because the coloration of the corresponding colonies was reduced compared to the colony producing $MipZ_{WT}$ (Figure 2.8A). As a control, the mutant MipZ variants were also tested for interaction with the T18 fraction alone. As expected, there was no interaction detected between them (Figure 2.8). The defective interactions between the different MipZ variants and ParB were further indicated by lower β-galactosidase activity in the corresponding *E. coli* BTH101 strains (Figure 2.8 B). The results of β-galactosidase activity assay largely fit to the coloration of the corresponding colonies on the MacConkey agar. However, $MipZ_{L248A}$ exhibited a

pronounced red color, only yielded a very low β-galactosidase activity. The reason for the differences is unclear, but it may be due to the limited sensitivity of the plate assay.

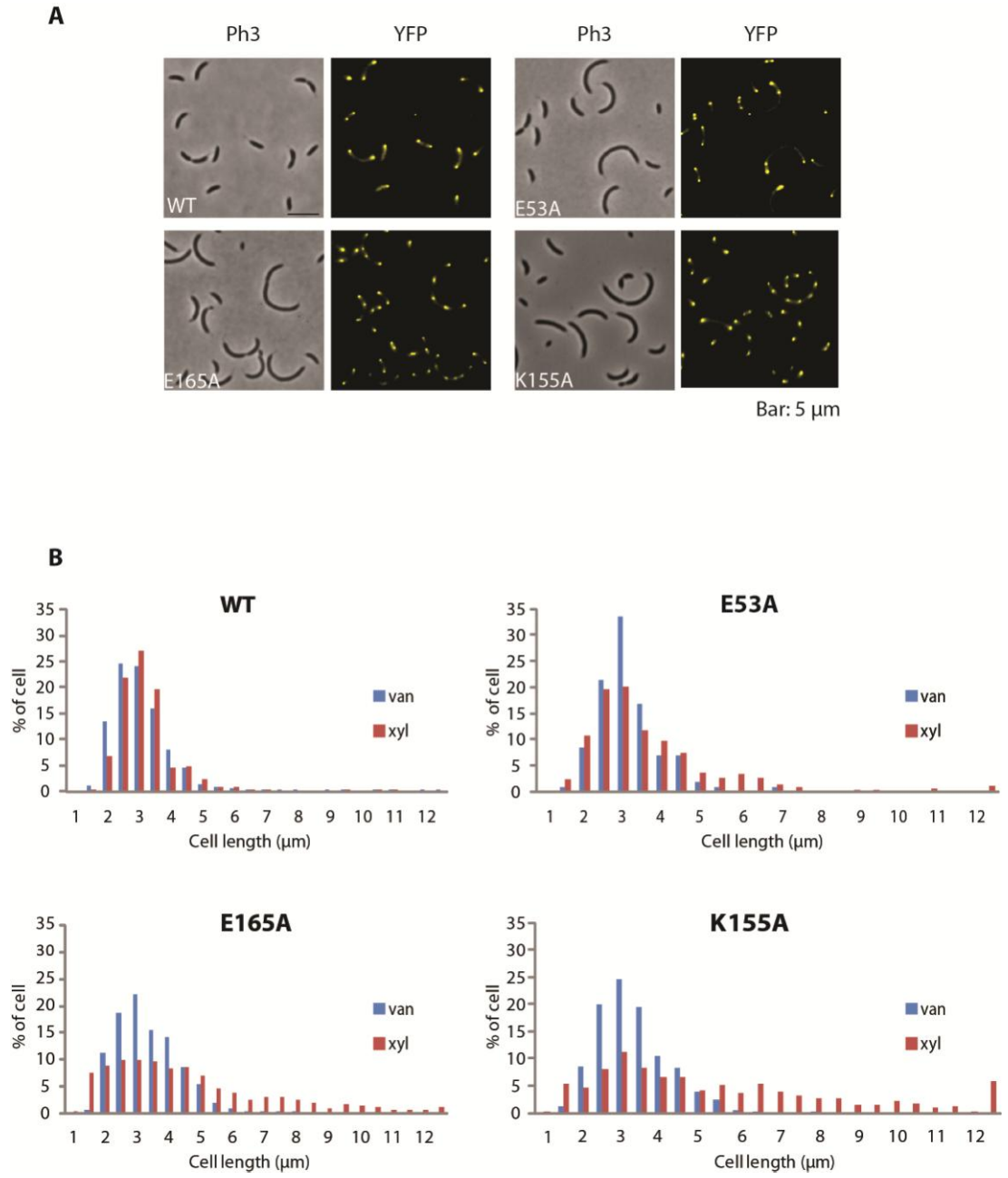

Figure 2.4 Phenotype of *C. crescentus* mutants producing FtsZ-binding defective MipZ variants. (A) Microscopic analysis of mutants producing FtsZ-binding defective MipZ variants. BH64 (WT), BH68 (E53A), BH82 (E165A) and BH97 (K155A) were cultivated and visualized as described in Figure 2.1 C. **(B)** Cell length distribution of mutants producing $MipZ_{WT}$ and FtsZ-bindng defective MipZ variants. The strains were cultivated in PYE supplemented either with 0.3% xylose to induce the synthesis of MipZ*-eYFP fusion or with 0.5 mM vanillate to induce the synthesis of $MipZ_{WT}$ for 8 h. Cells were visualized by phase contrast microscopy. 'Van' indicates a vanillate-induced culture, and 'xyl' indicates a xylose induced culture. The cell lengths of strains BH64 (van, n=747; xyl, n=343), BH68 (van, n=317; xyl, n=690), BH82 (van, n=680; xyl, n=891) and BH97 (van, n=429, xyl, n=429) were determined using MicrobeTracker.

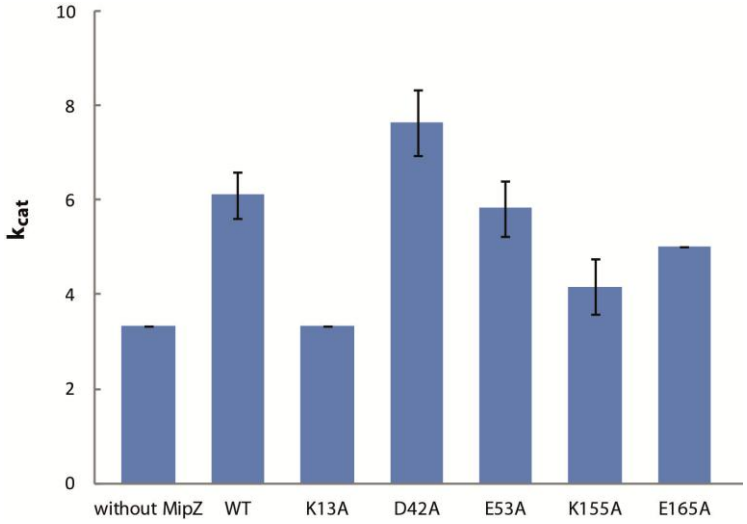

Figure 2.5 Effect of MipZ and its variants on the GTPase activity of FtsZ. 3 µM FtsZ was incubated with 2 mM GTP and 1 mM ATP in the presence of 6 µM $MipZ_{WT}$ or the indicated mutant variants. The turnover numbers (k_{cat}) represent the averages (±SD) of two independent measurements, each measurement was performed in triplicate.

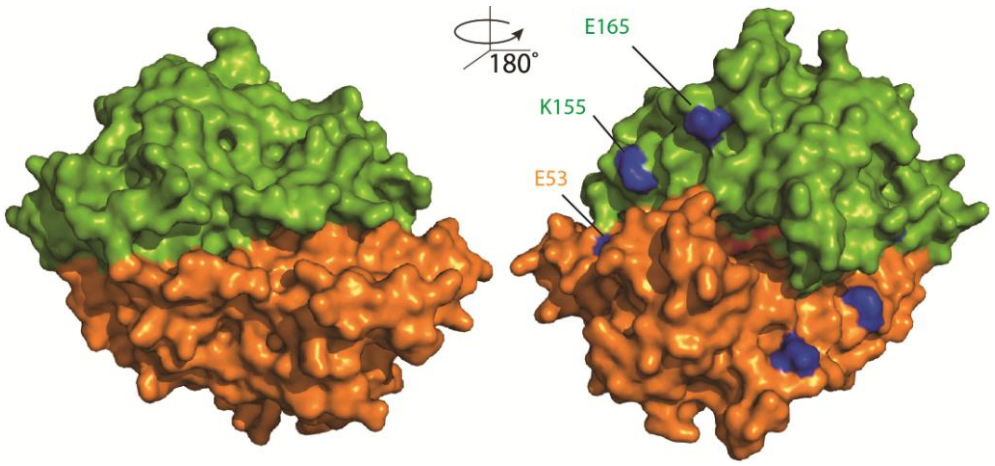

Figure 2.6 FtsZ interaction region of MipZ. The three residues E53, K155 and E165, which are involved in FtsZ interaction, were highlighted on MipZ dimer structure in blue.

The bacterial-two hybrid results suggest that all the seven MipZ mutations analyzed caused a defect in ParB-binding, indicating that the corresponding residues W58, D147, L172, R221, D236, V246 and L248 are involved in ParB interaction. Interestingly, these residues form two separated interaction regions on the MipZ dimer (Figure 2.9A) the five residues W58, R221, D236A, V246 and L248 are located at the front face of MipZ (Figure 2.9A left), close to the edge of dimer interface, while the other two, D147 and L172 are located a considerable distance at the back face of MipZ (Figure 2.9A, right). Since both monomeric and dimeric MipZ interact with ParB, we also highlighted these seven residues on the MipZ monomeric structure in Figure 2.9 B. These residues do not assemble into an obvious cluster, but are scattered along the rim of MipZ.

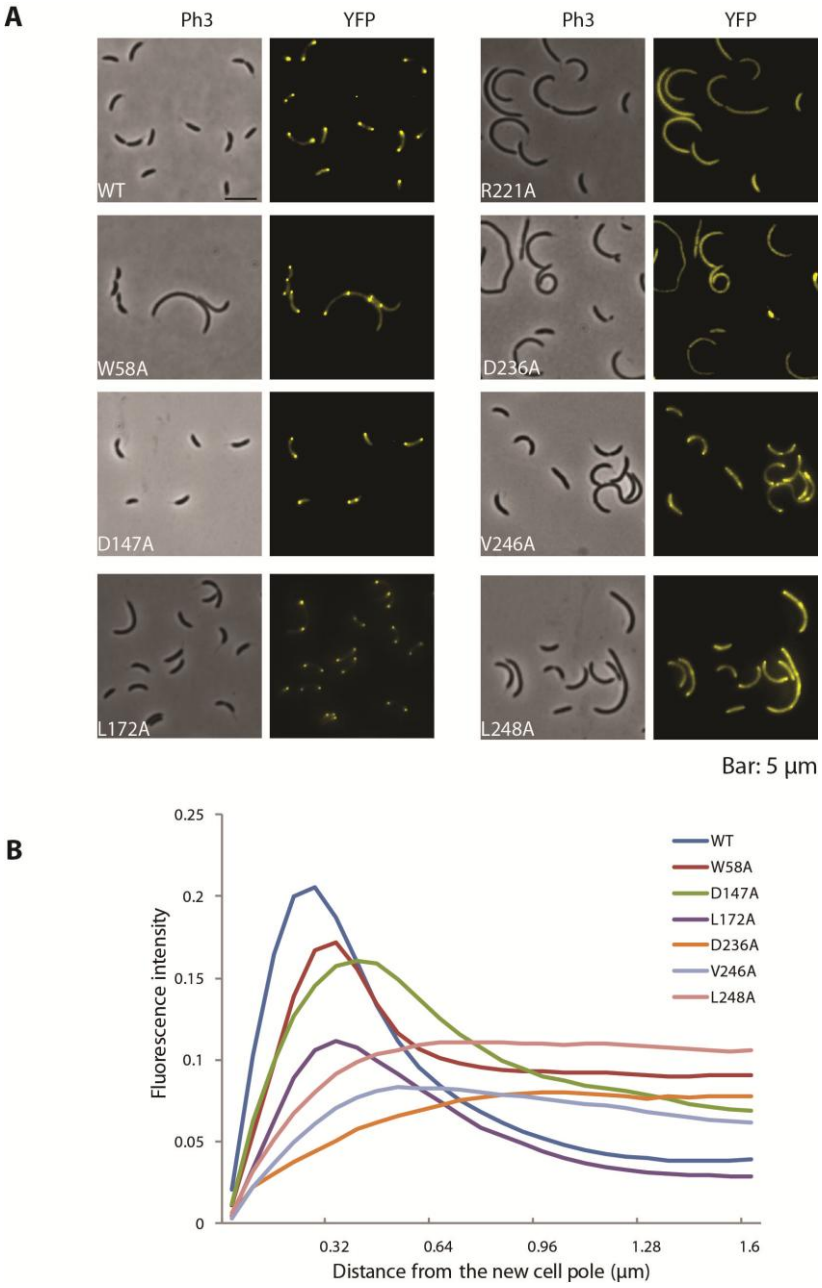

Figure 2.7 Phenotype of *C. crescentus* mutants producing ParB-binding defective MipZ variants. (A) Microscopic analysis of mutants producing ParB-binding defective MipZ variants. Strains BH64 (WT), BH70 (W58A) BH78 (D147A), BH83 (L172A), BH90 (D236A), BH93 (V246A), BH94 (L248A) and BH118 (R221A) were cultivated and visualized as Figure 2.1 C. **(B)** Subcellular distribution of MipZ and its ParB-binding defective mutant variants. The fluorescence intensity profiles of strain BH64 (n=75), BH70 (n=60), BH78 (n=39), BH83 (n=49), BH90 (n=10), BH93 (n=45), and BH94 (n=38) were analyzed by MicrobeTracker, and the fluorescence intensity values from each strain were averaged and plotted against the distance from the cell pole to the midcell. Note that only cells with WT morphology were analyzed.

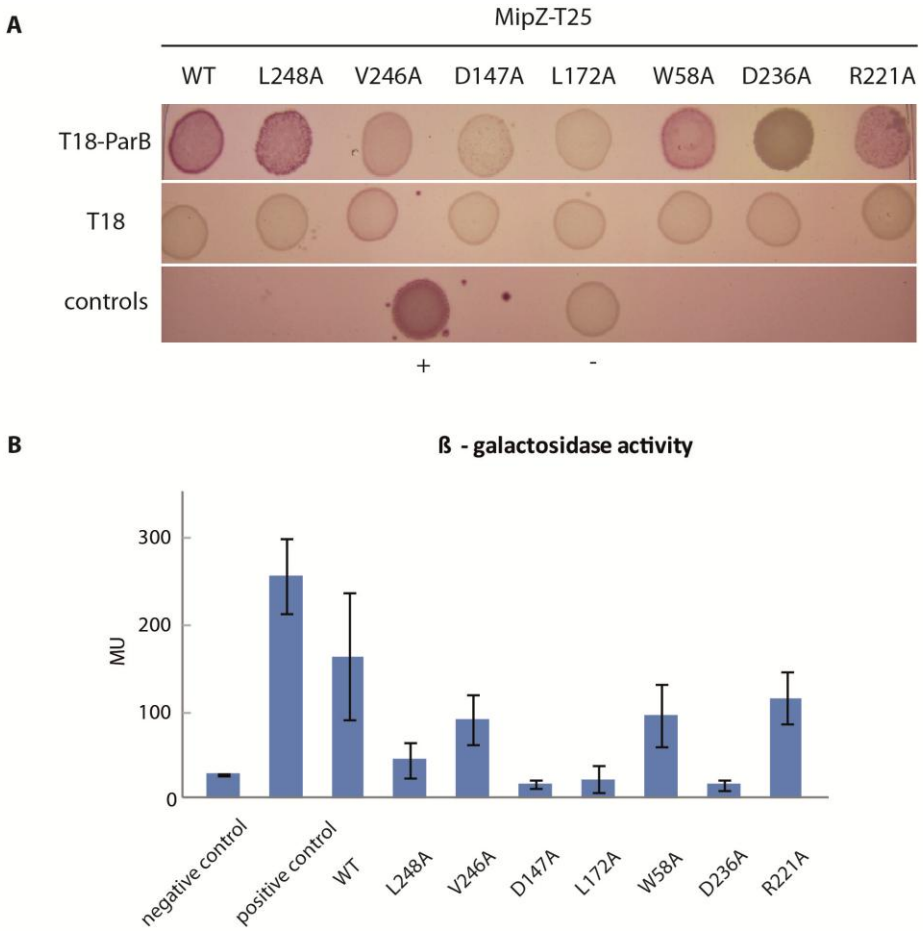

Figure 2.8 Interaction of MipZ variants with ParB. **(A)** Bacterial two-hybrid assay to detect the interaction between MipZ or its ParB-binding defective variants and ParB. *E. coli* BTH101 was transformed with pairs of plasmids encoding T18-ParB or only the T18 fragment and fusion of T25 to $MipZ_{WT}$ or its mutant derivatives. Red color indicates a positive interaction. Positive control (+): T25-zip: T18-zip, negative control (-): T25: T18. **(B)** Quantification of the ParB-MipZ interactions. *E.coli* BTH101 strains used in (A) were subjected to a β-galactosidase assay. MU values indicate the β-galactosidase activity. The results shown are the averages from two independent measurements, each performed in triplicate.

2.4 Residues involved in DNA interaction

Several mutants that showed filamentous growth (Figure 2.10) displayed the phenotype expected for DNA-binding defective MipZ mutants. DNA-binding is the basis for the formation of the MipZ gradient in *C. crescentus* (20). Chromosomal DNA retains the MipZ dimer in the polar regions, so that the MipZ dimer concentration decreases as a function of distance from the cell pole, which leaves midcell free of MipZ and allows Z-ring assembly. DNA-binding defective MipZ variants fail to establish the gradient-like distribution pattern and the freely diffusing MipZ dimers interrupt the Z-ring formation in the whole cell, resulting in filamentation (Figure 2.10). These potential DNA-binding defective MipZ mutants result in different extents of filamentous growth (Figure 2.10). The strains BH84 ($MipZ_{R194A}$), BH86 ($MipZ_{R198A}$) and BH89 ($MipZ_{R219A}$) appeared to mainly form filamentous cells, whereas the other strains exhibited mixed cell lengths ranging from WT-like cells to filamentous cells. Remarkably, mutants BH118 ($MipZ_{R221A}$), BH90 ($MipZ_{D236A}$) and BH94 ($MipZ_{L248A}$) displayed

largely diminished or even invisible YFP foci, suggesting a concomitant ParB-binding defect (Figure 2.7). In the case of BH118 ($MipZ_{R221A}$), this effect could be due to the release of YFP from the fusion protein (Figure 2.3)

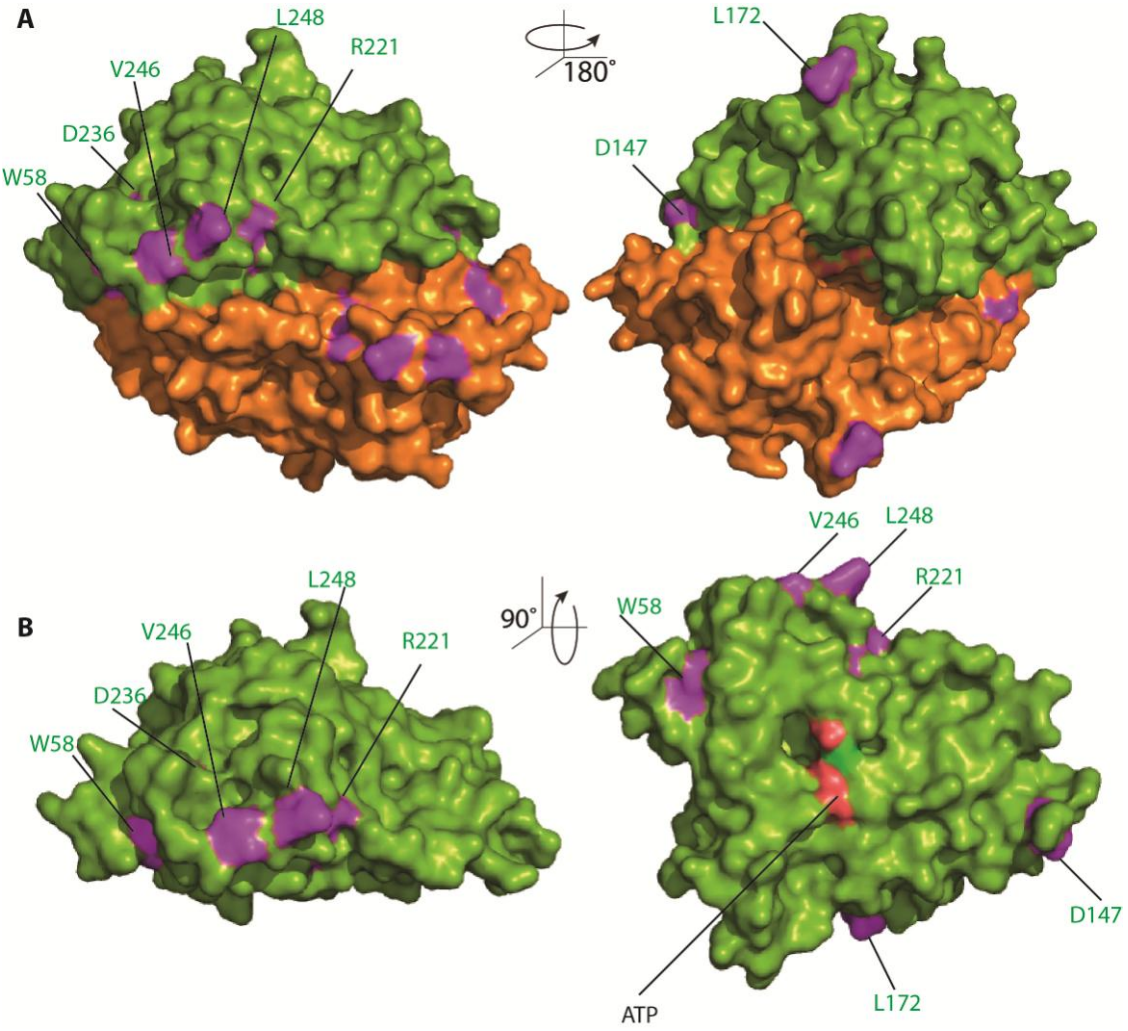

Figure 2.9 ParB interaction region of MipZ. **(A)** Location of the ParB interaction region on the MipZ dimer structure. W58, D147, L172, R221, D236, V246, L248 are highlighted in magenta. **(B)** Location of the ParB interaction region on the MipZ monomer structure. The same residues as in (A) are highlighted and indicated on the MipZ monomer, D236 is invisible in this view. ATP is indicated in red.

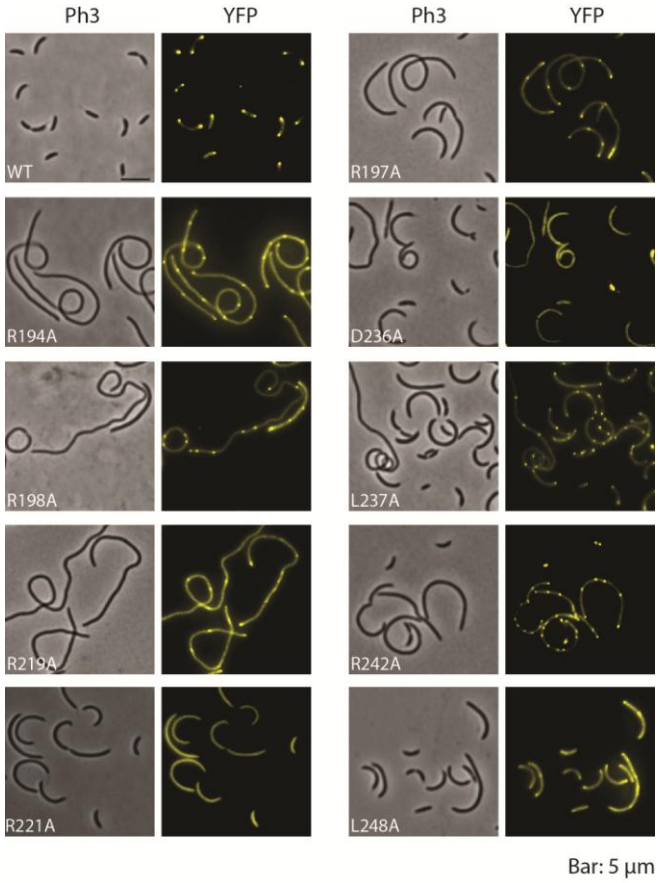

Figure 2.10 Phenotype of *C. crescentus* cells producing DNA-binding defective MipZ variants. *C. crescentus* strains BH64 (WT), BH84 (R194A), BH85 (K197A), BH86 (R198A), BH89 (R219A), BH118 (R221A), BH90 (D236A), BH91 (L237A), BH92 (R242A), and BH94 (L248A) were cultivated and analyzed as in Figure 2.1 C.

2.4.1 Verification of the DNA-binding defective MipZ variants *in vivo*

A previous study showed that heterologously overproduced $MipZ_{D42A}$-eYFP colocalizes with the *E. coli* nucleoid (20), because it is largely trapped in the DNA-binding proficient dimeric state. Upon introduction of a mutation conferring a DNA-binding defect into the D42A variant, the resulting double-mutant MipZ variant should no longer colocalize with the *E. coli* nucleoid. Based on this expectation, I constructed *E. coli* strains producing MipZ double-mutant derivatives under the control of an arabinose-inducible promoter. After induction, the localization of the fusion proteins and the nucleoid were analyzed microscopically. To facilitate the analysis, the cells were treated with cephalexin and chloramphenicol to induce the filamentous growth and nucleoid condensation. The results (Figure 2.11) showed that $MipZ_{D42A}$-eYFP carrying the R194A, K197A, R219A and L248A mutations still colocalized with the nucleoid, suggesting that the DNA-binding activities of these proteins are unaffected. $MipZ_{K197A}$ and $MipZ_{L248A}$ displayed weak filamentation in the corresponding *C. crescentus* mutants. However, the $MipZ_{R194}$ and $MipZ_{R219}$ caused completely filamentous growth in *C. crescentus* (Figure 2.10). Moreover, *in vitro* assays (Figure 2.15, 2.16, 2.17) strongly suggested that $MipZ_{R194A}$, $MipZ_{R219A}$ and $MipZ_{K197A}$ are defective in DNA-binding. Due to these contradictory results, I closely examined the *E. coli* strains by immunoblot analysis using an anti-MipZ

antibody. *C. crescentus* strain BH64, which produces MipZ-eYFP under the control of P_{xylX}, and CB15N, the WT *C. crescentus* strain, were included as controls. The results showed that MipZ-eYFP fusions were cleaved in the linker connecting MipZ with its eYFP fusion partner. Moreover, a pronounced band corresponding to a shortened MipZ-eYFP fusion is detected (Figure 2.12), whereas only a very small faction of the full-length fusion proteins was detected. Furthermore, an immunoblot analysis with the same samples but an anti-GFP antibody showed multiple bands, indicating the degradation of the eYFP tag (data not shown). These results suggest that production of MipZ-YFP fusions in *E. coli* may not be a reliable method to investigate the DNA-binding activity of MipZ.

Due to the fact that the results from the heterologous production of MipZ variants in *E. coli* were not conclusive, I went on to study the interaction of the mutant MipZ variants and DNA *in vitro*. To start these analyses, I set out to purify all the potentially DNA-binding defective variants in C-terminally hexahistidin-tagged form (Figure. 2.13). Surprisingly, the purification of $MipZ_{D236A}$-His_6 failed. Although $MipZ_{D236A}$-eYFP was stable in *C. crescentus*, its hexahistidin-tagged form was hardly overproduced in *E. coli* Rosetta (DE3)pLysS. Moreover, after purification, it was barely detected in the elution fractions. Due to the instability of $MipZ_{D236A}$-His_6, we wondered whether the D236A mutation in fact impaired the interaction with ParB and DNA or rather acted by changing the structure of MipZ. The *C. crescentus* cell producing $MipZ_{D236A}$-eYFP displayed a broad spectrum of cell lengths and the YFP signal was almost evenly distributed throughout the whole cell. Although the filamentous cells and the diminished YFP foci speak for a DNA and ParB interactions defect, it is also possible that these phenotypes are caused by the instability of $MipZ_{D236A}$. Moreover, in the MipZ structure, D236 is not fully exposed to the surface but hiding in a cleft (Figure 2.13 C), suggesting that it may not be directly involved in the interactions. Altogether, the function of residue D236 is not clear. Nevertheless, it was still provisionally counted as a ParB-binding residue in Figure 2.9. However, it is not included in the DNA-binding residue because we are unable to determine its DNA-binding activity with *in vitro* methods due to the lack of purified protein. Moreover, the negatively charged aspartic acid is unlikely to be involved in non-specific DNA-binding.

2.4.2 DNA-binding defective MipZ variants

After purifying the eight potentially DNA-binding defective MipZ variants, I started to determine the ATPase activity of these proteins. Because production of the ATPase defective mutant $MipZ_{D42A}$ in *C. crescentus* also leads to a filamentous phenotype similar to that of the DNA-binding defective mutants, it is important to distinguish the origin of the observed phenotype (20, 21).

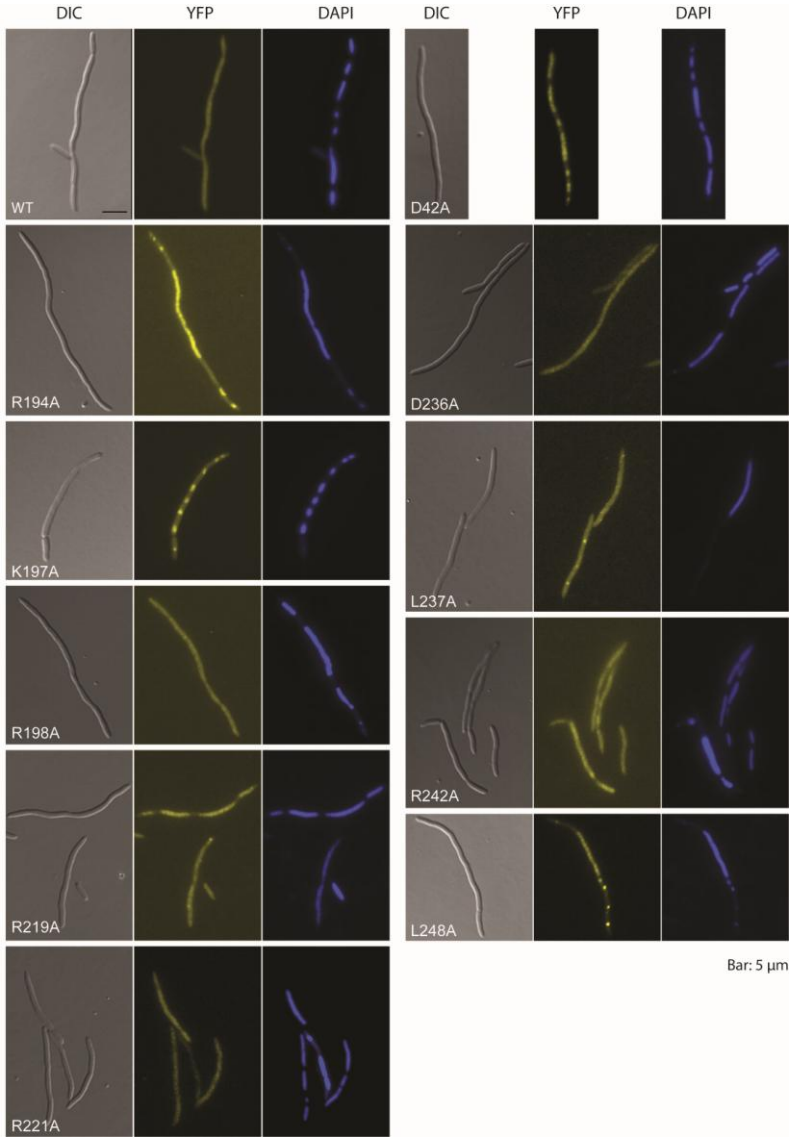

Figure 2.11 Co-localization of heterologously produced MipZ double mutant variants and nucleoid in *E. coli*. *E. coli* TOP10 was transformed with overproduction plasmids encoding the indicated $MipZ_{D42A}$-eYFP double mutation variants, together with the two control strains, which contained plasmids producing either $MipZ_{WT}$-eYFP or the single mutant $MipZ_{D42A}$-eYFP variant. Cells were treated with 5 µg/ml cephalexin and 10µg/ml chloramphenicol to induce filamentous growth and nucleoid condensation, respectively. The nucleoid was stained with DAPI.

In order to rule out the possibility that the observed filamentation was due to a defect in MipZ ATPase activity, I analyzed the ATPase activity of all purified MipZ variants. As showed in Table 2.2, all the DNA-binding defective MipZ variants had k_{cat} values that were similar to that of $MipZ_{WT}$, and about 10-times higher than that of the ATP hydrolysis-defective $MipZ_{D42A}$ variant. It can be concluded that all the MipZ variants tested are not deficient in ATPase activity, indicating that the filamentous growth of the corresponding mutants is likely due to the impaired DNA-binding activity.

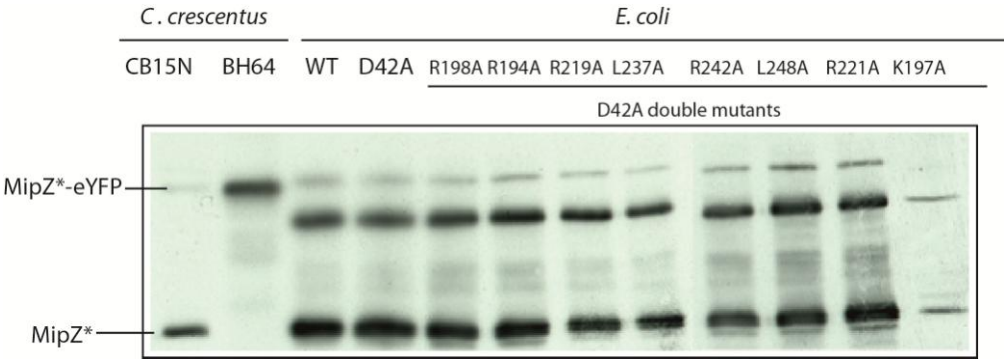

Figure 2.12 Immunoblot of *E. coli* cells heterologously overproducing the double mutant MipZ-eYFP derivatives. The corresponding *E. coli* cells used in Figure 2.11 and the *C. crescentus* control strain CB15N and BH64 (MipZ-eYFP) were subjected to immunoblot analysis using an anti-MipZ antibody.

Table 2.2 ATPase activity of purified MipZ and its variants

MipZ	**k_{cat} (min^{-1})**
WT	0.40 ± 0.05
D42A	0.034 (21)
R194A	0.39 ± 0.03
K197A	0.62 ± 0.08
R198A	0.56 ± 0.08
R219A	0.50 ± 0.05
R221A	0.33 ± 0
L237A	0.46 ± 0.06
R242A	0.60 ± 0.05
L248A	0.51 ± 0.05

The DNA-binding activities of the MipZ mutant variants were tested by a gel shift assay (Figure 2.14). Different MipZ variants were incubated with the linearized plasmid pMCS-2 in a buffer containing the slowly hydrolysable ATP analogue ATPγS, which blocks MipZ in the dimer form. $MipZ_{WT}$ and $MipZ_{D42A}$ were used as positive controls; $MipZ_{K13A}$ and BSA were employed as negative controls. The monomeric variant $MipZ_{K13A}$ displayed only weak DNA binding activity in this assay by showing a DNA smear in the lane (Figure 2.14). $MipZ_{K13A}$ still contains many of the residues constituting the DNA-binding site of the dimer and may therefore still be able to weakly interact with the phosphate backbone of the plasmid. Interestingly, the eight potential DNA-binding defective variants displayed different band-shift patterns. The R194A, K197A, R198A, R219A and L237A variants barely shifted the DNA bands. In particular, the R194A and R198A variants exhibited a similar pattern as BSA, implying that R194 and R198 play crucial roles in the MipZ-DNA interaction. $MipZ_{R242A}$ caused a smear, indicating a higher DNA-binding activity than the previous five variants. $MipZ_{R221A}$ displayed a smear pattern along half of the lane, indicating a defect but even better DNA-binding activity than $MipZ_{R242A}$. Notably, $MipZ_{L248A}$ exhibited a similar pattern as $MipZ_{WT}$, although not all of the plasmid DNA was shifted. The different gel shift patterns suggest that the different variants are defective in

DNA-binding to varying extents: the DNA-binding defect of the R194A, K197A, R198A, R219A and L237A variants is more severe than that of the R242A and R221A. By contrast, L248A showed only a subtle defect in binding to the linear plasmid.

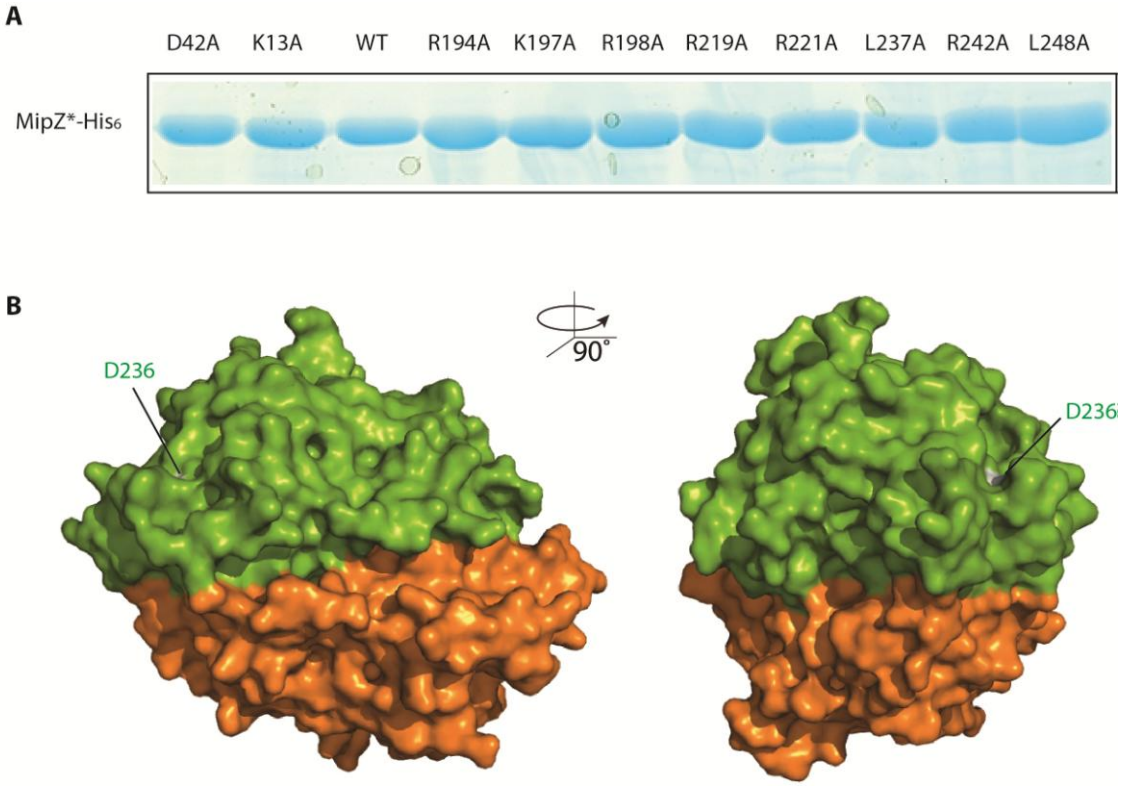

Figure 2.13 Purification of MipZ and its variants in C-terminal hexahistidine-tagged form and location of D236 on the surface of MipZ. (A) SDS-PAGE of purified MipZ*-His_6. 5 µM of purified MipZ and its indicated variants were subjected to SDS-PAGE and stained with InstantBlue. **(B)** Location of D236 on MipZ dimer surface. D236 is highlighted in white.

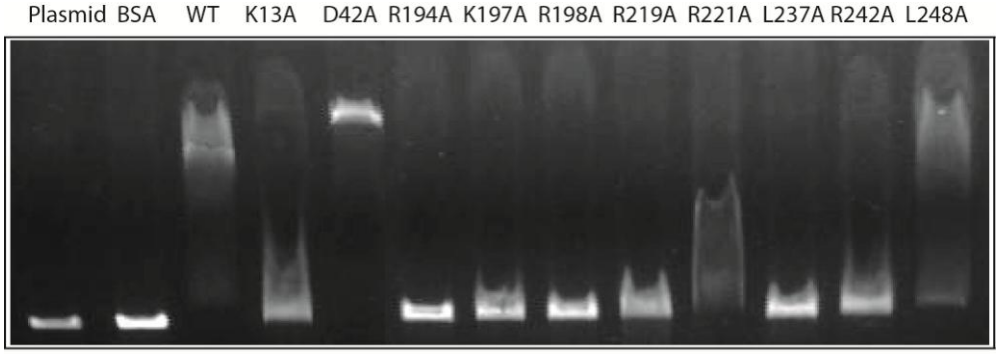

Figure 2.14 Gel shift assay of MipZ and its variants. 10 µM WT MipZ or its variants were incubated with 10 nM linearized plasmid pMSC-2 and 0.46 mM ATPγS at room temperature for 15 min and then subjected to agarose gel electrophoresis.

To further characterize the interaction of the eight DNA-binding defective MipZ variants, I performed surface plasmon resonance (SPR) analysis. To this end, a double stranded (ds, henceforth) oligonucleotide (rand-1-biotin and rand-rev, 26 bp) was immobilized on a sensor

chip and probed with $MipZ_{WT}$ or one of its mutant variants. Interaction between the MipZ variant and the oligonucleotide leads to a response signal, and a higher response value suggests a better binding. The result (Figure 2.15) showed that $MipZ_{WT}$ and its dimeric variant $MipZ_{D42A}$ exhibited a much higher response than the eight MipZ variants and the monomeric variant $MipZ_{K13A}$. The SPR results also indicate that the eight variants are defective in DNA binding to different extents (Figure 2.15). R221A, L248A and K197A displayed moderate responses, although the values were much lower than that obtained for the $MipZ_{WT}$. These data imply that R221A, L248A and K197A can still interact with dsDNA albeit weakly. This result largely fits with the gel shift assay, which suggests that R221A and L248A still interact weakly with the plasmid. The L248A variant, however, showed a very low response in the SPR analysis, only about 1/6 of the $MipZ_{WT}$ response, whereas it displayed a pronounced band shift in the gel shift assay.

The results from the gel shift assay and the SPR analysis suggest that, except for $MipZ_{L248A}$, all of the other seven potential DNA-binding defective variants indeed have a significantly reduced affinity for DNA. I continued the study by assessing the binding affinities between MipZ variants and the ds-oligonucleotide using MST analysis.

MST is short for microscale thermophoresis, a method that detects the motion of molecules in a temperature gradient (117, 118). MST is a new technology to quantify biomolecular interactions based on binding-induced changes of molecular properties, such as size, charge, hydration shell, or conformation (117, 118). In the MST assays, a temperature gradient is induced by an infrared laser, and the motion of the biomolecule to be analyzed along this gradient is monitored by changes of fluorescence, which requires fluorescent labeling of one of the interacting biomolecules (117, 118). Given the dynamic equilibrium between MipZ monomers and dimmers, the optimal way to measure the MipZ-DNA binding affinity would be to label the MipZ variants with a fluorescent dye and keep their concentration constant, while titrating with different concentrations of ds-oligonucleotide. Unfortunately, we were unable to detect any interaction after labeling of the MipZ proteins with a fluorescent dye; the labeling might impair the interaction between MipZ and DNA or even denature the proteins. Therefore, we had to change the titration scheme, by using a constant concentration of labeled ds-oligonucleotide and titrating with varying concentrations of MipZ proteins. The drawback of this approach is that increasing the concentration of MipZ variants shifts the equilibrium of MipZ dimerization toward the dimer form. Therefore, the reaction observed is the result of both dimerization and DNA-binding. We tried to diminish the influence of MipZ dimerization by using the slowly hydrolyzing ATP analogue ATPγS, which keeps MipZ in its dimeric form, but we are unable to completely exclude an influence of MipZ dimerization on the measured values for the MipZ-DNA interaction.

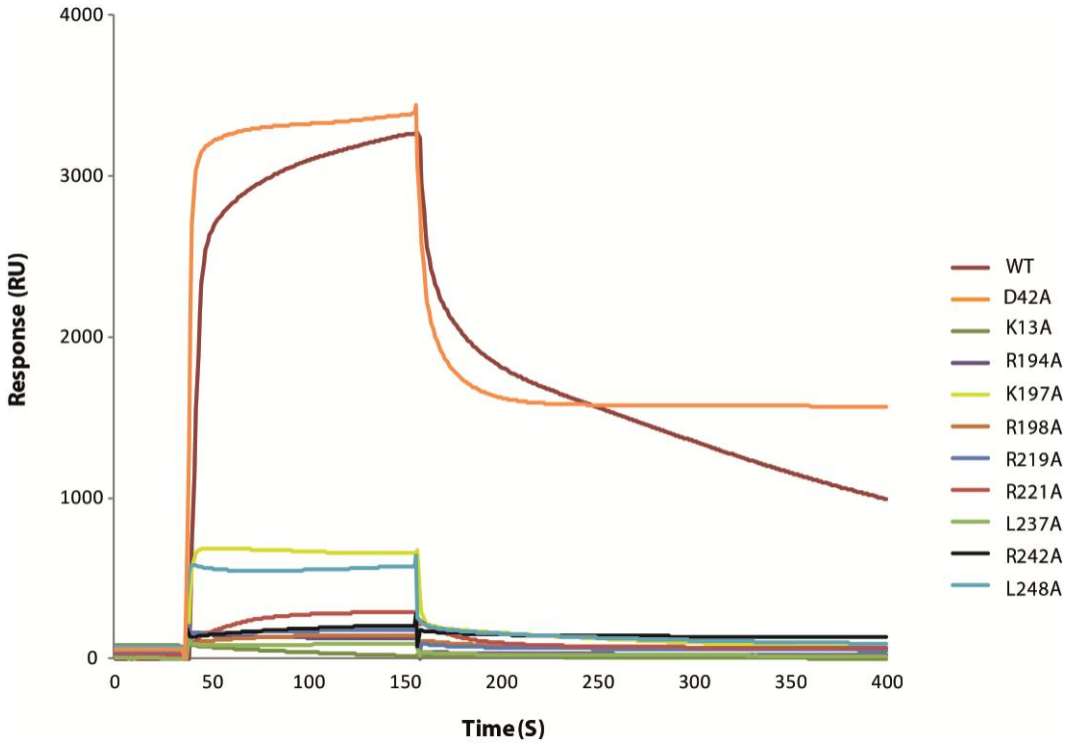

Figure 2.15 SPR analysis of the interaction of MipZ or its variants with a 26 bp double-stranded oligonucleotide. A 26 bp double-stranded oligonucleotide was immobilized on an SA sensor chip, and 6 µM WT MipZ or its variants were injected one by one in the SPR buffer containing 0.46 mM ATPγS. The measurements were performed triplicate, similar results were obtained throughout.

For the measurements, the DNA oligonucleotide was labeled with Cy3 at the 5'end and kept at a constant concentration of 50 nM in a buffer containing ATPγS, and varying concentrations of the MipZ variants. The binding curves and K_d values obtained are listed in Figure 2.16 and Table 2.3. The binding curves of the proteins $MipZ_{WT}$, $MipZ_{D42A}$, $MipZ_{L248A}$ and $MipZ_{R219A}$ were almost reached saturation and accurate K_d values were determined. The variants K197A, L237A and R242A exhibited unsaturated binding curves, which indicate lower binding affinities between these three variants and the oligonucleotide. As for R194A, R198A and R221A, the interactions were barely detected, suggesting the abolishment of their DNA-binding activities. As expected, DNA binding was also very low for the monomeric $MipZ_{K13A}$ variant, in accordance with the SPR result. $MipZ_{L248A}$ has a very similar K_d (6.8 µM) as $MipZ_{WT}$ (6.3 µM) implying a normal DNA-binding activity. The result of the SPR analysis (Figure 2.15), however, suggests a defective DNA-binding activity of L248A. The ds-oligonucleotide, used in the SPR and the MST experiments, had the same sequence and only differed in the kind of label attached to them: the one in the SPR analysis was biotin-labeled, whereas the one used in the MST assay was Cy3-labeled. Based on these contradictory results, it is still unclear if $MipZ_{L248A}$ is defective in DNA-binding. Nevertheless, L248 is for the moment still regarded as part of the DNA-binding region (Figure 2.18). $MipZ_{R219A}$ displayed mainly filamentous cells in the *C. crescentus* BH89 and almost abolished DNA binding ability in the gel shift and SPR assays, whereas it exhibited the best binding affinity to the ds-oligonucleotide among all the binding defective MipZ mutant variants in the MST assay. This may be due to the differences in the assay conditions. In general, the apparent K_d values obtained from MST measurements,

although semi-quantitatively due to the influence of dimerization, demonstrated that monomeric MipZ as well as the variants R194A, K197A, R198A, R219A, R221A, L237A and R242A are defective in DNA binding to different extents. Taking together all results from the three *in vitro* assays, we can conclude that R194 and R198 play crucial roles in the DNA binding, with mutations in these two residues abolishing the interaction. Residues K197, R219, R221, L237 and R242 are also important for the interaction, but their mutation still allows for some DNA binding. The L248 residue might be involved in DNA interaction, albeit possibly indirectly.

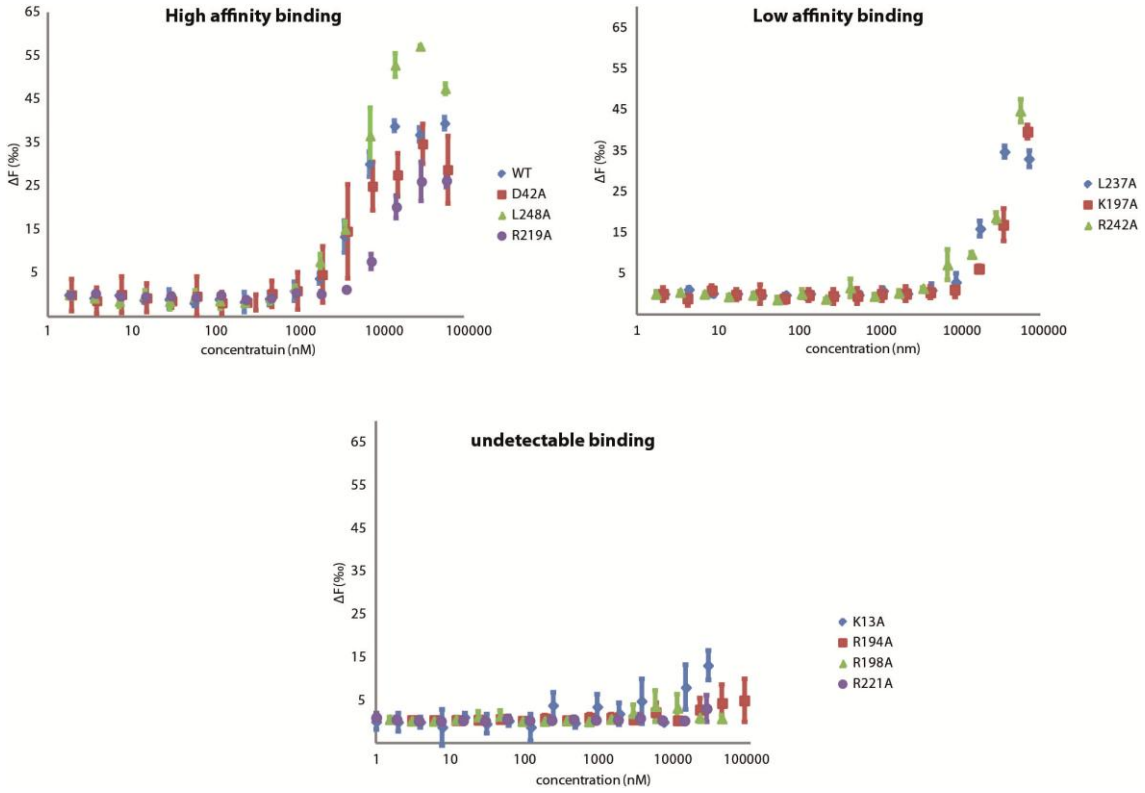

Figure 2.16 MST analysis of the binding of MipZ and its variants to a 26bp double-stranded oligonucleotide. The MipZ variants were categorized into three groups according to the different shapes of binding curves namely, almost saturated curves (high affinity binding), unsaturated curves (low affinity binding) and almost undetectable binding 50 nM Cy3-labeled ds-oligonucleotide was titrated with MipZ variants, every measurement was repeated three times with standard deviation indicated.

Table 2.3 Apparent dissociated constants (K_d) for the interaction of MipZ variants with a 26 bp ds-oligonucleotide

MipZ*	***K*$_d$ (µM)**
WT	6.32 ± 0.56
K13A	u.d
D42A	5.49 ± 0.95
R194A	u.d
K197A	>40
R198A	u.d
R219A	21.8 ± 1.76
R221A	u.d
L237A	>40

MipZ*	K_d (μM)
R242A	>40
L248A	6.81 ± 0.60

u.d: undetectable

Based on the above results, we mapped the DNA-binding region on the MipZ dimer (Figure 2.17). The interaction region is close to the dimer interface and only the dimer has a complete DNA binding region, consistent with the importance of MipZ dimerization for DNA interaction. Among the eight DNA-binding residues, six are positively charged, including five arginine residues and one lysine, and the other two are leucine residues including the ambiguous L248. This composition strongly suggests that the interaction of MipZ with DNA is largely based on electrostatic forces between positively charged MipZ residues and the negatively charged DNA phosphate backbone. This is also in agreement with the previously studied non-specific DNA-binding manner of MipZ (20). Taking a closer look at the DNA-interaction region, we found that the DNA interaction region and one of the ParB interaction regions are close to each other, with two residues overlapping (Figure 2.18). This overlapping binding region may explain the competition between ParB and DNA for binding to MipZ observed in a previous study (20). Given that the affinities of MipZ for ParB (20) and DNA appear to be similar and that there are considerably more DNA target sites than ParB molecules in a cell, the MipZ dimer will preferentially associate with the chromosome rather than ParB. These findings support the model that, after dimerization, MipZ dissociates from ParB and binds to chromosomal DNA (20).

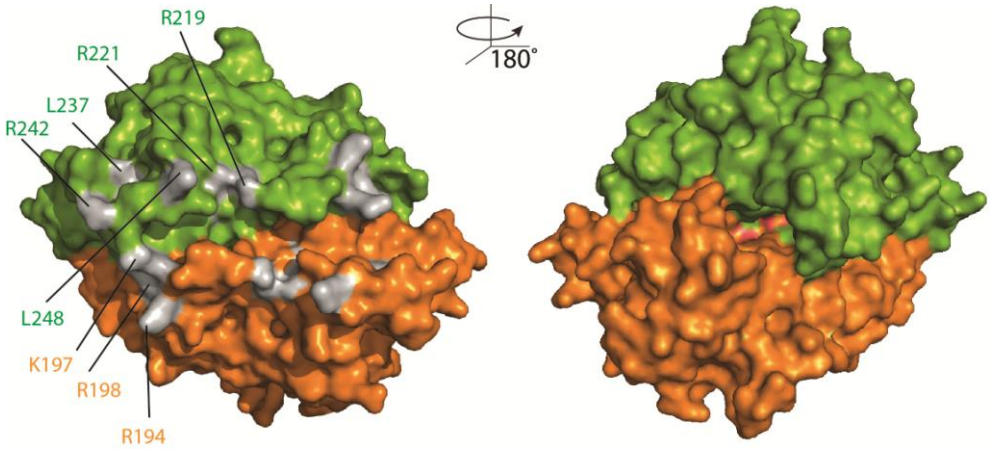

Figure 2.17 DNA interaction region of the MipZ dimer. Residues R194, K197, R198, R219, R221, L237, R242 and L248, which are involved in DNA interaction, are highlighted in gray color on the MipZ dimer structure.

In summary, based on the results from this study, we were able to map the interactive regions of MipZ, which are illustrated in Figure 2.19. The front face of the MipZ dimer (Figure 2.19, left) is responsible for DNA and ParB binding. The DNA binding region is mostly composed of positively charged residues and is close to the dimer interface in line with the non-specific DNA binding activity of MipZ and the importance of dimerization for DNA binding. The overlapping ParB and DNA-binding regions help the MipZ dimer form a gradient-like distribution: after dimerization, the MipZ dimer relocates from ParB to the chromosomal DNA, and the filter effect of the chromosomal DNA leads to the typical gradient-like distribution of MipZ, with the

highest concentration at the two polar regions and the lowest at midcell. The back face of MipZ (Figure 2.19 right) interacts with ParB and FtsZ. Although we have no clear explanation for the existence of two separated ParB interaction regions, the different oligomeric states of MipZ and the complexity of the ParB structure at the cell poles may require multiple models of interaction. For the FtsZ binding region we have so far been able to identify only three residues on each monomer. However, the complete binding site consisting of residues from both monomers, is in agreement with the observation that dimerization is a prerequisite for FtsZ interaction (20). Although the precise effect of MipZ on FtsZ polymerization is not clear, we can show that this cluster is required for stimulating the GTPase activity of FtsZ. Moreover, the separation of the DNA and FtsZ binding regions on the MipZ surface is in agreement with the observation that DNA and FtsZ interact independently with MipZ (20), with the DNA-bound dimer representing the active form of MipZ that is able to productively interact with FtsZ to prevent Z-ring formation close to the poles.

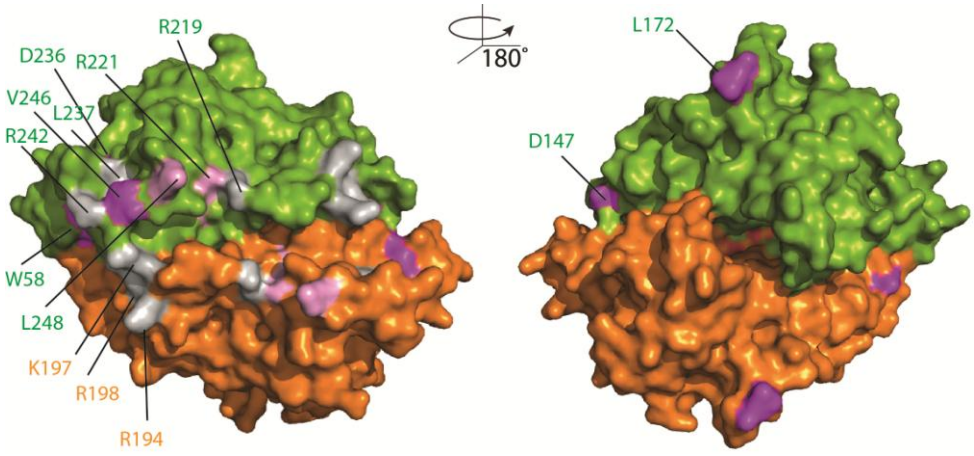

Figure 2.18 Partial overlap of the DNA- and ParB-binding regions. Residues involved in DNA binding are highlighted in gray, residues involved in ParB interaction are highlighted in magenta, and the two residues R221 and L248 involved in both interactions are highlighted in pink.

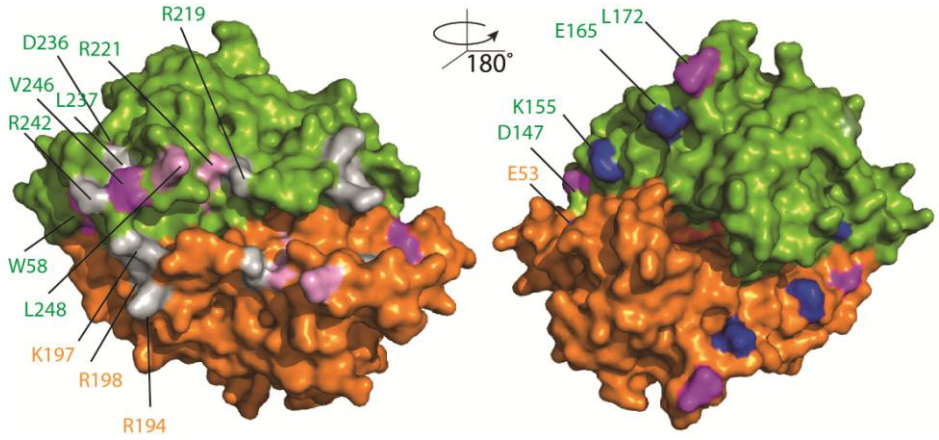

Figure 2.19 Mapping of the DNA, ParB and FtsZ binding regions on the MipZ dimer. Residues involved in FtsZ (blue), ParB (magenta), DNA (gray) interaction and residues contacting both ParB and DNA (pink) are highlighted on MipZ dimer structure.

3 DISCUSSION

3.1 The interactive map of MipZ

MipZ negatively regulates Z-ring positioning in *C. crescentus* by disrupting FtsZ polymerization and thus restricting Z-ring formation to the midcell, the point of lowest MipZ concentration in the cell (21). MipZ has been shown to directly interact with FtsZ *in vitro*, stimulating its GTPase activity and changing the straight FtsZ protofilaments into an inactive curved form (21). We continued the study of the MipZ-FtsZ interaction and identified a putative FtsZ interaction region on the MipZ dimer surface (Figure 2.6), which consists of three residues per monomer: K155, E165 and E53. Notably, these three residues form a cluster across the dimer interface (Figure 2.6), in line with the previous observation that MipZ dimerization is crucial for FtsZ interaction.

MipZ, as a member of the MinD/Mrp P-loop ATPase family, shares structural and functional similarities with ParA and MinD. However, in contrast to MipZ, neither ParA nor MinD interacts with FtsZ, and this distinct function of MipZ may be reflected in its structure. A comparison of the structures of MipZ, ParA and MinD revealed that MipZ has several unique features that have been speculated to be involved in FtsZ interaction (20). Interestingly, K155, one of the FtsZ interactive residues identified in this study, is located in a unique loop. Moreover, this loop changes its conformation dramatically upon dimerization (Figure 3.2), suggesting that it may be responsible for contacting FtsZ. However, the *C. crescentus* mutant producing the $MipZ_{\Delta D147\text{-}E152}$ variant, in which this loop is largely deleted, exhibited a dimerization defect instead of an FtsZ interaction defect (119). However, this observation does not exclude an FtsZ-binding function for this loop, because the deletion of six amino acids may severely change the structure of MipZ, which may result in a pleiotropic phenotype. The complexity of the MipZ-FtsZ interaction is also reflected by results from FtsZ sedimentation assays (120), which indicate that these three FtsZ-binding defective variants $MipZ_{E53A}$, $MipZ_{K155A}$, $MipZ_{E165A}$ can still interact with FtsZ *in vitro*, raising the possibility that MipZ might use different regions for FtsZ binding and GTPase stimulation. However to verify this idea, further investigations are needed.

In this study, we identified seven MipZ residues putatively involved in ParB interaction. Surprisingly, these residues are separated into two clusters, with a cluster of five residues (W58, R221, D236, V246 and L248) located on the front face of MipZ close to the dimer interface, and a cluster of two residues located on the back side of MipZ (Figure 2.9). Why does MipZ possess two ParB interaction regions, and how does ParB stimulate MipZ dimerization? These two questions are still open. In contrast to most bacteria, the ParAB-*parS* system is essential in *C. crescentus*, possibly due to its multiple roles in chromosome segregation, Z-ring positioning and cell pole organization (6, 21, 46, 47). In *C. crescentus*, ParB interacts with several components, including ParA, the *parS* sequence, MipZ, and PopZ. How does ParB, a relatively small protein, manage to interact with all these different components? One possibility is that ParB forms oligomers or even higher-order structures, which extends its interaction surface and

establishes an interaction platform for all the interacting components. Although ParB was reported to form dimers in *C. crescentus* (121), both plasmid- and chromosome-encoded ParB proteins have been shown to form oligomers in other bacteria (122, 123). The separated ParB-binding regions on MipZ may be important for interaction with oligomeric ParB. Moreover, the two ParB-binding regions may help MipZ to compete with other ParB-binding components. As another possibility, the two distinct forms of MipZ may use different modes to interact with ParB. It is important to note that unlike for the DNA and FtsZ interaction, both monomeric and dimeric MipZ interact with ParB; furthermore, ParB was proposed to stimulate MipZ dimerization (20), suggesting that the split interaction regions may be differentially used by monomeric and dimeric MipZ. In support of this idea, we found that the two residues D147 and L172 that locate at the back side of MipZ, (Figure 2.19; Figure 2.9) display conformational changes upon dimerization (Figure 3.2).

The eight DNA-binding residues of MipZ identified in this study (R194, K197, R198, R219, R221, L237, R242 and L248) are mostly positively charged arginines and lysine, as well as two leucines. Except for the residues identified in this study, there are two more arginines R196 and R258, probably also involved in DNA-binding (120). These findings support the previous result showing that MipZ binds to DNA in a sequence non-specific manner (20), suggesting that the binding of MipZ to DNA is mainly mediated through interaction of positively charged residues with the negatively charged DNA phosphate backbone. Moreover, these DNA-binding residues span the MipZ dimer interface, indicating an important role of MipZ dimerization in DNA interaction. It has been shown for many non-specific DNA-binding proteins, including chromosome-encoded ParA and ParA-like proteins, that positively charged residues play a central role (124, 125) in the binding process. Hester and Lukenhaus revealed that two arginines R189 and R218, are essential for the DNA-binding activity of the *B. subtilis* ParA homologue Soj; moreover, these two arginines are conserved among chromosomal ParA proteins, including *C. crescentus* ParA (125). It has been characterized that a variant of *C. crescentus* ParA carrying a mutation in one of these residues ($ParA_{R195E}$) has a severe defect in DNA-binding (14). Similar to ParA proteins, the DNA-binding region of MipZ identified here also mainly consist of positively charged residues. Moreover, one of the two most important DNA-binding residues, R198, is conserved among MipZ proteins (Figure 3.1). The other two residues involved in DNA-binding, R221 and L237 are even more conserved (Figure 3.1). R221 is not only involved in DNA binding but also implicated in ParB binding. In addition, the $MipZ_{R221A}$-eYFP fusion is partially instable in *C. crescentus*, suggesting a possible structural role of R221. The mutation of L237, on the other hand, caused severe defects in DNA binding in all the experiments tested in this study. Although positively charged residues are favored for DNA binding, non-charged residues, such as L237, may also contribute to DNA binding, for instance, through interaction with the aromatic rings of nucleotides. It appears that MipZ employs a flexible mode of interaction with DNA, involving both positively charged and uncharged residues.

The DNA-binding region comprises residues from both monomeric subunits, suggesting that only dimeric MipZ possesses a complete DNA-binding region. This result is in agreement with our previous observation that only dimeric MipZ is able to interact with DNA (20). In the gel shift assay, the monomeric $MipZ_{K13A}$ also displayed a weak DNA binding activity, suggesting that under certain conditions, a partial binding site may still have some affinity to DNA. However, this interaction is rather weak compared with $MipZ_{WT}$ and the dimeric $MipZ_{D42A}$.

Furthermore, in both the SPR and MST assays, which used short oligonucleotide as target DNA, and a higher salt concentration, the monomeric mutant $MipZ_{K13A}$ barely exhibited any binding activity. Notably, several DNA-binding residues, including R194, K197, R198 and L248 (Figure 3.2), undergo slight conformational changes upon dimerization, which may facilitate the access of these residues to DNA.

An alignment of MipZ homologues from selected α-proteobacteria (Figure 3.1) shows that seven residues (W58, D147, R198, R221, D236, L237, and L248) implicated in the interaction with FtsZ, ParB or DNA are conserved. Strikingly, three residues, R221, D236 and L248, which showed both ParB- and DNA-binding defective phenotype during the mutation screening, are conserved. The conservation of D236 and R221 may be due to their important role in ParB or/and DNA interaction, although it is also possible that they are crucial for stabilizing the MipZ structure, because $MipZ_{D236A}$ and $MipZ_{R221A}$ are somehow unstable (Figures 2.3 and 2.13). Notably, the residues located between R221 and L237 are quite conserved, implying an important function of this region. Characterization of $MipZ_{L248A}$ led to ambiguous results, and it is still unclear whether D236 and L248 are in fact involved in the interaction with DNA. Nevertheless, it appears that the overlapping ParB- and DNA-binding region may have important functional roles, in regulating the oscillation of the MipZ dimer between ParB and DNA and stabilizing MipZ structure.

3.2 MipZ as a member of the Mrp/MinD family

Phylogenetic analysis suggests that MipZ belongs to a distinct subfamily of the Mrp/MinD family of P-loop ATPases (20, 126). Proteins in this family are involved in many cellular processes, including chromosome or plasmid segregation (ParA), chemoreceptor and carboxysome segregation (PpfA and ParA), Z-ring positioning (MipZ and MinD), or the polar positioning of proteins (ParC, TadZ/CpaE) (53, 127, 128). A common feature of proteins in this family is that presence of a KGGh motif in the P-loop and retention of N in the NKXD motif (126). It has been shown that mutations in the KGGh motif (K13A and G14V) severely impact regulatory function of MipZ (20). ATP binding and hydrolysis determine the oligomeric states of Mrp/MinD proteins (53). ATP binding usually triggers the dimerization of these proteins, whereas hydrolysis disassembles the dimers (53). Notably, ATP binding and hydrolysis not only change the oligomeric state of these proteins but also serve to alter their affinities to their corresponding binding partners (19, 129). ParA and MipZ dimers have higher affinity to chromosomal DNA, whereas the MinD dimer binds to the cytoplasmic membrane. Importantly, binding a largely immobile scaffold, such as the membrane or chromosomal DNA for MinD and ParA/MipZ respectively, limits the diffusion rate of the dimmers, thereby establishing their specific cellular localization (19). In addition, dimerization of MinD generates the binding regions for MinE and MinC (20, 53, 98). Similarly, as shown in this study, the MipZ dimer also harbors binding regions for chromosomal DNA and FtsZ.

MipZ has a unique feature compared with other Mrp/MinD proteins, it does not depend on other proteins to trigger its ATPase activity (20, 53). As mentioned above, ParB stimulates the ATPase activity of ParA, thereby regulating the dynamics of ParA (6). MinD, similar to ParA, relies on MinE to stimulate its ATPase activity, which drives the pole-to-pole oscillation of

MinD (53). Interestingly, ParB triggers MipZ dimerization but stimulates ParA disassembly. However, the mechanism underlying the positive effect of ParB on MipZ dimer formation is still unclear.

Both chromosome and plasmid-encoded ParA proteins were shown to bind chromosomal DNA non-specifically (125, 130, 131). In some cases, DNA binding was proposed to induce the polymerization of ParA proteins, such as SopA from the F plasmid and ParA2 from *Vibrio cholerae* (131, 132). However, so far there is no evidence suggests that MipZ can form higher-order structures upon DNA binding. Another difference between ParA and MipZ is their DNA-binding specificity. Some ParA proteins have been shown to bind specifically to certain DNA sequences to control gene expression. For instance, *E. coli* P1 plasmid-encoded ParA in the ADP-bound form can bind specifically to the *parAB* promoter region and regulate the expression of *parAB*, whereas in the ATP-bound form, it interacts non-specifically with the chromosome to segregate newly replicated plasmids (133). In the case of P1, ParA contains an extended N-terminal region, which is responsible for specific DNA-binding but not encoded by chromosome-encoded ParA (124). Some chromosome-encoded ParA also bind to specific DNA sequences, even though they lack this N-terminal DNA-binding domain, as exemplified by Soj, which was shown to regulate the expression of several sporulation-related genes by specific DNA binding (13, 134). There are several sequence-specific DNA binding proteins once were considered non-specifically bound to DNA, for instance, the nucleoid occlusion proteins Noc and SlmA. The DNA-binding specificities of the two proteins were revealed recently by ChIP–Seq (Chromatin Immuno-Precipitation DNA-Sequencing) (110, 135). Moreover, some bacterial nucleoid-associated proteins (NAPs) also demonstrate a bias for certain binding motifs. For instance, H-NS prefers AT-rich sequences and the TCGATAAATT motif, HU has a mild preference for AT-rich sequences and distorted DNA regions (136). Up to date, there is no evidence suggesting that MipZ binds to specific DNA sequences. However, our ongoing ChIP-Seq analysis may provide deeper insights into the interaction between MipZ and chromosomal DNA. In particular it will reveal whether the MipZ monomer ($MipZ_{K13A}$) or the dimer ($MipZ_{D42A}$) interact preferentially with specific DNA sequences, or have a bias for sequences with certain properties such as a skewed base composition.

3.3 Gradient formation of MipZ and remarks

In eukaryotes, the formation of protein concentration gradient is a common strategy to regulate biological processes, and Morphogen gradients serve as a good example. Morphogens are produced and secreted by certain types of cells, they diffuse to neighboring cells and trigger gene expression in these cells in a concentration dependent manner (19, 137). Protein concentration gradients are also used by multicellular bacteria, such as filamentous cyanobacteria, in which a gradient of protein regulators control the development of heterocysts (19, 138). Although protein gradients that range over long distance are a widespread phenomenon, there are very few examples of steady state intracellular protein concentration gradients. The MipZ system in *C. crescentus* is a relatively well-studied example for this type of gradient.

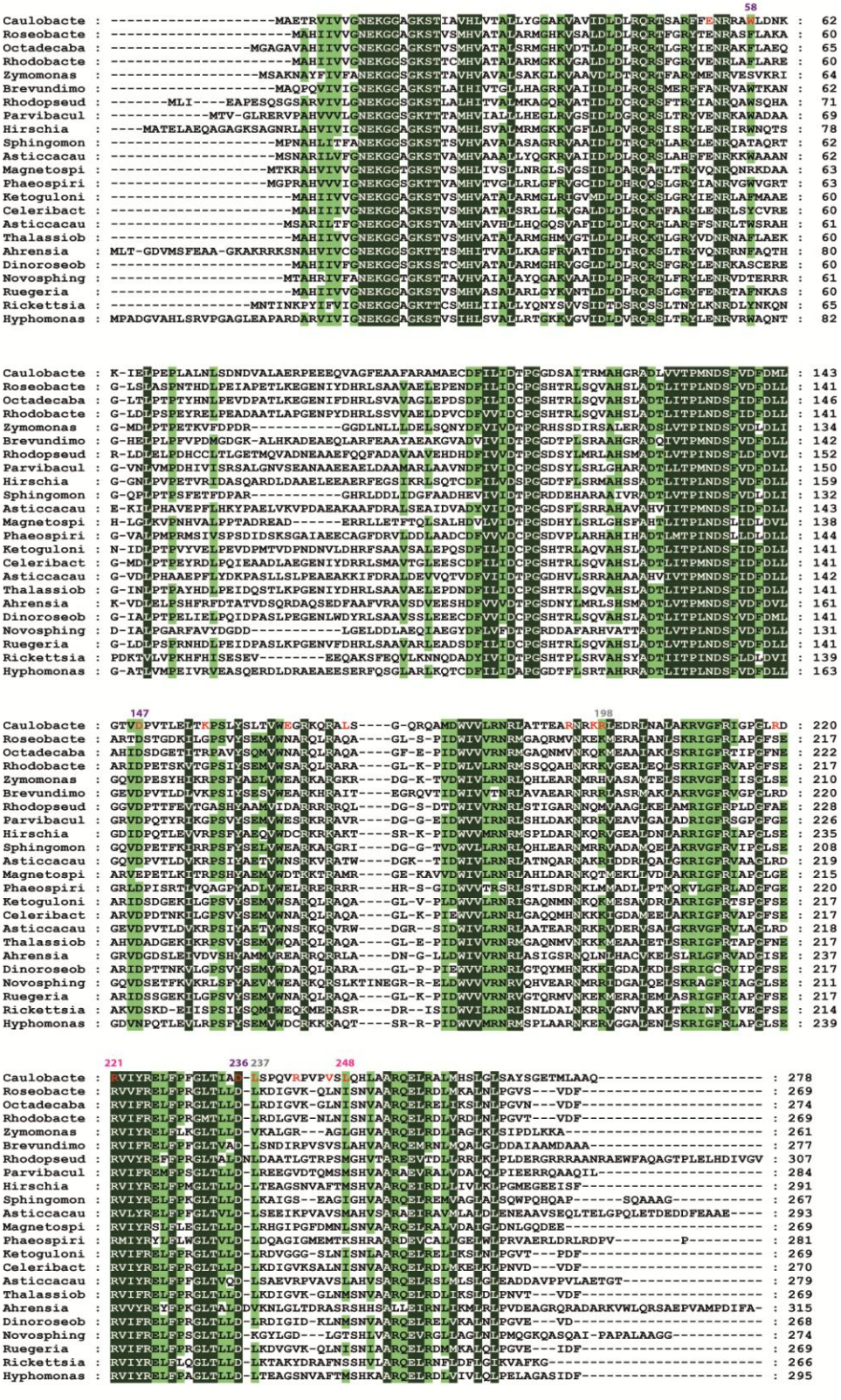

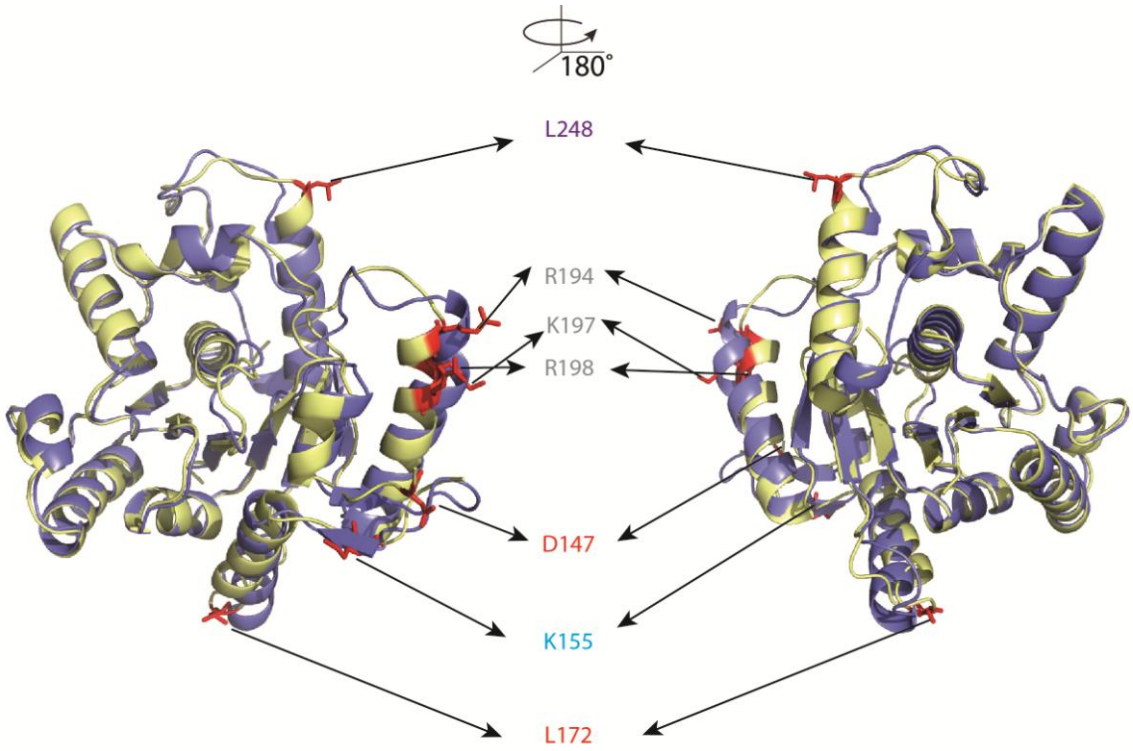

Figure 3.2. Dimerization induced conformational changes in MipZ. The monomeric structure of MipZ is shown in purple and the structure of a single subunit of dimeric MipZ is shown in yellow. Residues that are both involved in interaction and undergo conformational changes upon dimerization are highlighted in red color. The positions of DNA-binding residues are indicated in gray, ParB-binding residues are in red, bifunctional ParB and DNA-binding residue is in purple, and FtsZ-binding residue is in blue.

The mechanism of gradient formation by *C. crescentus* MipZ relies on the following facts. First, MipZ molecules are recruited to cell pole regions through direct interaction with polarly localized ParB. Previous studies revealed that there are approx. 1000 MipZ molecules in a cell. Most of them are probably in the dimeric form, based on the high cellular ATP/ADP ratio and the low ATP hydrolysis activity of MipZ dimers (20, 21). Second, the diffusion of MipZ dimers is restricted by chromosomal DNA. The MipZ concentration decreases with increasing distance from the poles, which is due to the retention of dimers by chromosomal DNA (20). Upon dimerization, MipZ forms the DNA binding region, which overlaps with one of the ParB interaction regions. Non-specific chromosomal DNA competes with ParB for the overlapping binding sites, leading to the release of newly formed dimers from the polarly localized ParB and relocalize to chromosomal regions in the vicinity of the poles. Third, ATP binding and hydrolysis regulate the different affinities of MipZ for its interaction partners and the dynamics of the whole regulatory network.

Figure 3.1 Amino acids sequence alignment of MipZ proteins from 23 α-proteobacteria species. The bacteria listed in the alignment are *Caulobacter crescentus, Roseobacter litoralis, Octadecabacter antarcticus, Rhodobacter capsulatus, Zymomonas mobilis, Brevundimonas diminuta, Rhodopseudomonas palustris, Parvibaculum lavamentivorans, Hirschia baltica, Sphingomonas wittichii, Asticcacaulis excentricus, Magnetospirillum gryphiswaldense, Phaeospirillum fulvum, Ketogulonicigenium vulgare, Celeribacter baekdonensis, Asticcacaulis biprosthecum, Thalassiobium sp. R2A62, Ahrensia sp. R2A130, Dinoroseobacter shibae, Novosphingobium sp. AP12, Ruegeria pomeroyi, Rickettsia monacensis and Hyphomonas neptunium* respectively. The interaction-implicated *C. crescentus* MipZ residues identified in this study are highlighted with red colors.The positions of conserved and ParB-binding, DNA-binding and bifunctional ParB and DNA-binding implicated residues are highlated in pink, purple and orange, respectively. The alignment was generated with Clustal omega available at https://www.ebi.ac.uk/Tools/msa/clustalo/

Upon ATP binding, MipZ forms dimer, which results in the completion of the DNA- and FtsZ-binding regions, thereby allowing concomitant interaction of MipZ with both DNA and FtsZ. On the other hand, the MipZ dimer disassembles after hydrolyzing ATP spontaneously. The resulting monomers can diffuse back to ParB efficiently without retention by the chromosome. In summary, the recruitment by polarly localized ParB, the oscillation between ParB and chromosomal DNA, the interaction with chromosomal DNA, as well as the intrinsic ATPase activity coordinate and regulate the bipolar concentration gradient of MipZ in *C. crescentus*.

In this study, we further explored the regulatory function of MipZ by mapping its interaction regions. We showed that FtsZ and DNA have distinct binding regions on MipZ dimer, and their binding regions are close to the dimer interface but remote from each other. Notably, ParB has two separate binding regions, one of which overlaps the DNA binding region. These data support a model in which only the dimeric MipZ interacts with chromosome and FtsZ, and in which ParB and chromosomal DNA compete for MipZ. However, several questions remained unsolved. The FtsZ interaction region of MipZ may not yet be complete. Moreover, the effect of MipZ on FtsZ should be further characterized. What is the reason behind the split ParB-binding regions and how is ParB involved in MipZ dimerization? The on-going ChIP-Seq analysis may also raise new questions about the interaction of MipZ with chromosomal DNA. Obtaining a more detailed and clearer picture of the MipZ regulatory network will provide new insights into the spatial regulation of protein localization and thus understanding the regulation of cell division in bacteria better.

4 MATERIALS AND METHODS

4.1 Materials

4.1.1 Chemicals and enzymes

Common chemicals used in this study were acquired from Bioline (Germany), Carl-Roth (Germany), Difco (Spain), GE Healthcare (Germany), Invitrogen (Germany), Merck (Germany), Nanotemper (Germany), Perkin Elmer (USA), Peqlab (USA), Qiagen (Germany), SIGMA-Aldrich (Germany) and Thermo Scientific (USA). Radioactive [α-^{32}P]-ATP and [α-^{32}P]-GTP were produced by Hartmann Analytic (Germany)

Enzymes used for DNA cloning were acquired from Fermentas (Canada) or New England Biolabs (USA). KOD hot start DNA polymerase used for standard PCR (Polymerase Chain Reaction) and BioMix Red for colony PCR were from Merck (Germany) and Bioline (Germany), respectively.

4.1.2 Buffers and solutions

Buffers and solutions were prepared in deionized water. If necessary, buffers and solutions were autoclaved at 121 °C for 20 min or sterilized by filtration through a 0.2 µm filter (Sarstedt, Germany)

4.1.3 Media

Media used in this study were autoclaved at 121 °C for 20 min unless mentioned otherwise. The antibiotics, carbohydrates or amino acids were first filter-sterilized and then add to the cooled down (approx. 60 °C) media. The solid media were supplemented with 1.5% (w/v) agar before autoclave.

LB (Lysogeny broth)	1.0% (w/v) Tryptone
	0.5 % (w/v) Yeast extract
	1.0% (w/v) NaCl
McConkey agar	1.7% (w/v) Peptone
	0.3% (w/v) Casein peptone
	1% (w/v) Lactose
	0.15% (w/v) Bile salts

	0.5% (w/v) NaCl 0.003% (w/v) Neutral red 0.0001% (w/v) Crystal violet 1.35% (w/v) Agar
PYE (peptone yeast extract)	0.2% (w/v) Bacto Peptone 1.0% (w/v) Yeast extract 1 mM $MgSO_4$ 0.5 mM $CaCl_2$

Additives

Antibiotics, carbohydrates and other additives were prepared as stock solutions.

Table 4.1 Antibiotics

Antibiotics	**Stock concentrations (mg/ml)**	**Final concentrations (µg/ml)**			
		E. coli liquid	*E. coli* solid	*C. crescentus* liquid	*C. crescentus* solid
Ampicillin	100	50	200	-	-
Chloramphenicol (in 70% ethanol)	10	20	30	-	-
Gentamicin	10	-	-	0.5	5
Kanamycin	20	30	50	5	25
Spectinomycin	20	50	100	25	50+Sreptomycin 5
Streptomycin	10	30	30	5	5

Table 4.2 Carbohydrates

Carbohydrate	**Stock concentrations (w/v)**	**Final concentrations (w/v)**
D(+)-arabinose	15%	0.2%
D(+)-glucose	20% and 40%	0.2%, 0.5% or 2%
Isopropyl-β-D-thiogalactopyranoside (IPTG)	1 M	0. 5 mM
Vanillate	50 mM	0.5 mM
D(+)-xylose	20%	0.3%

4.1.4 Oligonucleotides

Oligonucleotides used in this study were designed with the softwares GeneTool Lite 1.0 (BioTools Inc., Canada) and QuickChange Primer Design tool (Agilent Technologies, Germany) and synthesized either by SIGMA-Aldrich (Germany) or Eurofins MWG Operon (Germany). All oligonucleotides used in this study are listed in the Appendix.

4.1.5 Strains

C. crescentus CB15N (NA1000) was used as wild-type strain. *E. coli* host strains are listed in Table 4.3.

Table 4.3 *E. coli* host strains

Strains	**Application**	**Genotype**
TOP10	Molecular cloning	F⁻ *mcrA* Δ(*mrr-hsdRMS-mcrBC*) Φ80*lacZ*ΔM15 *ΔlacX74 recA1 araD139* Δ(*ara leu*) 7697 *galU galK rpsL* (StrR) *endA1 nupG*
Rosetta™2(DE3)pLysS	Protein overproduction	F⁻ *ompT hsdS*$_B$ (r_{B-} m_{B-}) *gal dcm* (DE3) pLysSpRARE2 (Cam^R)
BTH101	Bacterial-two hybrid assay	F⁻ *cya-99 araD13 galE15 galK16 rpsL1* (Str^R) *hsdR2 mcrA1 mcrB1*

4.2 Microbiological methods

4.2.1 Cultivation of *E. coli*

E. coli strains was aerobically grown in liquid LB medium at 37°C with shacking speed of 210 rpm or grown on LB agar plates, supplemented with corresponding antibiotics or carbohydrates listed in Table 4.1 and 4.2. Only the single colonies grown on the plates were used for the further experiments. BTH101 cells were cultivated on MacConkey agar plates at 28 °C for bacterial two-hybrid assay.

4.2.2 Cultivation of *C. crescentus*

C. crescentus strains was aerobically grown in PYE medium at 28 °C with shacking speed of 210 rpm or grown on PYE agar plates, supplemented with the corresponding antibiotics and carbohydrates listed in Table 4.1 and 4.2.

4.2.3 Storage of bacteria

For the short period storage (one or two weeks), bacteria were kept on agar plates and stored at 4°C. For the long term storage, the overnight cultures of bacteria were supplemented with sterile DMSO (dimethy sulfoxid) to final concentration of 20% (v/v) and stored at -80°C.

4.2.4 Bacterial Adenylate Cyclase Two-Hybrid (BACTH) assay

The BACTH system was performed as described by Ladant and coworkers (116), with the modification according to the instruction of BACTH System Kit (Euromedex, France). BACTH was used to detect the interaction between MipZ or its mutant variants and ParB. *C. crescentus parB* was inserted into pUT18 to produce a T18-ParB fusion protein, and sequences of *mipZ* or its mutant variants were inserted into pKNT25 to form MipZ*-T25 fusion proteins after co-transformation and synthesis in host strain BTH101. The resulting strains were streaked on McConkey agar plates supplemented with ampicillin and kanamycin. Positive interactions were indicated by red color of the colonies. Moreover the interactions of the corresponding colonies can be quantified by analyzing β-galactosidase activity.

To measure the β-galactosidase activity, three single colonies of one resulting transformant were inoculated separately in LB medium supplemented with ampicillin and kanamycin. The cultures were grown to mid-log phase, and the OD values were recorded. 3 ml of each culture was pelletized and resuspended in 1 ml Z buffer (60 mM Na_2HPO_4, 40 mM NaH_2PO_4, 10 mM KCl, 1 mM $MgSO_4$, pH 7.0), and then 50 µl chloroform and 25 µl 0.1% SDS buffer were added to lyze the cells, followed by a 10 s vigorously vortex, and a 30 min incubation at room temperature. 500 µl lysate from last step and 500 µl of Z buffer supplemented with 50 mM β-mercaptoethanol were transferred into a new tube as a reaction system. A tube containing 1 ml Z buffer supplemented with 50 mM β-mercaptoethanol was used as the blank control. The reaction was started by adding 200 µl 4 mg/ml O-nitrophenyl β-D-galactopyranoside (ONPG) into the 1 ml reaction system. When the samples turn yellow, 400 µl of 1 M Na_2CO_3 was added in immediately to stop the reaction. The reaction time was recorded. The reaction samples were then pelletized, the clear supernatant was collected and the A_{420} was measured against the blank control. The β-galactosidase activity (MU) can be calculated according to the equation:

$$\text{MU} = 1000 \times A_{420}/t \times V \times OD_{600}$$

t: Reaction time in minutes

V: applied culture volume in ml

4.2.5 Protein overproduction in *E. coli*

Hexahistidine-tagged forms of MipZ and its mutant variants were overproduced in Rosetta2(DE3)/pLysS which was transformed with pET21a (+) backbone plasmids carrying the corresponding *mipZ* variants. Protein overproduction was induced by adding 0.5 mM IPTG into cell culture when the OD_{600} reached 1. Cells was cultivated for another 3 h and then harvested and stored in -80 °C freezer.

MipZ*-eYFP fusion proteins were overproduced in TOP10 strain, which was transformed with pBAD24-CB backbone plasmids carrying respective *mipZ* double mutation alleles. Protein overproduction and cell filamentation were induced by 1% arabinose and 5 µg/ml cephalexin respectively, when cells were grown to early exponential phase. Cells were cultivated for another 2.5 h and 20 µg/ml chloramphenicol was added to induce nucleoid condensation. After 30 min cultivation, samples were subjected to microscopy.

4.3 Molecular biological methods

4.3.1 Construction of plasmids

Plasmids containing *mipZ* point mutation alleles

These plasmids were constructed containing different mutations in *mipZ* allele. The wild-type *mipZ* was amplified from pMT182 by primers CC2165-uni2 and CC2165-rev2 (21), the PCR product was inserted into the blunt end plasmid pJET1.2 (Thermo Scientific, USA) and the resulting plasmid was named pBH8. And then, pBH8 was used as the template for the site-directed mutagenesis PCR with the corresponding primers to introduce different point mutations in *mipZ* alleles.

Plasmids for production *mipZ* or its derivatives C-terminal *eyfp* fusions in *C. crescentus*

These plasmids would integrate into *C. crescentus* chromosome at *xylX* locus by single homologous recombination. pXYFPC-2 was used as the backbone vector and was digested with endonuclease NdeI and SacI. The insertion genes were amplified by PCR from pBH8 and its derivative plasmids containing *mipZ* point mutation alleles, using CC256uni-2 and MipZ-rev as primers, followed by digestion with NdeI and SacI. Finally, the resulting digested vector and insertions were ligated as described in 4.3.4.

Plasmids for production of *mipZ* or its derivatives C-terminal *eyfp* fusions in *E. coli* TOP10

These plasmids replicate and overproduce MipZ or its derivative eYFP fusion protein in TOP10 upon induction with arabinose. pDK3 (20) was used as backbone vector and introduced an extra mutation in $mipZ_{D42A}$ sequence by using mutagenesis PCR (4.3.3) with corresponding primers. The resulting PCR product was digested with endonuclease NdeI and SacI, the small fragment containing *mipZ* mutation allele was then ligated with pDK3 whose $mipZ_{D42A}$ gene was released by restriction with NdeI and SacI.

Plasmids for overproduction *mipZ* or its derivatives in C-terminal hexahistidine-tagged forms in *E. coli* Rosetta2(DE3)/pLysS

These plasmids were used to synthesis MipZ or its derivative in C-terminal hexahistidine tagged form in Rosetta2(DE3)/pLysS. pET21a (+) was used as backbone vector and digested with endonuclease NdeI and HindIII, the insertion genes were amplified from corresponding templates, which are the pXYFPC-2 backbone plasmid with corresponding *mipZ* mutation

alleles, with CC2165 uni-2 and CC2165-HindIII rev as primers, followed by digestion with NdeI and HindIII. The digested vector and insertions were ligated as described in 4.3.4.

Plasmids for bacterial two-hybrid analysis

These plasmids were constructed to detecting the interaction between MipZ mutant variants and ParB. pKNT25 was used as backbone vector and digested with EcoRI and BamHI. Insertion genes were amplified from corresponding templates with MipZ-BACTH-for and MipZ-pKNT25-rev as primers, followed by digestion with EcoRI and BamHI. The digested vector and insertion were ligated as described in 4.3.4.

4.3.2 DNA extraction and sequencing

Plasmids from *E. coli* were extracted using GenElute™ Plasmid Kit (SIGMA-Aldrich, Germany) following the instruction provided by the manufacturer. The concentration of extracted plasmids was measured by Nanodrop ND-1000 (Nanodrop,USA).

Sequencing was performed by Eurofins MWG Operon (Germany) with providing 50-100 ng/µl DNA samples and the corresponding primers.

4.3.3 Polymerase Chain Reaction (PCR)

To amplify a specific DNA fragment, KOD PCR was performed with following reagents: 10-200 ng template plasmids, a pair of 1 µM specific DNA primers, KOD Hot Start DNA Polymerase, the supplied $MgSO_4$ solution and the reaction buffer (Merk, Germany), plus 5% DMSO.

To introduce a point mutation into the wild-type *mipZ* gene, a site-directed mutagenesis PCR was performed with following reagents: 10 ng template plasmids, a pair of 0.4 µM specific primers, the rest was the same as KOD PCR. The product of site-directed mutagenesis PCR was incubated with 1 µl restriction enzyme DpnI (Fermantas, Canada) at 37 °C for 1 h to digest the template.

To confirm plasmids uptaken or insertion into the chromosome loci correctly, a colony PCR was performed. The reaction system contained 1× BioMix™Red (bioline,Germany), 5% DMSO, a pair of 1 µM primers and a tip of *E. coli* or *C. crescentus* cells from a corresponding colony.

All the PCR reactions were carried out in a thermocycler (Biometra, Germany) with parameters listed in Table 4.4.

Table 4.4 Standard PCR cycling parameters

Steps	Temperature	Time
Initial denaturation	95°C	5 min
Denaturation	95°C	45 s

Steps	Temperature	Time
Annealing	50-65°C (depending on the primers)	45 s
Elongation	72°C	30 s/kb
Final elongation	72°C	4 min

4.3.4 Restriction digestion and ligation of DNA fragments

Plasmids or PCR products were digested with proper restriction enzymes to remove certain parts and generate matched ends to ligate into new plasmids. DNA fragments were incubated with proper FastDigest restriction enzymes (Fermantas, Canada) in the supplied buffer at 37°C for 0.5-2 h. For plasmids restriction shrimp alkaline phosphatase (SAP; Fermentas, Canada) was added into the digestion solution to prevent the re-ligation of the digested plasmid by dephosphorylating 5'-end.

The DNA fragments were ligated by T4 DNA ligase in the supplied buffer (Fermentas, Canada) and incubated at room temperature for 1- 2 h.

4.3.5 Agarose gel electrophoresis

DNA samples were separated and visualized by agarose gel electrophoresis. The samples was mixed with 10 times diluted 10× DNA loading buffer (50% glycerin, 0.2% bromophenol blue, 0.2% xylene cyanol, 0.2 M EDTA), loaded on the agarose gel, and run the electrophoresis at 160 volt for 20 min. The agarose gel was prepared with 1% agarose in 0.5× TAE buffer (20 mM Tris, 0.175% acetic acid, 0.5 mM EDTA) and supplemented with 0.005% ethidium bromide. After electrophoresis, the agarose gel was visualized under the UV light of the UV-Transilluminator (UVP-BioDoc-IT™ Imaging System, UniEquip, Germany).

4.3.6 Preparation and transformation of chemically competent *E. coli*

To prepare chemically competent cells, *E. coli* was routinely cultivated overnight, and diluted 100 times into fresh LB medium, cultivated till an OD_{600} of 0.6. The culture was placed on ice for 10 min. In the following steps the cell culture, solutions and equipments were kept on ice or at 4 °C. Cell culture was centrifuged at 3000× g for 10 min, afterwards the pellet was resuspended with 0.1 M $CaCl_2$ and incubated on ice for 30 min. Cells were centrifuged again with the same condition and the pellet was resuspended with 1/50 original culture volume of solution containing 0.1 M $CaCl_2$ and 15% glycerol. Aliquots of 100-150 µl cells were snap-frozen in liquid nitrogen and stored at -80 °C.

Transformation of *E. coli* was performed as following steps: the competent cells were thawed on ice, added with approx. 5 ng plasmids followed by 30 min incubation on ice, 90 s heat shock at 42 °C, and 2 min on ice. Subsequently, cells were cultivated with 500 µl LB medium at 37 °C for 1 h, and then spread on agar plates with the respective resistant antibiotics.

4.3.7 Preparation and transformation of electrocompetent *C.crescentus*

The overnight culture of *C. crescentus* cells was diluted 50 times into fresh 2x PYE medium, cultivated till an OD_{600} of 1. In the following steps the cell culture, solutions and equipment were kept on ice or at 4 ℃. The culture was first centrifuged at 6500× g, 10 min and washed with the 1× culture volume of 10% glycerol, pelletized at 8600× g for 10 min, and repeated this step once. After resuspension with 1/10 culture volume of 10% glycerol, cells were harvested by centrifugation at 11000× g for 10 min. Subsequently, cells were resuspended with 1/50 culture volume of 10% (v/v) glycerol and first snap-frozen in liquid nitrogen and stored at -80°C in 80 µl aliquots.

Transformation of *C. cresentus* was performed as following steps: the competent cells were thawed on ice, added with 5-10 µg plasmid solution and transferred into an ice-cold electroporation cuvette (bio-Red, Germany), followed by an electroporation with a pulse of 1500 V, 400 Ω, 25 µF. Afterwards, cells were cultivated with 900 µl 2× PYE at 28°C for 2 h and then spread on PYE plates with the respective resistant antibiotics.

4.4 Biochemical methods

4.4.1 SDS-polyacrylamide gel electrophoresis (SDS-PAGE)

SDS-PAGE was used to separate proteins according to their sizes (139).This method is suitable for both purified protein and cell lysate. For purified protein samples, they were diluted with 1× SDS buffer [300 mM Tris base, 50% (v/v) glycerol, 5% (w/v) SDS, 500 mM dithiothreitol, 0.05% bromophenol blue, pH6.8] to 5-10 µM. For cell lysate samples, the OD_{600} of cell culture was recorded. Cell culture was pelletized and resuspended with 1× SDS buffer to its original OD_{600} of 10. The prepared samples were first heated at 95 ℃ for 5 or 15 min for purified protein and cell lysate samples, respectively. After cooling down, the samples can be subjected to SDS-PAGE directly or stored at -20 ℃. 10-15 µl samples were usually loaded into the SDS gel and subjected to electrophoresis. The SDS-PAGE electrophoresis was run with 15 mA/ gel for the upper layer and 30 mA/ gel for the lower gel layer in SDS running buffer [25 mM Tris Base, 192 mM glycine, 0.1 % (w/v) SDS] using PerfectBlue™ Twin S system (Peqlab, USA).

After electrophoresis, SDS gel was either stained for visualization or transferred to a PVDF (polyvinylidene fluoride) membrane for immunoblot analysis (4.4.2). The staining of SDS gels was either with coomassie solution [40 % methanol, 10 % acidic acid, 0.1 % (w/v) Brilliant Blue R 250] for 1 h or with Instant Blue™ (Gentaur, Germany) for 20-60 min. Coomassie staining was destained with a solution containing 20 % ethanol and 10 % acidic acid, by gently shacking the SDS gels in the detaining solution for approx. 10 min, repeated for 3-4 times. Instant blue was destained with tap water till excess dye washed away.

Table 4.5 Composition of a SDS gel

Component	Upper gel (5% stacking gel)	Lower gel (11% resolving gel)
H_2O	1.43 ml	1.9 ml
Upper gel buffer [500 mM Tris Base pH6.8 0.4 % (w/v) SDS]	625 µl	-
Lower gel buffer [1.5 M Tris Base pH 8.8 0.4 % (w/v) SDS]	-	1.25 ml
N,N,N,N-Tetramethylethylenediamine (TEMED)	1.9µl	3 µl
10% (W/V) Ammonium persulfat (APS)		
30% NR-Acrylamide/Bis- (29:1)	417 µl	1.9 ml

4.4.2 Immunoblot analysis

Immunoblot analysis was used for detecting specific proteins. Proteins were first separated by SDS-PAGE and transferred onto a PVDF membrane (Millipore, USA) using semi-dry westen-blot transfer by the PerfectBlue™ Semi-Dry-Elektro Blotter (Peqlab, USA). The PVDF membrane was first activated in methanol for 15 s, washed in water for 2 min followed a 5 min incubation in western-blot transfer buffer [25 mM Tris Base, 192 mM glycine, 10% (v/v) methanol]. The SDS gel was laid upon the activated PVDF membrane and transferred by PerfectBlue™ Semi-Dry-Elektro Blotter (Peqlab, USA) at 2 mA/cm² for 1.5 h. The transferred membrane was then incubated with blocking buffer, which is the TBST buffer [10 mM Tris Base, 150 mM NaCl, 0.1% (w/v) Tween20, pH 7.5]containing 1.5% (w/v) non-fat milk power, for 1-2 h at room temperature or overnight at 4 °C. Subsequently, the membrane was incubated with a specific antibody in blocking buffer for 1.5 h at room temperature. After three times washing in TBST buffer each time 5 min, the membrane was then incubated with the secondary antibody, an anti-rabbit IgG conjugated with horseradish perioxidase (HRP), in blocking buffer for 2 h at room temperature. Subsequently, the membrane was washed five times with TBST buffer, followed by 1 min incubation in 0.8 ml chemiluminescence substrate (Western Lightning™ Chemiluminescence Reagent Plus; Perkin Elmer, USA). The detected protein signal was visualized by exposing the membrane to Amersham Hyperfilm™ ECL-Chemiluminenscence films (GE Healthcare, Germany), which were developed in an LAS-4000 Luminescent Image Analyzer (Fujifilm, Germany).

4.4.3 Protein purification

MipZ and its mutant variants in hexahistidine-tagged forms were synthesized in Rosetta™2(DE3)pLysS (4.2.7) and the cell pellets were collected and frozen at -80 °C. To purify the proteins, the pellet was thawed and resuspended in buffer B3 (50 mM NaH_2PO_4, 300 mM NaCl, 20 mM imidazole, 1 mM β-mercaptoethanol, pH8.0) with 3-5×pellet volume, supplemented with 100 µg/ml PMSF (phenylmethylsulfonyl fluoride) and 10 U/ml DNase I. Afterwards, cells were lyzed by passing through French press two times at 16000 psi, and the cell debris were removed by centrifugation at 3000× g for 30 min, the supernatant was then

passed through a 0.2 µm filter (Sarstedt, Germany) and then loaded onto a HisTrap column (GE Healthcare, Germany), and followed by a step of equilibrium with B3, subsequently, the protein was eluted with linear gradient of imidazole buffer (50 mM NaH_2PO_4, 300 mM NaCl, 20-250 mM imidazole, pH8). The elution fractions were collected in 2 ml aliquots, the fractions containing interesting protein were collected and dialyzed against 3 L B6 buffer (50 mM HEPES, pH 7.2, 50 mM NaCl, 5 mM $MgCl_2$, 0.1 mM EDTA, 10% glycerol) overnight at 4˚C. The resulting protein sample was centrifuged at 3000× g for 30 min to remove the percipient. To this end, the protein was snap frozen in liquid nitrogen and stored at -80˚C in 100 µl aliquots.

4.4.4 Nucleotide hydrolysis assays

The ATPase activity of hexahistidine-tagged form of MipZ or its derivatives, and the GTPase activity of tag-free FtsZ were analyzed as described (20, 21). Briefly, to determine the nucleotide hydrolysis activity, 6 µM MipZ or its variants were pre-incubated in P buffer (50 mM Hepes/NaOH, pH 7.2, 50 mM KCl, 10 mM $MgCl_2$) at 30 °C for 10 min. Afterwards 1 mM ATP containing 25 Ci/mmol [α-32P]-ATP was added into the protein samples, time was recorded. In every 10 min interval, 2 µl samples were taken and immediately spotted onto PEI cellulose F thin-layer chromatography plates (Merck, Germany) samples were taken and spotted for 60 min. The plates were then subjected to the chromatography in a solvent system containing 0.5 M LiCl and 1 M formic acid. To this end, the air-dried plates were expose to a storage phosphor screen (GE Healthcare, Germany) and scanned with a Storm 840 PhosphorImager (GE Healthcare, Germany), the amount of [α-32P]-ADP present in the samples was quantified using ImageQuant 5.2. The GTPase activity of FtsZ was measured the same way but with 3 µM FtsZ as the starting sample, 2 mM GTP containing 25 Ci/mmol [α-32P]-GTP in every starting sample, and the reaction sample was taken in 5 min interval till 30 min.

4.4.5 Gel shift assay

Gel shift assay is a method to detect DNA binding activities of MipZ and its variants. 10 µM proteins together with 20 nM super coiled plasmid pMCS-2 or 10 nM EcoRI linearized pMCS-2 were incubated with 1 mM ATP or 0.46 mM ATPγS in SPR buffer (10 mM Hepes/NaOH pH 7.2, 150 mM NaCl, 10 mM $MgCl_2$, 0.05% Tween 20) at room temperature for 15 min and then samples were applied for a standard DNA agarose gel electrophoresis (4.3.5).

4.4.6 Surface Plasmon Resonance (SPR)

SPR is used to detect the interactions between MipZ or its mutant variants and oligonucleotide. The experiment was performed in Biacore T100 System (GE Healthcare, Germany) at 10 °C in SPR buffer with flow rate of 30 µl/min. To detect the interaction a pair of oligonucleotide (rand1-biotin and rand1-rev), was first annealed and immobilized on a streptavidin coated SA sensor Chip (GE Healthcare, Germany) following the manufacturer's instruction. 6 µM proteins supplemented with 1 mM ATP/ADP or without nucleotide were diluted in SPR buffer and loaded onto the Biacore T100 System, after the protein binding step, the chip was washed with

the SPR buffer. After that, the chip was regenerated by injecting the buffer (2M NaCl in SPR buffer). To correct the unspecific binding, a mock-treated cell in the chip without oliogonucleotides was used as the reference.

4.4.7 MicroScale Thermophoresis (MST) analysis

Using microscale thermophoresis to determine biomolecules interaction was developed by Baaske *et al* (140). This method is used to determine the binding affinities between oligonucleotide and MipZ or its variants. We had two different titration approaches to determine the dissociation constants (k_d): either titrated the constant concentration of the fluorescently labeled oligonucleotide with increased concentration of proteins or titrate the constant concentration of fluorescently labeled proteins with increased concentration of oligonucleotide. For the first approach, oligonucleotide, a 5' end Cy3 labeled oligonucleotide cy3-rand1 and an unlabeled oligonucleotide rand1-rev was annealed and diluted to a final concentration of 50 nM. Proteins were serially diluted 16 times with the SPR buffer supplemented with 1 mM ATP or 0.46 mM ATPγS and mixed with the double stranded-oligonucleotide. The reaction solution was loaded into hydrophilic capillaries (NanoTemper, Germany), which were arranged into Monolith NT.115 (NanoTemper, Germany). The MST measurements were performed with 20-40% LED power, 20% MST power. For the second titration approach, the two unlabeled oligonucleotides strands rand1 and rand1-rev were annealed. The proteins were either labeled at amine with protein labeling Kit RED-NHS (NanoTemper, Germany) or at cysteine with protein labeling Kit RED-MALEIMIDE (NanoTemper, Germany) following the manufacturer's instruction. The double-stranded oligonucleotide was serially diluted 12-16 times in SPR running buffer supplemented with 1 mM ATP or 0.46 mM ATPγS with the maximum concentration of 200 µM. Proteins were mixed with the serially diluted double-stranded DNA, and loaded into hydrophilic capillaries and then subjected to MST measurements with 60-80% LED power and 20% MST power.

4.5 Microscopy

Microscopy was used to visualize *C. crescentus* and *E. coli* cells and their cellular fluorescently-labeled proteins. Cell samples were immobilized by 1.5% agarose pads and imaged by an Axio Imager.M1 microscope (Zeiss, Germany) having a Photometrics Cascade: 1K CCD camera or a Zeiss Axio Imager Z1 microscope having a pco.edge sCMOS camera. DIC (differential interference contrast) images, Ph (phase contrast) images were acquired via Zeiss Plan-Apochromat 100x/1.40 Oil DIC objective and Objective Plan-Apochromat 100x/1.40 Oil Ph3 M27 respectively. Fluorescent images were taken via the X-Cite®120PC metal halide light source (EXFO, Canada) and ET-DAPI, ET-CFP, ET-YFP, ET-GFP or ET-TexasRed filter cubes (Chroma, USA). The acquired images were analyzed with Metamorph 7.7 (Universal Imaging Group).

To detect the localization of MipZ*-eYFP fusion proteins, the corresponding *C. crescentus* cells were induced with 0.3% xylose for 6-8 h. To visualize nucleoid of *E. coli*, the cells were stained with 0.5 µg/ml DAPI (4', 6-diamidino-2-phenylindole) for 30 min in dark.

4.6 Bioinformatic analysis

Amino acid sequences of MipZ proteins were obtained either from the national center for biotechnology information (NCBI) (http://www.ncbi.nlm.nih.gov/) or Pfam (http://pfam.sanger.ac.uk/). Sequence alignments were conducted by Clustal Omega at https://www.ebi.ac.uk/Tools/msa/clustalo/, and the alignment results were analyzed by GeneDoc.

APPENDIX

Table 4.6 oligonucleotides

Name	Sequence (5' to 3')
CC2165-uni2	ttttcatatggccgaaacgcgcgttatcgtcg
CC2165-rev2	ttgagctcctgcgccgccagcatcgtctcgcc
CC2165-rev-HindIII	ccgcaagcttgtcgacggcctgcgccgccagcatcgtctcgcc
eGYC-down	gctgctgcccgacaaccactacctgag
eGYC-up	cttcccgtaggtggcatcgccctcg
IntSpec-1 (RecUni-1)	atgccgtttgtgatggcttccatgtcg
IntXyl-2 (RecXyl-2)	tcttccggcaggaattcactcacgcc
MipZE53A- for	cgcggttcttcgcgaaccgccgcgc
MipZE53A -rev	gcgcggcggttcgcgaagaaccgcg
MipZR55A- for	gttcttcgagaacgcccgcgcgtggctg
MipZR55A-rev	cagccacgcgcgggcgttctcgaagaac
MipZW58A-for	gaaccgccgcgcggcgctggacaacaag
MipZW58A-rev	cttgttgtccagcgccgcgcggcggttc
MipZE65A-for	caacaagaagatcgcgcttcccgagccgc
MipZE65A-rev	gcggctcgggaagcgcgatcttcttgttg
MipZD76A-for	cttgaacctcagcgccaacgacgtcgccc
MipZD76A-rev	gggcgacgtcgttggcgctgaggttcaag
MipZE94A-for	tggccggtttcgcagccgccttcgc
MipZE94A-rev	gcgaaggcggctgcgaaaccggcca
MipZR99A-for	gccgccttcgccgcggccatggccga
MipZR99A-rev	tcggccatggccgcggcgaaggcggc
MipZE103A-for	cagggccatggccgcatgcgacttcatcc
MipZE103A-rev	ggatgaagtcgcatgcggccatggccctg
MipZL161A-for	cccagcctctattcggcgaccgtctgggaagg
MipZL161A-rev	ccttcccagacggtcgccgaatagaggctggg
MipZE165A-for	ctgaccgtctgggcaggtcgcaagcag
MipZE165A-rev	ctgcttgcgacctgcccagacggtcag
MipZL172A-for	aagcagcgcgccgcgtcgggccagcg
MipZL172A-rev	cgctggcccgacgcggcgcgctgctt
MipZR213A-for	cgcgtcggcttcgcgatcgggcccgg
MipZR213A-rev	cgcggttcttcgcgaaccgccgcgc
MipZD236A-for	gcgcggcggttcgcgaagaaccgcg
MipZD236A-rev	gttcttcgagaacgcccgcgcgtggctg
MipZL237A-for	cagccacgcgcgggcgttctcgaagaac
MipZL237A-rev	gaaccgccgcgcggcgctggacaacaag
MipZR242A-for	cgccgcaggtggccccggtcccgg

Name	Sequence (5’ to 3’)
MipZR242A-rev	ccgggaccggggccacctgcggcg
MipZV246A-for	cccggtcccggcgtcgctgcagc
MipZV246A-rev	gctgcagcgacgccgggaccggg
MipZL248A-for	ggtcccggtgtcggcgcagcatctggcg
MipZL248A-rev	cgccagatgctgcgccgacaccgggacc
MipZY269A-for	gggtctgtcggccgcttccggcgagacg
MipZY269A-rev	cgtctcgccggaagcggccgacagaccc
MipZK35A-for	gtacggcggcgccgcggtcgctgtcatc
MipZK35A-rev	gatgacagcgaccgcggcgccgccgtac
MipZE86A-for	gctgaaaggccggcggaggagcaggtg
MipZE86A-rev	cacctgctcctccgccggcctttcagc
MipZR125A-for	catggcccacggcgctgcggacctggtg
MipZR125-rev	caccaggtccgcagcgccgtgggccatg
MipZD147-for	ctgggcaccgttgctcccgtcaccctg
MipZD147-rev	cagggtgacgggagcaacggtgcccag
MipZE152A-for	ccgtcaccctggcgctgaccaagcc
MipZE152-rev	ggcttggtcagcgccagggtgacgg
MipZW164A-for	ctattcgctgaccgtcgcggaaggtcgcaagcag
MipZW164A-rev	ctgcttgcgaccttccgcgacggtcagcgaatag
MipZR194 A-for	caccaccgaggcggcgaaccgcaagcgt
MipZR194A-rev	acgcttgcggttcgccgcctcggtggtg
MipZK197A-for	ggcgcggaaccgcgcgcgtctggaggac
MipZK197A-rev	gtcctccagacgcgcgcggttccgcgcc
MipZR198A-for	gcggaaccgcaaggctctggaggaccgc
MipZR198A-rev	gcggtcctccagagccttgcggttccgc
MipZE200A-for	cgcaagcgtctggcggaccgcctcaac
MipZE200A-rev	gttgaggcggtccgccagacgcttgcg
MipZR219A-for	ggcccggcctggccgaccgcgtga
MipZR219A-rev	tcacgcggtcggccaggccgggcc
MipZH262A-for	ctgcgtgctctgatggccagcctgggtctgtc
MipZH262A-rev	gacagacccaggctggccatcagagcacgcag
MipZK155A-for	accctggagctgaccgcgcccagcctctattc
MipZK155A-rev	gaatagaggctgggcgcggtcagctccagggt
MipZE3A-for	gaccatatggccgcaacgcgcgttatc
MipZE3A-rev	gataacgcgcgtttcggccatatggtc
MipZR5A-for	gaccatatggccgaaacggccgttatcgtcgtc
MipZR5A-rev	gacgacgataaccggcgtttcggccatatg
MipZR221A-for	ccggcctgcgcgacgccgtgatctatcgc
MipZR221A-rev	gcgatagatcacggcgtcgcgcaggccgg
MipZ rev-EcoI	ttgaattcttactgcgccgccagcatcgtctc
MipZ-rev	ttgagctcgcgccgccagcatcgtctcgccgga
MipZ-BACTH-for	ttttggatcccatggccgaaacgcgcgttatcgtcg
MipZ-KT25-rev	aaaagaattctttactgcgccgccagcatcgtctcgcc
MipZ-KNT25-rev	aaaagaattcgactgcgccgccagcatcgtctcgcc

Name	Sequence (5' to 3')
pBAD24-rev	accgcttctgcgttctgatttaatc
pBAD24-uni	cctacctgacgctttttatcgcaac
pET-for	cacgatgcgtccggcgtagaggatc
PvanA-for	gacgtccgtttgattacgatcaagattgg
Pxyl-1	cccacatgttagcgctaccaagtgc
rand1-Cy3	Cy3-gaggcagactagatcttctagttcgg
rand1-biotin	Biothin-gaggcagactagatcttctagttcgg
rand1-rev	ccgaactagaagatctagtctgcctc

Table 4.7 plasmids

Plasmid	Description	Reference
pET21a+	Vector for overexpression of C-terminally His_6-tagged proteins, Amp^R	Novagen
pXYFPC-2	Integration plasmid fuse 3' end of a target gene to *eyfp* under the control of P_{xyl}, Kan^R	(141)
pVCERN-1	Integration plasmid fuse 5' end of a target gene to *venus* under the control of P_{van}, $Spec^R$	
pUT18	Plasmid for constructing C-terminal fusions to T18, Amp^R	(142)
pKNT25	Plasmid for constructing C-terminal fusions to T25, Kan^R	(142)
pUT18C-zip	Derivative of pUT18C in which the leucine zipper of GCN4 is fused in frame to the T18 fragment , Amp^R	(142)
pKT25-zip	Derivative of pKT25 in which the leucine zipper of GCN4 is fused in frame to the T25 fragment, $Kcan^R$	(142)
pGADT7	Plasmid for constructing N-terminal fusion of activation domain of Gal4	Clontech
pGBKT7	Plasmid for constructing N-terminal fusion of DNA-binding domain of Gal4	Clontech
pBAD24-CB	Plasmid for the expression of genes in *E. coli* under the control of P_{BAD}, Amp^R	(143)
pDK3	pBAD24-CB carrying $mipZ_{D42A}$	(20)
pJET1.2	Plasmid for blunt end ligation	Thermo scientific
pMT182	pMR31carrying *mipZ*	(21)

Plasmid	Description	Reference
pBH8	pJET1.2 carrying *mipZ*	This study
pBH46	pXYFPC-2 carring $mipZ_{K35A}$	This study
pBH47	pXYFPC-2 carring $mipZ_{E53A}$	This study
pBH48	pXYFPC-2 carring $mipZ_{R55A}$	This study
pBH49	pXYFPC-2 carring $mipZ_{W58A}$	This study
pBH50	pXYFPC-2 carring $mipZ_{D76A}$	This study
pBH51	pXYFPC-2 carring $mipZ_{R84A}$	This study
pBH52	pXYFPC-2 carring $mipZ_{E86A}$	This study
pBH53	pXYFPC-2 carring $mipZ_{E94A}$	This study
pBH54	pXYFPC-2 carring $mipZ_{R99A}$	This study
pBH55	pXYFPC-2 carring $mipZ_{E103A}$	This study
pBH56	pXYFPC-2 carring $mipZ_{R125A}$	This study
pBH57	pXYFPC-2 carring $mipZ_{D147A}$	This study
pBH58	pXYFPC-2 carring $mipZ_{E152A}$	This study
pBH59	pXYFPC-2 carring $mipZ_{L161A}$	This study
pBH60	pXYFPC-2 carring $mipZ_{W164A}$	This study
pBH61	pXYFPC-2 carring $mipZ_{E165A}$	This study
pBH62	pXYFPC-2 carring $mipZ_{L172A}$	This study
pBH63	pXYFPC-2 carring $mipZ_{R194A}$	This study
pBH64	pXYFPC-2 carring $mipZ_{K197A}$	This study
pBH65	pXYFPC-2 carring $mipZ_{R198A}$	This study
pBH66	pXYFPC-2 carring $mipZ_{E200A}$	This study
pBH67	pXYFPC-2 carring $mipZ_{R213A}$	This study
pBH68	pXYFPC-2 carring $mipZ_{R219A}$	This study
pBH69	pXYFPC-2 carring $mipZ_{D236A}$	This study
pBH70	pXYFPC-2 carring $mipZ_{L237A}$	This study

Plasmid	Description	Reference
pBH71	pXYFPC-2 carring *mipZ*$_{R242A}$	This study
pBH72	pXYFPC-2 carring *mipZ*$_{V246A}$	This study
pBH73	pXYFPC-2 carring *mipZ*$_{L248A}$	This study
pBH74	pXYFPC-2 carring *mipZ*$_{H262A}$	This study
pBH75	pXYFPC-2 carring *mipZ*$_{Y269A}$	This study
pBH76	pXYFPC-2 carring *mipZ*$_{K155A}$	This study
pBH77	pXYFPC-2 carring *mipZ*$_{E65A}$	This study
pBH78	pXYFPC-2 carring *mipZ*	This study
pBH79	pXYFPC-2 carring *mipZ*$_{K13A}$	This study
pBH80	pXYFPC-2 carring *mipZ*$_{G14V}$	This study
pBH81	pXYFPC-2 carring *mipZ*$_{D42A}$	This study
pBH100	pVCERN-1 carring mipZ	This study
pBH103	pXYFPC-2 carring *mipZ*$_{3EA}$	This study
pBH104	pXYFPC-2 carring *mipZ*$_{R5A}$	This study
pBH135	pXYFPC-2 carring mipZR221A	This study
pBH82	pGADT7 carring *mipZ*	This study
pBH83	pGADT7 carring *mipZ*$_{R194A}$	This study
pBH84	pGADT7 carring *mipZ*$_{R219A}$	This study
pBH85	pGADT7 carring *mipZ*$_{R242A}$	This study
pBH105	pGADT7 carring *mipZ*$_{L248A}$	This study
pBH121	pGADT7 carring *mipZ*$_{K13A}$	This study
pBH122	pGADT7 carring *mipZ*$_{G14V}$	This study
pBH123	pGADT7 carring *mipZ*$_{D42A}$	This study
pBH124	pGADT7 carring *mipZ*$_{R198A}$	This study
pBH125	pGADT7 carring *mipZ*$_{D236A}$	This study
pBH126	pGADT7 carring *mipZ*$_{L237A}$	This study

Plasmid	Description	Reference
pBH89	pGADT7 carring *mipZ*$_{K197A}$	This study
pBH90	pGADT7 carring *mipZ*$_{L248A}$	This study
pBH91	pGADT7 carring *mipZ*$_{R194A}$	This study
pBH92	pGADT7 carring *mipZ*$_{R219A}$	This study
pBH98	pGADT7 carring *mipZ*$_{L237A}$	This study
pBH101	pGADT7 carring *mipZ*$_{R242A}$	This study
pBH102	pGADT7 carring *mipZ*$_{V246A}$	This study
pBH107	pGADT7 carring *mipZ*$_{D147A}$	This study
pBH108	pGADT7 carring *mipZ*$_{W58A}$	This study
pBH109	pGADT7 carring *mipZ*$_{R198A}$	This study
pBH110	pGADT7 carring *mipZ*$_{D236A}$	This study
pBH132	pGADT7 carring *mipZ*$_{R221A}$	This study
pBH94	pET21a+ carring *mipZ*$_{L237A}$	This study
pBH95	pET21a+ carring *mipZ*$_{R219A}$	This study
pBH97	pET21a+ carring *mipZ*$_{R194A}$	This study
pBH117	pET21a+ carring *mipZ*$_{R198A}$	This study
pBH118	pET21a+ carring *mipZ*$_{D236A}$	This study
pBH119	pET21a+ carring *mipZ*$_{R242A}$	This study
pBH120	pET21a+ carring *mipZ*$_{L248A}$	This study
pBH130	pET21a+ carring *mipZ*$_{R221A}$	This study
pBH106	pBAD24-CB carrying *mipZ*$_{D42AR194A}$-*eyfp*	This study
pBH111	pBAD24-CB carrying *mipZ*$_{D42AR198}$-*eyfp*	This study
pBH112	pBAD24-CB carrying *mipZ*$_{D42AR219A}$-*eyfp*	This study
pBH113	pBAD24-CB carrying *mipZ*$_{D42AL237A}$-*eyfp*	This study
pBH114	pBAD24-CB carrying *mipZ*$_{D42AR242A}$-*eyfp*	This study
pBH115	pBAD24-CB carrying *mipZ*$_{D42AL248A}$-*eyfp*	This study

Plasmid	Description	Reference
pBH116	pBAD24-CB carrying *mipZ*$_{D42AD236A}$-*eyfp*	This study
pBH131	pBAD24-CB carrying *mipZ*$_{D42AR212A}$-*eyfp*	This study
pBH88	pKNT25 carrying *mipZ*$_{L172A}$	This study
pBH89	pKNT25 carrying *mipZ*$_{K197A}$	This study
pBH90	pKNT25 carrying *mipZ*$_{L248A}$	This study
pBH91	pKNT25 carrying *mipZ*R$_{194A}$	This study
pBH92	pKNT25 carrying *mipZ*$_{R219A}$	This study
pBH98	pKNT25 carrying *mipZ*$_{L237A}$	This study
pBH101	pKNT25 carrying *mipZ*$_{R242A}$	This study
pBH102	pKNT25 carrying *mipZ*$_{V246A}$	This study
pBH107	pKNT25 carrying *mipZ*$_{D147A}$	This study
pBH108	pKNT25 carrying *mipZ*$_{W58A}$	This study
pBH109	pKNT25 carrying *mipZ*$_{R198A}$	This study
pBH110	pKNT25 carrying *mipZ*$_{D236A}$	This study
pBH132	pKNT25 carrying *mipZ*$_{R221A}$	This study

Table 4.8 Strains

strains	Description/ genotype	Reference
CB15N	Wild-type strain of *C. crescentus*	(144)
Rosetta2(DE3)pLysS	*E.coli* Strain for protein overproduction	Invitrogen
TOP10	*E.coli* strain for general cloning strain/MipZ *-YFP production strain	Invitrogen
BTH101	*E.coli* strain for bacterial two-hybrid	Euromedex

strains	Description/genotype	Reference
BH64	CB15N *ΔmipZ* P_{vanA}::P_{vanA}-*mipZ* P_{xylX}::P_{xylX}-*mipZ-eyfp*	This study
BH65	CB15N *ΔmipZ* P_{vanA}::P_{vanA}-*mipZ* P_{xylX}::P_{xylX}-$mipZ_{E3A}$-*eyfp*	This study
BH66	CB15N *ΔmipZ* P_{vanA}::P_{vanA}-*mipZ* P_{xylX}::P_{xylX}-$mipZ_{R5A}$-*eyfp*	This study
BH67	CB15N *ΔmipZ* P_{vanA}::P_{vanA}-*mipZ* P_{xylX}::P_{xylX}-$mipZ_{K35A}$-*eyfp*	This study
BH68	CB15N *ΔmipZ* P_{vanA}::P_{vanA}-*mipZ* P_{xylX}::P_{xylX}-$mipZ_{E53A}$-*eyfp*	This study
BH69	CB15N *ΔmipZ* P_{vanA}::P_{vanA}-*mipZ* P_{xylX}::P_{xylX}-$mipZ_{R55A}$-*eyfp*	This study
BH70	CB15N *ΔmipZ* P_{vanA}::P_{vanA}-*mipZ* P_{xylX}::P_{xylX}-$mipZ_{W58A}$-*eyfp*	This study
BH71	CB15N *ΔmipZ* P_{vanA}::P_{vanA}-*mipZ* P_{xylX}::P_{xylX}-$mipZ_{D76A}$-*eyfp*	This study
BH72	CB15N *ΔmipZ* P_{vanA}::P_{vanA}-*mipZ* P_{xylX}::P_{xylX}-$mipZ_{R84A}$-*eyfp*	This study
BH73	CB15N *ΔmipZ* P_{vanA}::P_{vanA}-*mipZ* P_{xylX}::P_{xylX}-$mipZ_{E86A}$-*eyfp*	This study
BH74	CB15N *ΔmipZ* P_{vanA}::P_{vanA}-*mipZ* P_{xylX}::P_{xylX}-$mipZ_{E94A}$-*eyfp*	This study
BH75	CB15N *ΔmipZ* P_{vanA}::P_{vanA}-*mipZ* P_{xylX}::P_{xylX}-$mipZ_{R99A}$-*eyfp*	This study
BH76	CB15N *ΔmipZ* P_{vanA}::P_{vanA}-*mipZ* P_{xylX}::P_{xylX}-$mipZ_{E103A}$-*eyfp*	This study
BH77	CB15N *ΔmipZ* P_{vanA}::P_{vanA}-*mipZ* P_{xylX}::P_{xylX}-$mipZ_{R125A}$-*eyfp*	This study
BH78	CB15N *ΔmipZ* P_{vanA}::P_{vanA}-*mipZ* P_{xylX}::P_{xylX}-$mipZ_{D147A}$-*eyfp*	This study
BH79	CB15N *ΔmipZ* P_{vanA}::P_{vanA}-*mipZ* P_{xylX}::P_{xylX}-$mipZ_{E152A}$-*eyfp*	This study
BH80	CB15N *ΔmipZ* P_{vanA}::P_{vanA}-*mipZ* P_{xylX}::P_{xylX}-$mipZ_{L161A}$-*eyfp*	This study
BH81	CB15N *ΔmipZ* P_{vanA}::P_{vanA}-*mipZ* P_{xylX}::P_{xylX}-$mipZ_{W164A}$-*eyfp*	This study
BH82	CB15N *ΔmipZ* P_{vanA}::P_{vanA}-*mipZ* P_{xylX}::P_{xylX}-$mipZ_{E165A}$-*eyfp*	This study
BH83	CB15N *ΔmipZ* P_{vanA}::P_{vanA}-*mipZ* P_{xylX}::P_{xylX}-$mipZ_{L172A}$-*eyfp*	This study
BH84	CB15N *ΔmipZ* P_{vanA}::P_{vanA}-*mipZ* P_{xylX}::P_{xylX}-$mipZ_{R194A}$-*eyfp*	This study
BH85	CB15N *ΔmipZ* P_{vanA}::P_{vanA}-*mipZ* P_{xylX}::P_{xylX}-$mipZ_{K197A}$-*eyfp*	This study
BH86	CB15N *ΔmipZ* P_{vanA}::P_{vanA}-*mipZ* P_{xylX}::P_{xylX}-$mipZ_{R198A}$-*eyfp*	This study
BH87	CB15N *ΔmipZ* P_{vanA}::P_{vanA}-*mipZ* P_{xylX}::P_{xylX}-$mipZ_{E200A}$-*eyfp*	This study
BH88	CB15N *ΔmipZ* P_{vanA}::P_{vanA}-*mipZ* P_{xylX}::P_{xylX}-$mipZ_{R213A}$-*eyfp*	This study
BH89	CB15N *ΔmipZ* P_{vanA}::P_{vanA}-*mipZ* P_{xylX}::P_{xylX}-$mipZ_{R219A}$-*eyfp*	This study

strains	Description/ genotype	Reference
BH90	CB15N *ΔmipZ* P_{vanA}::P_{vanA}-*mipZ* P_{xylX}::P_{xylX}-*mipZ*$_{D236A}$-*eyfp*	This study
BH91	CB15N *ΔmipZ* P_{vanA}::P_{vanA}-*mipZ* P_{xylX}::P_{xylX}-*mipZ*$_{L237A}$-*eyfp*	This study
BH92	CB15N *ΔmipZ* P_{vanA}::P_{vanA}-*mipZ* P_{xylX}::P_{xylX}-*mipZ*$_{R242A}$-*eyfp*	This study
BH93	CB15N *ΔmipZ* P_{vanA}::P_{vanA}-*mipZ* P_{xylX}::P_{xylX}-*mipZ*$_{V246A}$-*eyfp*	This study
BH94	CB15N *ΔmipZ* P_{vanA}::P_{vanA}-*mipZ* P_{xylX}::P_{xylX}-*mipZ*$_{L248A}$-*eyfp*	This study
BH95	CB15N *ΔmipZ* P_{vanA}::P_{vanA}-*mipZ* P_{xylX}::P_{xylX}-*mipZ*$_{H262A}$-*eyfp*	This study
BH96	CB15N *ΔmipZ* P_{vanA}::P_{vanA}-*mipZ* P_{xylX}::P_{xylX}-*mipZ*$_{Y269A}$-*eyfp*	This study
BH97	CB15N *ΔmipZ* P_{vanA}::P_{vanA}-*mipZ* P_{xylX}::P_{xylX}-*mipZ*$_{K155A}$-*eyfp*	This study
BH98	CB15N *ΔmipZ* P_{vanA}::P_{vanA}-*mipZ* P_{xylX}::P_{xylX}-*mipZ*$_{E65A}$-*eyfp*	This study
BH99	CB15N *ΔmipZ* P_{vanA}::P_{vanA}-*mipZ* P_{xylX}::P_{xylX}-*mipZ*$_{D42A}$-*eyfp*	This study
BH100	CB15N *ΔmipZ* P_{vanA}::P_{vanA}-*mipZ* P_{xylX}::P_{xylX}-*mipZ*$_{K13A}$-*eyfp*	This study
BH101	CB15N *ΔmipZ* P_{vanA}::P_{vanA}-*mipZ* P_{xylX}::P_{xylX}-*mipZ*$_{G14V}$-*eyfp*	This study
BH118	CB15N *ΔmipZ* P_{vanA}::P_{vanA}-*mipZ* P_{xylX}::P_{xylX}-*mipZ*$_{R221A}$-*eyfp*	This study

REFERENCES

1. Murray SM, Panis G, Fumeaux C, Viollier PH, Howard M. 2013. Computational and genetic reduction of a cell cycle to its simplest, primordial components. *PLoS biology* 11:e1001749.

2. Poindexter JS. 1964. Biological Properties and Classification of the *Caulobacter* Group. *Bacteriological reviews* 28:231-295.

3. Thanbichler M. 2009. Spatial regulation in *Caulobacter crescentus*. *Current opinion in microbiology* 12:715-721.

4. Willard M. 2002. Rapid directional translocations in virus replication. *Journal of virology* 76:5220-5232.

5. Reyes-Lamothe R, Nicolas E, Sherratt DJ. 2012. Chromosome replication and segregation in bacteria. *Annual review of genetics* 46:121-143.

6. Wang X, Montero Llopis P, Rudner DZ. 2013. Organization and segregation of bacterial chromosomes. *Nature reviews. Genetics* 14:191-203.

7. Harms A, Treuner-Lange A, Schumacher D, Sogaard-Andersen L. 2013. Tracking of chromosome and replisome dynamics in *Myxococcus xanthus* reveals a novel chromosome arrangement. *PLoS genetics* 9:e1003802.

8. Thadani R, Uhlmann F, Heeger S. 2012. Condensin, chromatin crossbarring and chromosome condensation. *Current biology* : CB 22:R1012-1021.

9. Stouf M, Meile JC, Cornet F. 2013. FtsK actively segregates sister chromosomes in *Escherichia coli*. *Proc Natl Acad Sci U S A* 110:11157-11162.

10. Nolivos S, Sherratt D. 2013. The bacterial chromosome: architecture and action of bacterial SMC and SMC-like complexes. *FEMS microbiology reviews*.

11. Kaur T, Al Abdallah Q, Nafissi N, Wettig S, Funnell BE, Slavcev RA. 2011. ParAB-mediated intermolecular association of plasmid P1 *parS* sites. *Virology* 421:192-201.

12. Donovan C, Schwaiger A, Kramer R, Bramkamp M. 2010. Subcellular localization and characterization of the ParAB system from *Corynebacterium glutamicum*. *Journal of bacteriology* 192:3441-3451.

13. Leonard TA, Butler PJ, Lowe J. 2005. Bacterial chromosome segregation: structure and DNA binding of the Soj dimer--a conserved biological switch. *The EMBO journal* 24:270-282.

14. Ptacin JL, Lee SF, Garner EC, Toro E, Eckart M, Comolli LR, Moerner WE, Shapiro L. 2010. A spindle-like apparatus guides bacterial chromosome segregation. *Nature cell biology* 12:791-798.

15. Mierzejewska J, Jagura-Burdzy G. 2012. Prokaryotic ParA-ParB-*parS* system links bacterial chromosome segregation with the cell cycle. *Plasmid* 67:1-14.

16. Banigan EJ, Gelbart MA, Gitai Z, Wingreen NS, Liu AJ. 2011. Filament depolymerization can explain chromosome pulling during bacterial mitosis. *PLoS computational biology* 7:e1002145.

17. Hwang LC, Vecchiarelli AG, Han YW, Mizuuchi M, Harada Y, Funnell BE, Mizuuchi K. 2013. ParA-mediated plasmid partition driven by protein pattern self-organization. *The EMBO journal* 32:1238-1249.

18. Vecchiarelli AG, Hwang LC, Mizuuchi K. 2013. Cell-free study of F plasmid partition provides evidence for cargo transport by a diffusion-ratchet mechanism. *Proc Natl Acad Sci U S A* 110:E1390-1397.

19. Kiekebusch D, Thanbichler M. 2013. Spatiotemporal organization of microbial cells by protein concentration gradients. *Trends Microbiol*.

20. Kiekebusch D, Michie KA, Essen LO, Lowe J, Thanbichler M. 2012. Localized dimerization and nucleoid binding drive gradient formation by the bacterial cell division inhibitor MipZ. *Mol Cell* 46:245-259.

21. Thanbichler M, Shapiro L. 2006. MipZ, a spatial regulator coordinating chromosome segregation with cell division in *Caulobacter*. *Cell* 126:147-162.

22. Bowman GR, Comolli LR, Zhu J, Eckart M, Koenig M, Downing KH, Moerner WE, Earnest T, Shapiro L. 2008. A polymeric protein anchors the chromosomal origin/ParB complex at a bacterial cell pole. *Cell* 134:945-955.

23. Donovan C, Schauss A, Kramer R, Bramkamp M. 2013. Chromosome segregation impacts on cell growth and division site selection in *Corynebacterium glutamicum. PloS one* 8:e55078.

24. Ireton K, Gunther NWt, Grossman AD. 1994. *spo0J* is required for normal chromosome segregation as well as the initiation of sporulation in *Bacillus subtilis. Journal of bacteriology* 176:5320-5329.

25. Flardh K, Buttner MJ. 2009. *Streptomyces* morphogenetics: dissecting differentiation in a filamentous bacterium. *Nature reviews*. Microbiology 7:36-49.

26. Livny J, Yamaichi Y, Waldor MK. 2007. Distribution of centromere-like *parS* sites in bacteria: insights from comparative genomics. *Journal of bacteriology* 189:8693-8703.

27. Mohl DA, Easter J, Jr., Gober JW. 2001. The chromosome partitioning protein, ParB, is required for cytokinesis in *Caulobacter crescentus*. *Molecular microbiology* 42:741-755.

28. Iniesta AA. 2014. ParABS System in Chromosome Partitioning in the Bacterium *Myxococcus xanthus. PloS one* 9:e86897.

29. Jensen RB, Shapiro L. 2003. Cell-cycle-regulated expression and subcellular localization of the *Caulobacter crescentus* SMC chromosome structural protein. *Journal of bacteriology* 185:3068-3075.

30. Sawitzke JA, Austin S. 2000. Suppression of chromosome segregation defects of *Escherichia coli muk* mutants by mutations in topoisomerase I. *Proc Natl Acad Sci U S A* 97:1671-1676.

31. Britton RA, Lin DC, Grossman AD. 1998. Characterization of a prokaryotic SMC protein involved in chromosome partitioning. *Genes & development* 12:1254-1259.

32. Danilova O, Reyes-Lamothe R, Pinskaya M, Sherratt D, Possoz C. 2007. MukB colocalizes with the oriC region and is required for organization of the two *Escherichia coli* chromosome arms into separate cell halves. *Molecular microbiology* 65:1485-1492.

33. Gruber S, Errington J. 2009. Recruitment of condensin to replication origin regions by ParB/SpoOJ promotes chromosome segregation in *B. subtilis. Cell* 137:685-696.

34. Gruber S, Veening JW, Bach J, Blettinger M, Bramkamp M, Errington J. 2014. Interlinked Sister Chromosomes Arise in the Absence of Condensin during Fast Replication in *B. subtilis*. *Current biology* : CB 24:293-298.

35. Schwartz MA, Shapiro L. 2011. An SMC ATPase mutant disrupts chromosome segregation in *Caulobacter*. *Molecular microbiology* 82:1359-1374.

36. Toro E, Hong SH, McAdams HH, Shapiro L. 2008. *Caulobacter* requires a dedicated mechanism to initiate chromosome segregation. *Proc Natl Acad Sci U S A* 105:15435-15440.

37. Cattoni DI, Le Gall A, Nollmann M. 2014. Chromosome organization: original condensins. *Current biology* : CB 24:R111-113.

38. Marko JF. 2009. Linking topology of tethered polymer rings with applications to chromosome segregation and estimation of the knotting length. *Physical review*. E, Statistical, nonlinear, and soft matter physics 79:051905.

39. Grainge I. 2013. Simple topology: FtsK-directed recombination at the *dif* site. *Biochemical Society transactions* 41:595-600.

40. Lee JY, Finkelstein IJ, Crozat E, Sherratt DJ, Greene EC. 2012. Single-molecule imaging of DNA curtains reveals mechanisms of KOPS sequence targeting by the DNA translocase FtsK. *Proc Natl Acad Sci U S A* 109:6531-6536.

41. Bigot S, Saleh OA, Lesterlin C, Pages C, El Karoui M, Dennis C, Grigoriev M, Allemand JF, Barre FX, Cornet F. 2005. KOPS: DNA motifs that control *E. coli* chromosome segregation by orienting the FtsK translocase. *The EMBO journal* 24:3770-3780.

42. Aussel L, Barre FX, Aroyo M, Stasiak A, Stasiak AZ, Sherratt D. 2002. FtsK Is a DNA motor protein that activates chromosome dimer resolution by switching the catalytic state of the XerC and XerD recombinases. *Cell* 108:195-205.

43. Steiner W, Liu G, Donachie WD, Kuempel P. 1999. The cytoplasmic domain of FtsK protein is required for resolution of chromosome dimers. *Molecular microbiology* 31:579-583.

44. Bigot S, Marians KJ. 2010. DNA chirality-dependent stimulation of topoisomerase IV activity by the C-terminal AAA+ domain of FtsK. *Nucleic acids research* 38:3031-3040.

45. Grainge I. 2010. FtsK--a bacterial cell division checkpoint? *Molecular microbiology* 78:1055-1057.

46. Mohl DA, Gober JW. 1997. Cell cycle-dependent polar localization of chromosome partitioning proteins in *Caulobacter crescentus. Cell* 88:675-684.

47. Laloux G, Jacobs-Wagner C. 2013. Spatiotemporal control of PopZ localization through cell cycle-coupled multimerization. *J Cell Biol* 201:827-841.

48. Schofield WB, Lim HC, Jacobs-Wagner C. 2010. Cell cycle coordination and regulation of bacterial chromosome segregation dynamics by polarly localized proteins. *The EMBO journal* 29:3068-3081.

49. Bowman GR, Comolli LR, Gaietta GM, Fero M, Hong SH, Jones Y, Lee JH, Downing KH, Ellisman MH, McAdams HH, Shapiro L. 2010. *Caulobacter* PopZ forms a polar subdomain dictating sequential changes in pole composition and function. *Molecular microbiology* 76:173-189.

50. Ebersbach G, Briegel A, Jensen GJ, Jacobs-Wagner C. 2008. A self-associating protein critical for chromosome attachment, division, and polar organization in *Caulobacter. Cell* 134:956-968.

51. Lam H, Schofield WB, Jacobs-Wagner C. 2006. A landmark protein essential for establishing and perpetuating the polarity of a bacterial cell. *Cell* 124:1011-1023.

52. Huitema E, Pritchard S, Matteson D, Radhakrishnan SK, Viollier PH. 2006. Bacterial birth scar proteins mark future flagellum assembly site. *Cell* 124:1025-1037.

53. Lutkenhaus J. 2012. The ParA/MinD family puts things in their place. *Trends Microbiol* 20:411-418.

54. Margolin W. 2005. FtsZ and the division of prokaryotic cells and organelles. *Nature reviews*. Molecular cell biology 6:862-871.

55. Nogales E, Downing KH, Amos LA, Lowe J. 1998. Tubulin and FtsZ form a distinct family of GTPases. *Nature structural biology* 5:451-458.

56. Michie KA, Monahan LG, Beech PL, Harry EJ. 2006. Trapping of a spiral-like intermediate of the bacterial cytokinetic protein FtsZ. *Journal of bacteriology* 188:1680-1690.

57. Huang KH, Durand-Heredia J, Janakiraman A. 2013. FtsZ ring stability: of bundles, tubules, crosslinks, and curves. *Journal of bacteriology* 195:1859-1868.

58. Lutkenhaus J, Pichoff S, Du S. 2012. Bacterial cytokinesis: From Z ring to divisome. *Cytoskeleton* 69:778-790.

59. Fu G, Huang T, Buss J, Coltharp C, Hensel Z, Xiao J. 2010. In vivo structure of the *E. coli* FtsZ-ring revealed by photoactivated localization microscopy (PALM). *PloS one* 5:e12682.

60. Strauss MP, Liew AT, Turnbull L, Whitchurch CB, Monahan LG, Harry EJ. 2012. 3D-SIM super resolution microscopy reveals a bead-like arrangement for FtsZ and the division machinery: implications for triggering cytokinesis. *PLoS biology* 10:e1001389.

61. Li Z, Trimble MJ, Brun YV, Jensen GJ. 2007. The structure of FtsZ filaments in vivo suggests a force-generating role in cell division. *The EMBO journal* 26:4694-4708.

62. Holden SJ, Pengo T, Meibom KL, Fernandez Fernandez C, Collier J, Manley S. 2014. High throughput 3D super-resolution microscopy reveals *Caulobacter crescentus in vivo* Z-ring organization. *Proc Natl Acad Sci U S A.*

63. Li Y, Hsin J, Zhao L, Cheng Y, Shang W, Huang KC, Wang HW, Ye S. 2013. FtsZ protofilaments use a hinge-opening mechanism for constrictive force generation. *Science* 341:392-395.

64. Erickson HP. 2009. Modeling the physics of FtsZ assembly and force generation. *Proc Natl Acad Sci U S A* 106:9238-9243.

65. Erickson HP, Anderson DE, Osawa M. 2010. FtsZ in bacterial cytokinesis: cytoskeleton and force generator all in one. *Microbiology and molecular biology reviews* : MMBR 74:504-528.

66. Natale P, Pazos M, Vicente M. 2013. The *Escherichia coli* divisome: born to divide. *Environmental microbiology* 15:3169-3182.

67. Soderstrom B, Skoog K, Blom H, Weiss DS, von Heijne G, Daley DO. 2014. Disassembly of the divisome in *Escherichia coli*: Evidence that FtsZ dissociates before compartmentalisation. *Molecular microbiology*.

68. Du Toit A. 2013. Cytoskeleton: Remodelling the FtsZ network. *Nature reviews*. Molecular cell biology 15:3.

69. Du Toit A. 2014. Bacterial physiology: Remodelling the FtsZ network. *Nature reviews*. Microbiology 12:77.

70. Loose M, Mitchison TJ. 2014. The bacterial cell division proteins FtsA and FtsZ self-organize into dynamic cytoskeletal patterns. *Nature cell biology* 16:38-46.

71. Schwille P. 2014. Bacterial cell division: a swirling ring to rule them all? *Current biology* : CB 24:R157-159.

72. Kuchibhatla A, Bhattacharya A, Panda D. 2011. ZipA binds to FtsZ with high affinity and enhances the stability of FtsZ protofilaments. *PloS one* 6:e28262.

73. Gundogdu ME, Kawai Y, Pavlendova N, Ogasawara N, Errington J, Scheffers DJ, Hamoen LW. 2011. Large ring polymers align FtsZ polymers for normal septum formation. *The EMBO journal* 30:617-626.

74. Goley ED, Dye NA, Werner JN, Gitai Z, Shapiro L. 2010. Imaging-based identification of a critical regulator of FtsZ protofilament curvature in *Caulobacter*. *Mol Cell* 39:975-987.

75. Buss J, Coltharp C, Huang T, Pohlmeyer C, Wang SC, Hatem C, Xiao J. 2013. *In vivo* organization of the FtsZ-ring by ZapA and ZapB revealed by quantitative super-resolution microscopy. *Molecular microbiology* 89:1099-1120.

76. Goley ED, Yeh YC, Hong SH, Fero MJ, Abeliuk E, McAdams HH, Shapiro L. 2011. Assembly of the *Caulobacter* cell division machine. *Molecular microbiology* 80:1680-1698.

77. Ruiz-Avila LB, Huecas S, Artola M, Vergonos A, Ramirez-Aportela E, Cercenado E, Barasoain I, Vazquez-Villa H, Martin-Fontecha M, Chacon P, Lopez-Rodriguez ML, Andreu JM. 2013. Synthetic inhibitors of bacterial cell division targeting the GTP-binding site of FtsZ. *ACS chemical biology* 8:2072-2083.

78. Tsao DH, Sutherland AG, Jennings LD, Li Y, Rush TS, 3rd, Alvarez JC, Ding W, Dushin EG, Dushin RG, Haney SA, Kenny CH, Malakian AK, Nilakantan R, Mosyak L. 2006. Discovery of novel inhibitors of the ZipA/FtsZ complex by NMR fragment screening coupled with structure-based design. *Bioorganic & medicinal chemistry* 14:7953-7961.

79. Sass P, Josten M, Famulla K, Schiffer G, Sahl HG, Hamoen L, Brotz-Oesterhelt H. 2011. Antibiotic acyldepsipeptides activate ClpP peptidase to degrade the cell division protein FtsZ. *Proc Natl Acad Sci U S A* 108:17474-17479.

80. Schaffner-Barbero C, Martin-Fontecha M, Chacon P, Andreu JM. 2012. Targeting the assembly of bacterial cell division protein FtsZ with small molecules. *ACS chemical biology* 7:269-277.

81. Stokes NR, Baker N, Bennett JM, Chauhan PK, Collins I, Davies DT, Gavade M, Kumar D, Lancett P, Macdonald R, Macleod L, Mahajan A, Mitchell JP, Nayal N, Nayal YN, Pitt GR, Singh M, Yadav A, Srivastava A, Czaplewski LG, Haydon DJ. 2014. Design, synthesis and structure-activity relationships of substituted oxazole-benzamide antibacterial inhibitors of FtsZ. *Bioorganic & medicinal chemistry letters* 24:353-359.

82. Pilhofer M, Aistleitner K, Biboy J, Gray J, Kuru E, Hall E, Brun YV, VanNieuwenhze MS, Vollmer W, Horn M, Jensen GJ. 2013. Discovery of chlamydial peptidoglycan reveals bacteria with murein sacculi but without FtsZ. *Nature communications* 4:2856.

83. Erickson HP, Osawa M. 2010. Cell division without FtsZ--a variety of redundant mechanisms. *Molecular microbiology* 78:267-270.

84. Mercier R, Kawai Y, Errington J. 2013. Excess membrane synthesis drives a primitive mode of cell proliferation. *Cell* 152:997-1007.

85. Monahan LG, Harry EJ. 2013. Identifying how bacterial cells find their middle: a new perspective. *Molecular microbiology* 87:231-234.

86. Willemse J, Borst JW, de Waal E, Bisseling T, van Wezel GP. 2011. Positive control of cell division: FtsZ is recruited by SsgB during sporulation of *Streptomyces*. *Genes & development* 25:89-99.

87. Treuner-Lange A, Aguiluz K, van der Does C, Gomez-Santos N, Harms A, Schumacher D, Lenz P, Hoppert M, Kahnt J, Munoz-Dorado J, Sogaard-Andersen L. 2013. PomZ, a ParA-like protein, regulates Z-ring formation and cell division in *Myxococcus xanthus*. *Molecular microbiology* 87:235-253.

88. Jakimowicz D, van Wezel GP. 2012. Cell division and DNA segregation in *Streptomyces*: how to build a septum in the middle of nowhere? *Molecular microbiology* 85:393-404.

89. de Boer PA, Crossley RE, Rothfield LI. 1989. A division inhibitor and a topological specificity factor coded for by the minicell locus determine proper placement of the division septum in *E. coli*. *Cell* 56:641-649.

90. Woldringh CL, Mulder E, Huls PG, Vischer N. 1991. Toporegulation of bacterial division according to the nucleoid occlusion model. *Research in microbiology* 142:309-320.

91. Lutkenhaus J. 2007. Assembly dynamics of the bacterial MinCDE system and spatial regulation of the Z ring. *Annual review of biochemistry* 76:539-562.

92. Bernhardt TG, de Boer PA. 2005. SlmA, a nucleoid-associated, FtsZ binding protein required for blocking septal ring assembly over Chromosomes in *E. coli*. *Mol Cell* 18:555-564.

93. Shen B, Lutkenhaus J. 2010. Examination of the interaction between FtsZ and MinCN in *E. coli* suggests how MinC disrupts Z rings. *Molecular microbiology* 75:1285-1298.

94. Shen B, Lutkenhaus J. 2009. The conserved C-terminal tail of FtsZ is required for the septal localization and division inhibitory activity of MinC(C)/MinD. *Molecular microbiology* 72:410-424.

95. Dajkovic A, Lan G, Sun SX, Wirtz D, Lutkenhaus J. 2008. MinC spatially controls bacterial cytokinesis by antagonizing the scaffolding function of FtsZ. *Current biology* : CB 18:235-244.

96. Rowlett VW, Margolin W. 2013. The bacterial Min system. *Current biology* : CB 23:R553-556.

97. Rodrigues CD, Harry EJ. 2012. The Min system and nucleoid occlusion are not required for identifying the division site in *Bacillus subtilis* but ensure its efficient utilization. *PLoS genetics* 8:e1002561.

98. Wu W, Park KT, Holyoak T, Lutkenhaus J. 2011. Determination of the structure of the MinD-ATP complex reveals the orientation of MinD on the membrane and the relative location of the binding sites for MinE and MinC. *Molecular microbiology* 79:1515-1528.

99. Cho H, McManus HR, Dove SL, Bernhardt TG. 2011. Nucleoid occlusion factor SlmA is a DNA-activated FtsZ polymerization antagonist. *Proc Natl Acad Sci U S A* 108:3773-3778.

100. Tonthat NK, Milam SL, Chinnam N, Whitfill T, Margolin W, Schumacher MA. 2013. SlmA forms a higher-order structure on DNA that inhibits cytokinetic Z-ring formation over the nucleoid. *Proc Natl Acad Sci U S A* 110:10586-10591.

101. Wu LJ, Errington J. 2012. Nucleoid occlusion and bacterial cell division. *Nature reviews.* Microbiology 10:8-12.

102. Pavlendova N, Muchova K, Barak I. 2010. Expression of *Escherichia coli* Min system in *Bacillus subtilis* and its effect on cell division. *FEMS microbiology letters* 302:58-68.

103. Bramkamp M, Emmins R, Weston L, Donovan C, Daniel RA, Errington J. 2008. A novel component of the division-site selection system of *Bacillus subtilis* and a new mode of action for the division inhibitor MinCD. *Molecular microbiology* 70:1556-1569.

104. van Baarle S, Celik IN, Kaval KG, Bramkamp M, Hamoen LW, Halbedel S. 2013. Protein-protein interaction domains of *Bacillus subtilis* DivIVA. *Journal of bacteriology* 195:1012-1021.

105. Adams DW, Errington J. 2009. Bacterial cell division: assembly, maintenance and disassembly of the Z ring. *Nature reviews*. Microbiology 7:642-653.

106. Eswaramoorthy P, Erb ML, Gregory JA, Silverman J, Pogliano K, Pogliano J, Ramamurthi KS. 2011. Cellular architecture mediates DivIVA ultrastructure and regulates min activity in *Bacillus subtilis. mBio 2.*

107. van Baarle S, Bramkamp M. 2010. The MinCDJ system in *Bacillus subtilis* prevents minicell formation by promoting divisome disassembly. *PloS one* 5:e9850.

108. Bach JN, Albrecht N, Bramkamp M. 2014. Imaging DivIVA dynamics using photo-convertible and activatable fluorophores in *Bacillus subtilis*. *Frontiers in microbiology* 5:59.

109. Wu LJ, Errington J. 2004. Coordination of cell division and chromosome segregation by a nucleoid occlusion protein in *Bacillus subtilis. Cell* 117:915-925.

110. Wu LJ, Ishikawa S, Kawai Y, Oshima T, Ogasawara N, Errington J. 2009. Noc protein binds to specific DNA sequences to coordinate cell division with chromosome segregation. *The EMBO journal* 28:1940-1952.

111. Cambridge J, Blinkova A, Magnan D, Bates D, Walker JR. 2014. A replication-inhibited unsegregated nucleoid at mid-cell blocks Z-ring formation and cell division independently of SOS and the SlmA nucleoid occlusion protein in *Escherichia coli. Journal of bacteriology* 196:36-49.

112. Monahan LG, Liew AT, Bottomley AL, Harry EJ. 2014. Division site positioning in bacteria: one size does not fit all. *Frontiers in microbiology* 5:19.

113. Pinho MG, Kjos M, Veening JW. 2013. How to get (a)round: mechanisms controlling growth and division of coccoid bacteria. *Nature reviews*. Microbiology 11:601-614.

114. Veiga H, Jorge AM, Pinho MG. 2011. Absence of nucleoid occlusion effector Noc impairs formation of orthogonal FtsZ rings during *Staphylococcus aureus* cell division. *Molecular microbiology* 80:1366-1380.

115. Ramirez-Arcos S, Szeto J, Dillon JA, Margolin W. 2002. Conservation of dynamic localization among MinD and MinE orthologues: oscillation of *Neisseria gonorrhoeae* proteins in *Escherichia coli*. *Molecular microbiology* 46:493-504.

116. Ladant D, Ullmann A. 1999. *Bordatella pertussis* adenylate cyclase: a toxin with multiple talents. T*rends Microbiol* 7:172-176.

117. Seidel SA, Dijkman PM, Lea WA, van den Bogaart G, Jerabek-Willemsen M, Lazic A, Joseph JS, Srinivasan P, Baaske P, Simeonov A, Katritch I, Melo FA, Ladbury JE, Schreiber G, Watts A, Braun D, Duhr S. 2013. Microscale thermophoresis quantifies biomolecular interactions under previously challenging conditions. *Methods* 59:301-315.

118. Zhang W, Duhr S, Baaske P, Laue E. 2014. Microscale thermophoresis for the assessment of nuclear protein-binding affinities. *Methods in molecular biology* 1094:269-276.

119. Döhlemann J. 2013. Untersuchung der MipZ-FtsZ-Interaktion in *Caulobacter crescentus*. Master thesis. der Technischen Universität Kaiserslautern

120. Ringel ST. 2013. Untersuchungen zur Aufklärung der MipZ-FtsZ-Interaktion in *Caulobacter crescentus*. Master thesis. Philipps-Universität

121. Figge RM, Easter J, Gober JW. 2003. Productive interaction between the chromosome partitioning proteins, ParA and ParB, is required for the progression of the cell cycle in *Caulobacter crescentus. Molecular microbiology* 47:1225-1237.

122. Chaudhuri BN, Dean R. 2011. The evidence of large-scale DNA-induced compaction in the mycobacterial chromosomal ParB. *J Mol Biol* 413:901-907.

123. Huang L, Yin P, Zhu X, Zhang Y, Ye K. 2011. Crystal structure and centromere binding of the plasmid segregation protein ParB from pCXC100. *Nucleic acids research* 39:2954-2968.

124. Roberts MA, Wadhams GH, Hadfield KA, Tickner S, Armitage JP. 2012. ParA-like protein uses nonspecific chromosomal DNA binding to partition protein complexes. *Proc Natl Acad Sci U S A* 109:6698-6703.

125. Hester CM, Lutkenhaus J. 2007. Soj (ParA) DNA binding is mediated by conserved arginines and is essential for plasmid segregation. *Proc Natl Acad Sci U S A* 104:20326-20331.

126. Leipe DD, Wolf YI, Koonin EV, Aravind L. 2002. Classification and evolution of P-loop GTPases and related ATPases. *J Mol Biol* 317:41-72.

127. Savage DF, Afonso B, Chen AH, Silver PA. 2010. Spatially ordered dynamics of the bacterial carbon fixation machinery. *Science* 327:1258-1261.

128. Thompson SR, Wadhams GH, Armitage JP. 2006. The positioning of cytoplasmic protein clusters in bacteria. *Proc Natl Acad Sci U S A* 103:8209-8214.

129. Eun YJ, Zhou M, Kiekebusch D, Schlimpert S, Trivedi RR, Bakshi S, Zhong Z, Wahlig TA, Thanbichler M, Weibel DB. 2013. Divin: a small molecule inhibitor of bacterial divisome assembly. *Journal of the American Chemical Society* 135:9768-9776.

130. Ebersbach G, Gerdes K. 2005. Plasmid segregation mechanisms. *Annual review of genetics* 39:453-479.

131. Hui MP, Galkin VE, Yu X, Stasiak AZ, Stasiak A, Waldor MK, Egelman EH. 2010. ParA2, a *Vibrio cholerae* chromosome partitioning protein, forms left-handed helical filaments on DNA. *Proc Natl Acad Sci U S A* 107:4590-4595.

132. Lim GE, Derman AI, Pogliano J. 2005. Bacterial DNA segregation by dynamic SopA polymers. *Proc Natl Acad Sci U S A* 102:17658-17663.

133. Vecchiarelli AG, Havey JC, Ing LL, Wong EO, Waples WG, Funnell BE. 2013. Dissection of the ATPase active site of P1 ParA reveals multiple active forms essential for plasmid partition. *The Journal of biological chemistry* 288:17823-17831.

134. Quisel JD, Grossman AD. 2000. Control of sporulation gene expression in *Bacillus subtilis* by the chromosome partitioning proteins Soj (ParA) and Spo0J (ParB). *Journal of bacteriology* 182:3446-3451.

135. Tonthat NK, Arold ST, Pickering BF, Van Dyke MW, Liang S, Lu Y, Beuria TK, Margolin W, Schumacher MA. 2011. Molecular mechanism by which the nucleoid occlusion factor, SlmA, keeps cytokinesis in check. *The EMBO journal* 30:154-164.

136. Dillon SC, Dorman CJ. 2010. Bacterial nucleoid-associated proteins, nucleoid structure and gene expression. *Nature reviews*. Microbiology 8:185-195.

137. Wartlick O, Kicheva A, Gonzalez-Gaitan M. 2009. Morphogen gradient formation. *Cold Spring Harbor perspectives in biology* 1:a001255.

138. Flores E, Herrero A. 2010. Compartmentalized function through cell differentiation in filamentous *cyanobacteria*. *Nature reviews*. Microbiology 8:39-50.

139. Laemmli UK. 1970. Cleavage of structural proteins during the assembly of the head of bacteriophage T4. *Nature* 227:680-685.

140. Baaske P, Wienken CJ, Reineck P, Duhr S, Braun D. 2010. Optical thermophoresis for quantifying the buffer dependence of aptamer binding. *Angewandte Chemie* 49:2238-2241.

141. Thanbichler M, Iniesta AA, Shapiro L. 2007. A comprehensive set of plasmids for vanillate- and xylose-inducible gene expression in *Caulobacter crescentus*. *Nucleic acids research* 35:e137.

142. Karimova G, Pidoux J, Ullmann A, Ladant D. 1998. A bacterial two-hybrid system based on a reconstituted signal transduction pathway. *Proc Natl Acad Sci U S A* 95:5752-5756.

143. Moll A, Thanbichler M. 2009. FtsN-like proteins are conserved components of the cell division machinery in proteobacteria. *Molecular microbiology* 72:1037-1053.

144. Evinger M, Agabian N. 1977. Envelope-associated nucleoid from *Caulobacter crescentus* stalked and swarmer cells. *Journal of bacteriology* 132:294-301.

ACKNOWLEDGMENT

I love this chapter of my thesis the most, since I don't need to carefully cite the origin of the sentences or subjectively describe the results and the explanations, I can freely express what I feel, that is the true emotional me!

This thesis is the summary of my Ph.D work and also the reflection and the reminder of my life in the three and half years. During this time I got help from many people, without their contribution and support I would never finish my thesis.

Let me first express my gratitude to my supervisor Prof. Dr. Martin Thanbichler, who made the blue script of my thesis and kept leading me the way to complete this work. The entire project is preceded with his great ideas and helpful advices. Although I am far away from a good Ph.D student, he never gave up enlightening me with scientific minds and encouraging me to overcome difficulties.

I would also like to thank the members of my IMPRS committee and thesis committee: Prof. Dr. Lotte Søgaard-Andersen, Prof. Dr. Uwe Maier, Dr. Lennart Randau and Prof. Dr. Hans-Ulrich Mösch. Thank you for all the advices and suggestions during my whole Ph.D study, and kindly spend time on reading and reviewing my thesis.

It is a great pleasure to spend this three and half years in my working group. My open and helpful colleagues support me not only for my work but also during my daily life in Marburg. I want to give my gratitude to all of my lovely colleagues, both the current ones and the former ones, particularly, to Dani, Till and Johannes for their contribution to my project; to Emöke, Lin and Wolle for their great help on correcting my Chinglish writing style, writing the Zusammenfassung, clarifying my scientific ideas and showing me all the tricks to cope with the softwares used in my thesis. I am grateful to Alex, Ola, Maria, Emöke and Lin for their company during the lunch time in weekdays and "happy hours" in the weekends.

Of course, I cannot thank my family and friends enough. My parents and grandparents have to endure the absence of me in the lunar New Year eve, mid-autumn day, their birthdays and almost every important family event for six years. This situation will finish soon, and I promise to go back and stay with my family. I will also take the chance to express my gratitude to my non-blood related family in Bonn, my grandpa, sisters and brothers, who always rescue me from negative mood and encourage me to face the frustrating reality. Thank you so much to provide me a home in Germany. My beloved friend Niuniu, I cannot image how pale my Ph.D life would be without you. I'm so glad to have your company inside and outside of the lab, in and out of Marburg, in the virtual internet and in real life.

Last but not the least, I am appreciate the encouragement from lengyuegufen, who tried her best to persuade me to continue my study, extract the bad feelings and stress from my heart and in turn fulfill it with confidence.

ERKLÄRUNG

Ich versichere, dass ich meine Dissertation:

„ Study of a sociable molecule: mapping the binding interfaces of the cell division regulator MipZ in *Caulobacter crescentus* “ selbstständig, ohne unerlaubte Hilfe angefertigt und mich dabei keiner anderen als der von mir ausdrücklich bezeichneten Quellen und Hilfen bedient habe.

Die Dissertation wurde in der jetzigen oder einer ähnlichen Form noch bei keiner anderen Hochschule eingereicht und hat noch keinen sonstigen Prüfungszwecken gedient.

Marburg, den _____

Binbin He